USAARL Report No. 2020-04

Effect of Patient Weight as a Factor during Use of an Immobilization System versus No Immobilization System

By Sandra Conti[1,2], Amy Lloyd[1,2], Rachel Kinsler[1], Laura Kroening[1,3], Jeff Molles[1,2]

[1]U.S. Army Aeromedical Research Laboratory
[2]Goldbelt Frontier, LLC
[3]Oak Ridge Institute for Science and Education

United States Army Aeromedical Research Laboratory

Enroute Care Group

December 2019

Approved for public release; Distribution unlimited.

Notice

Qualified Requesters

Qualified requesters may obtain copies from the Defense Technical Information Center (DTIC), Fort Belvoir, Virginia 22060. Orders will be expedited if placed through the librarian or other person designated to request documents from DTIC.

Change of Address

Organizations receiving reports from the U.S. Army Aeromedical Research Laboratory on automatic mailing lists should confirm correct address when corresponding about laboratory reports.

Disposition

Destroy this document when it is no longer needed. Do not return it to the originator.

Disclaimer

Human Subject Use

In the conduct of research involving human subjects, the investigator(s) adhered to the policies regarding the protection of human subjects as prescribed by Department of Defense Instruction 3216.02 (Protection of Human Subjects and Adherence to Ethical Standards in Department of Defense (DoD)-Supported Research) dated 8 November 2011.

REPORT DOCUMENTATION PAGE	*Form Approved* *OMB No. 0704-0188*

1. REPORT DATE *(DD-MM-YYYY)*	2. REPORT TYPE	3. DATES COVERED *(From - To)*
20-12-2019	Final Technical Report	09 May 2019 - 04 Nov 2019

4. TITLE AND SUBTITLE

Effect of Patient Weight as a Factor during Use of an Immobilization System versus No Immobilization System

5a. CONTRACT NUMBER W81XWH-1-7-P-0315

5b. GRANT NUMBER DM167047

5c. PROGRAM ELEMENT NUMBER 6111102

6. AUTHOR(S)

Conti, Sandra; Lloyd, Amy; Kinsler, Rachel; Kroening, Laura; Molles, Jeff

5d. PROJECT NUMBER 2015-013

5e. TASK NUMBER

5f. WORK UNIT NUMBER ECG

7. PERFORMING ORGANIZATION NAME(S) AND ADDRESS(ES)

U.S. Army Aeromedical Research Laboratory
P.O. Box 620577
Fort Rucker, AL 36362

8. PERFORMING ORGANIZATION REPORT NUMBER

USAARL 2020-04

9. SPONSORING/MONITORING AGENCY NAME(S) AND ADDRESS(ES)

Department of Defense, Joint Program Committee 6
Combat Casualty Care Research Program, Congressionally Directed Medical Research Program
1077 Patchel Street
Fort Detrick, MD 21702

10. SPONSOR/MONITOR'S ACRONYM(S)

CDMRP

11. SPONSOR/MONITOR'S REPORT NUMBER(S)

12. DISTRIBUTION/AVAILABILITY STATEMENT

Approved for public release; Distribution unlimited.

13. SUPPLEMENTARY NOTES

Goldbelt Frontier, LLC; Oak Ridge Institute for Science and Education

14. ABSTRACT

This goal of this study was to evaluate the effect of patient weight as a factor when using an immobilization system versus no immobilization system (litter only) during patient transport. The hypothesis that patients with different weights produce different biodynamic responses was tested under two immobilization conditions: 1) immobilized with a U.S. Army Immobilization Kit while secured to a U.S. Army Decontaminable Litter with standard litter straps, and 2) non-immobilized where subjects were simply secured to the Decontaminable Litter with two litter straps. Subjects were divided into high- and low-weight groups. High-weight subjects were those who weighed 190 to 240 pounds (lb.) and low-weight subjects were those who weighed 110 to 150 lb. Accelerometers were placed on each subject's forehead, sternum, pelvis, and knee, as well as the input surface (litter mesh or spine board) and Multi-Axis Ride Simulator (MARS) platform surface. The subjects were placed in the immobilized and non-immobilized configurations ON THE mars, then ride signatures of a Mine-Resistant Ambush Protected ground vehicle, HH-60M helicopter, and constructed white-noise vibration profile were simulated. Significant differences were found between weight groups and immobilization configurations within weight groups, in regards to z-axis transmissibility, area under z-axis transmissibility curve, z-axis transmissibility resonance frequency, root mean square (RMS) z-axis acceleration, and RMS rotational velocity.

15. SUBJECT TERMS

Patient weight, immobilization, vibration, acceleration, rotational velocity, MEDEVAC, helicopter, ground vehicle, en route care, vibration mitigation, vibration transmissibility

16. SECURITY CLASSIFICATION OF: a. REPORT	b. ABSTRACT	c. THIS PAGE	17. LIMITATION OF ABSTRACT	18. NUMBER OF PAGES	19a. NAME OF RESPONSIBLE PERSON
UNCLAS	UNCLAS	UNCLAS	SAR	100	Loraine St. Onge, PhD
					19b. TELEPHONE NUMBER *(Include area code)* 334-255-6906

This page is intentionally blank.

Table of Contents

List of Figures

List of Tables

Introduction

Medical evacuation (MEDEVAC) of combat casualties is critical to obtaining life- and function-saving treatment. Prior to transport, casualties with serious or suspected head and/or spine injuries are required to be immobilized to prevent movement that may exacerbate injuries. In some circumstances, patients may get transported using only litters with no backboard. Casualties are then evacuated in medical transport vehicles, which are often sources of mechanical shock and vibration inputs to the patients.

During recent surveys of healthcare providers in the field, respondents reported severe discomfort and pain experienced by casualties during military ground and air transport. Pain was attributed to vibration and repeated shock associated with the transport (Kinsler, Barazanji, Lee, Fulton, & Hatzfeld, 2015). The forces and vibrations transmitted to the patient's body through the transport system could have severe consequences, especially for neurotrauma patients sensitive to increased intracranial pressure (ICP) (Ratanalert et al., 2004; Reno, 2010).

Subjective observations during field evacuations have revealed cases of patients experiencing unexpected mechanical shocks and motions during loading and unloading, including their litter being dropped. These transmitted forces and motions can have dramatic consequences on patient health outcome and well-being. Patients and care providers also reported adverse effects from the application of immobilization technologies in these environments, such as discomfort, pain, pressure sores, and possible exacerbation of injuries (Ben-Galim et al., 2010).

While motion transmitted to the human body is the main focus in most transmitted-vibration analysis studies (Meusch & Rahmatalla, 2014a, 2014b; DeShaw & Rahmatalla, 2016; Wanner, Mayer, Kinsler, DeShaw, & Rahmatalla, 2016), measurement of forces transmitted to different body segments of a supine patient during transport has not been reported in the literature. Insufficient research has been conducted to assess human response to whole-body vibration while secured to a litter or backboard in the supine position. Likewise, there has been little research on effects of vibration or shock on immobilization systems used for securing transported patients with head and/or spine injuries.

There is little information in the literature on effects of whole-body vibration on supine humans as compared to seated transport (DeShaw & Rahmatalla, 2014a, 2016; Meusch, 2012; Rahmatalla, DeShaw & Barazanji, 2017; Wang & Rahmatalla, 2013a, 2013b). The complexity of the biodynamic response of different body segments presents a challenging task for data collection and analysis. Unexpected large body motion can dramatically affect output of sensors attached to the body and transport system, which can generate significant assessment and conclusion errors. With advances in new motion measurement technologies, recent publications have outlined effective methodologies to deal with such complicated environments (DeShaw & Rahmatalla, 2012). This project used modernized data acquisition systems, an innovative motion platform, sensitive motion sensors, and unique data analysis software to characterize patient weight as a factor during the use of an immobilization system versus no immobilization system during simulated transport. The study team investigated various factors that could affect biodynamic response of the supine human under whole-body vibration and repeated shock. Results of the project provide significant information and tools that can be used toward increasing patient safety, reducing discomfort, and developing vibration mitigation systems.

Military Relevance

Studies reported in the literature and observations from Operation Enduring Freedom and Operation Iraqi Freedom indicated that repeated shock and vibration during aeromedical and ground transport can cause considerable patient motion and may adversely affect patient comfort and medical outcome. Patients with spinal immobilization required additional sedation when transported by ground vehicles. Casualties with spinal cord injury, traumatic brain injury, and/or other severe neurologic injuries are the most vulnerable to vehicle repeated shock and vibration. Patient management during military en route care is a complex process because of inconsistencies in patient clinical conditions, patient sizes, vehicle configurations, patient transport systems (e.g., litters and immobilizations systems), and environments associated with transport.

This project addressed the fiscal year 2016 Joint En Route Care Research Focus Area "research to understand the impact of transport on patient physiology, the impact of transport on clinician human performance, and the best time to transport." The team investigated patient weight, transport systems, and securing practices as factors affecting supine human biodynamic response. Mathematical models were produced and may be used to better understand patient en route care management. The long-term outcome from this work is to use the findings to develop guidelines for effective best practices that can reduce secondary damages to patients during transport. Material designers and developers will have assessment tools for developing better vibration mitigation technologies and more effective transport systems.

Objective

The overall objective of this study was to evaluate the effect of patient weight as a factor during use of an immobilization system versus no immobilization system (litter only). The hypothesis that patients with different weights produce different biodynamic responses was tested under the two immobilization conditions.

Specific Aims

(1) Specific Aim 1: The team measured vibration in supine healthy humans while subjected to ride profiles on the Advanced Motion Technologies, Inc. Multi-Axis Ride Simulator (MARS) while lying supine on a Decontaminable (Decon) Litter.

(2) Specific Aim 2: The team measured vibration of supine healthy humans while subjected to ride profiles on the MARS while lying supine on an immobilization system.

(3) Specific Aim 3: The team characterized the biodynamic response of humans with different weights using a) a Decon Litter and b) an immobilization system.

Materials

USAARL evaluated two patient setups and two weight groups during the study. Both setups simulated casualties exposed to vibration and mechanical shock using a MARS platform. The first setup included a National Industries for the Blind Defense Medical Board Medical

Litter (Decon Litter) and National Industries for the Blind Canvas Webbing Patient Securing Cargo Straps (litter straps) (Figures 1 and 2). The second setup was the immobilization system, which included a North American Rescue (NAR) Spine Board (Figure 3), Morrison Medical Black Head Immobilizer (Figure 4), and Emergency Products and Research Spider Strap™ XL (Figure 5) in conjunction with the Decon Litter and securing straps (Figure 6).

Figure 1. Decon Litter (National Stock Number (NSN): 6530-01-380-7309).

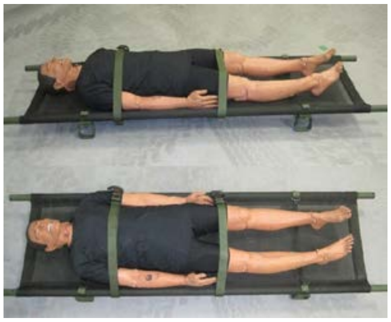

Figure 2. Decon Litter test setup.

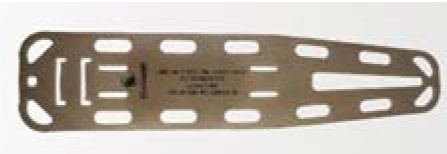

Figure 3. NAR Spine Board (item number: 50-0014, NSN# 6530-01-490-2487).

Figure 4. Black Head Immobilizer (item number: 261420, NSN# 6530-01-619-1**777**).

Figure 5. Spider Strap™ XL (item number: 01115OD, NSN# 6530-01-593-0010).

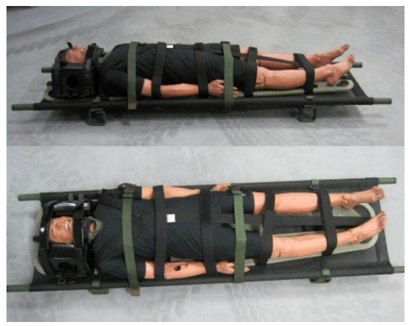

Figure 6. Immobilization system.

The litter configurations were attached to the MARS motion platform as shown in the Methods section. Simulated casualties (healthy human subjects) were exposed to three simulated vehicle ride signatures via the MARS platform: 1) Mine-Resistant Ambush Protected (MRAP) ground vehicle, 2) HH-60M helicopter, and 3) constructed white-noise vibration profile. Measurements included acceleration and motion capture.

Acceleration and angular velocity measurements were taken using six-degree-of-freedom (6DOF) sensors and triaxial accelerometers attached to the MARS, litter, backboard, and human subject. Data were collected using a Crystal Instruments CoCo-90® Dynamic Signal Analyzer and Data Collector. GoPro HERO3® and HERO4® cameras were used to collect video in the dynamic environment.

Methods

Sample Size Estimation, Volunteer Selection, and Grouping

Sample size estimation was calculated and the required number of subjects was defined assuming a confidence interval of 95% and an acceptable power of 80%. A minimum of 12 subjects per condition, for a total minimum of 24, was established to allow sufficient power in this study to either reject or accept the null hypotheses. The study group was able to recruit a total of 26 subjects, 13 in each of the two weight groups. The first group required a weight of 110 to 150 pounds (lb.) (low-weight [LW] group), and the second group required a weight of 190 to 240 lb. (high-weight [HW] group).

Subjects 19 years of age or older with general good health, no medical conditions that might be adversely affected by exposure to moderate low-frequency vibration, and no difficulties with the application of immobilization technologies were recruited for the study. Individuals with orthopedic injuries (especially back, neck, or head injuries), poor circulation, motion sickness, diabetes, known severe skin sensitivities or allergies to adhesives, or who were pregnant were denied participation. Refer to the Medical History Questionnaire for all excluding medical criteria (Attachment A). Subjects who did not fall within the target weight ranges were also excluded. Table 1 summarizes the gender and weights for each subject.

Table 1. Subjects by Group

Group	Gender	Weight (kg)
Upper Weight	Female	91.5
	Male	108.6
	Female	86.5
	Female	103.2
	Male	95.3
	Male	95.5
	Female	88.5
	Male	109.5
	Male	92.9
	Male	88.3
	Male	106.5
	Male	104.1
	Male	92.9
Lower Weight	Female	54.8
	Male	65.3
	Female	58.7
	Female	66.4
	Female	58.6
	Female	51.9
	Female	62.9
	Female	60.1
	Female	50.7
	Female	65.9
	Male	60.8
	Female	66.9
	Female	59.4

Data Collection

The primary data collected under this protocol were acceleration data, angular velocity data, anthropometric measures, verbal survey data, videos, and photographs (Table 2). Medical history was collected for determination of subject suitability against inclusion and exclusion criteria and was not included in the data analyses. The videos and photographs were collected for reference and qualitative viewing of the subjects’ experience. No quantitative measures were collected from the videos or photographs. Verbal survey data was used to determine subject discomfort and/or pain during the course of testing. These ratings were an indicator of whether testing needed to be halted for subject comfort or safety.

The study determined whether relationships existed between weight and transmissibility and presence or absence of an immobilization system and transmissibility. The relationship between weight and transmissibility was evaluated using one-way analysis of variance (ANOVA). The acceleration data, angular velocity data, anthropometric measures, and reporting of gender contributed to the biodynamic response characterization described in Specific Aim 3.

Table 2. Types of Data Collected

Data Element/Variable	Source(s)	Operational Specification
Acceleration (6DOF sensors)	Human subject forehead, sternum, and pelvis; spine board and litter.	200 millivolts per unit of gravity (mV/g) (± 10%)
Angular velocity	Human subject forehead, sternum, and pelvis; spine board and litter.	1 millivolt per degree per second (mV/deg/s) (± 10%)
Acceleration (triaxial sensors)	MARS platform, human subject knee.	174 mV/g (± 10%)
Discomfort rating	Human subject	Scale 1 to 10
Anthropometric measurements	Human subject	Weight, height, anthropometric measurements (kilogram per centimeter [kg/cm]
Video	Testing of subject on MARS	60 frames per second
Medical history	Human subject	N/A

The acceleration and angular velocity data required reduction and preparation prior to analysis. Sensor values were recorded as variable voltages that corresponded to acceleration values or angular velocity values. Data files from the two data acquisition systems were combined into common files, with channels from the two systems aligned in time by use of the timing signal (recorded by channel 16 of each data acquisition system). Once the files were combined, a conversion was applied to each channel as appropriate converting from voltage to acceleration values or angular velocity values. The data was also low-pass filtered.

The individual components of the acceleration data (x-, y-, and z-axes) were averaged and standard deviations were calculated across all subjects for each signal to verify that vibration excitation was consistent across all groups. Power spectral density (PSD) functions were also used on the dataset. When plotted across specific frequency bands, PSD describes the frequencies at which energy is present and at what levels. This is of particular interest when higher levels of energy are present in frequency bands that are known to have possible health effects on humans during whole-body vibration.

Analysis of acceleration data allowed characterization of transmitted vibration frequency and amplitude at various points in the human-litter system. These characterizations were used to calculate vibration transmissibility, which is a quantitative metric that defines how vibration is altered by passing through a material or structure and attenuating, amplifying, or shifting energy to different frequencies. Transmissibility has been used to characterize the human system as a single-input / single-output function or as a multiple-input /

multiple-output function (Paddan and Griffin, 1998; DeShaw and Rahmatalla, 2014b; Hinz, Menzel, Bluthner, & Seidel, 2010.) Transmissibility above 1.0 indicates amplification in the system, while transmissibility below 1.0 indicates attenuation. The transmissibility was calculated for each input-output directional combination in three dimensional (3D) space (three input / three output). Table 3 shows the matrix of transmissibility combinations. For this analysis, the input acceleration was the surface of the litter or immobilization system. The output acceleration was the acceleration at each body segment; consequently, there are multiple matrices for each subject.

Table 3. Directional Transmissibility Combinations

Fore-aft Input Fore-aft Output (Xx)	Lateral Input Fore-aft Output (Yx)	Vertical Input Fore-aft Output (Zx)
Fore-aft Input Lateral Output (Xy)	Lateral Input Lateral Output (Yy)	Vertical Input Lateral Output (Zy)
Fore-aft Input Vertical Output (Xz)	Lateral Input Vertical Output (Yz)	Vertical Input Vertical Output (Zz)

The area under each transmissibility curve was calculated and evaluated. Finding the area under the transmissibility curve helped to quantify the frequency distribution of the amplification and the overall energy transmission.

The accelerations were computed into a 3D resultant average by taking the root-mean-square (RMS) for each subject and sensor location. This resultant indicated the average total vibrational energy experienced by the subject at the sensor locations. Resultant RMS acceleration is the square root of the sum of each acceleration value (in all three axes) squared divided by the total number of values. The equation for this calculation is:

$$RMS = \sqrt{\frac{\left(\sum_{i=1}^{N} x(i)^2 + y(i)^2 + z(i)^2\right)}{N}}$$

These sums were averaged and standard deviations calculated across weight, body location, and input signals. An ANOVA was performed to determine if any significant differences existed across these groupings.

The resonant frequency is the frequency at which an object resonates, or stores energy, and increases the amplitude of its motion. The resonance frequency is found using two variables: the stiffness of the system, *k*, and the mass of the system, *m*. The equation used is:

$$\omega_n = \sqrt{\frac{k}{m}}$$

Additional data analyses determined the vibration transfer functions throughout the litter system and through the healthy human subject. The transfer functions, developed by the project's extramural partners, were employed to describe the transmissibility of vibration. The relationship between anthropometric characteristics and vibration transfer functions was identified, which allowed the development of the characterization of supine human vibration response.

Sensor Placement

Subjects were evaluated for inclusion by the study physician before testing. Healthy human subjects were then fitted with four sensors. The 6DOF sensors were placed in the center of the subject's forehead (Figure 7), on the upper sternum (Figure 8), and at the forward-most point of the left anterior superior iliac spine (Figure 9). A triaxial accelerometer was placed two inches above the top of the patella (Figure 10). Double sided tape, sensor holders, and athletic wrap were used to secure the sensors. Details of the sensors used are described in Attachment C. Test system sensor placements are shown in Figures 11 through 15.

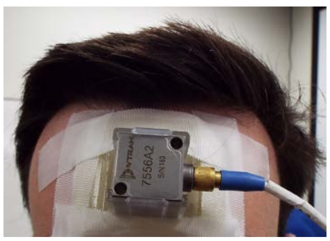
Figure 7. Forehead sensor.

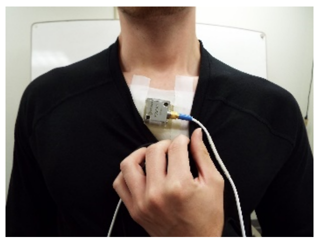
Figure 8. Sternum sensor.

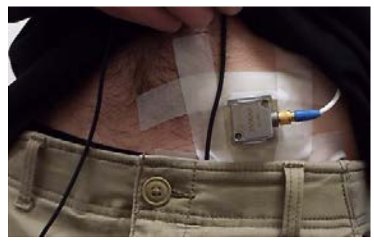
Figure 9. Hip sensor.


Figure 10. Knee sensor.

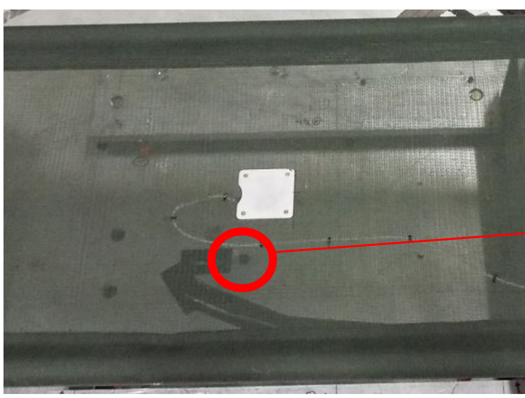
Figure 11. MARS and Decon Litter sensors.

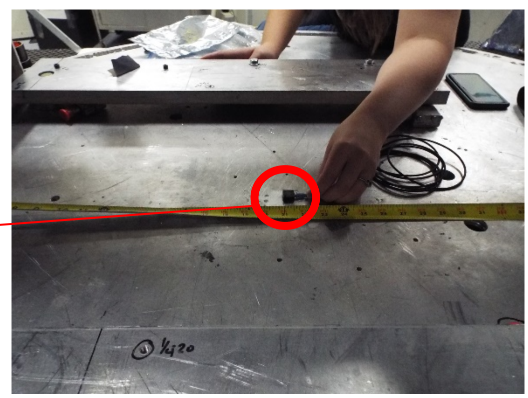
Figure 12. MARS platform sensor.

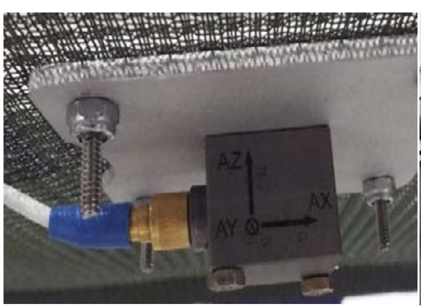

Figure 13. Decon Litter sensor.

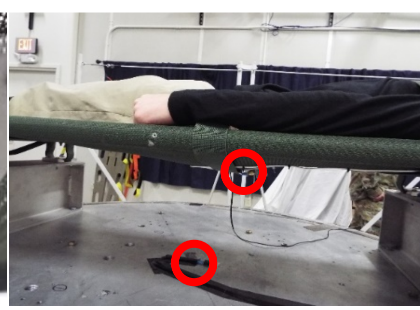
Figure 14. Test setup showing sensor positions.


Figure 15. NAR Spine Board sensor.

Ride Profiles

The ground vehicle profile was a ride signature collected from a ground ambulance that was driven over a rough road with bumps. This profile contained a predominant low frequency vibration of 2 Hertz (Hz) associated with the vehicle suspension and some higher frequency elements associated with engine operation and jolts from bumps in the road. The air vehicle profile was a compilation of collected signatures from an HH-60M series MEDEVAC helicopter that was performing standard maneuvers. This profile contained energy associated with a predominant frequency of approximately 17 Hz that is associated with the operation of the main rotor. There were also some minor jolts in the profile from landing maneuvers. The maximum amplitudes in each ride profile fell within the safety standards described in the ISO 2631 series.

Profile Performance

Subjects were asked to lay in a supine position on a Decon litter (henceforth referred to as "no board configuration" or "NB" to match the nomenclature of the data analysis report provided by USAARL's partner for this study, ActiBioMotion [ABM]), as seen in Figure 16, or an immobilization system (henceforth referred to as "spinal board configuration" or "SB" to match the nomenclature of ABM's report), as seen in Figure 17. Each configuration was rigidly attached to the MARS during testing (Figures 16 and 17). Litter straps and the Spider Strap™ XL were applied by a retired U.S. Army Flight Medic according to standard U.S. Army MEDEVAC guidelines with the same tension for all subjects. During testing with the SB configuration, the subject's head was secured with the head immobilizer. The sensor wires were connected to the data acquisition systems and cameras recorded the data collection event.

The three vibration profiles were played by the MARS operator. Each profile was approximately 60 seconds in duration, and at the end of each ride profile subjects were asked to rate their dynamic discomfort caused by the vibration input. Testing time from arrival to release took approximately 2.5 hours.

If a maximum discomfort rating of seven or above, or pain rating of three or above was indicated by a participant, the testing stopped so the subject could be evaluated by the study physician. Participants were evaluated by the study physician at the conclusion of testing.

Figure 16. NB configuration.

Figure 17. SB configuration.

Results

Data analysis was performed by ABM. The full report from ABM is included as Attachment D.

Vibration data from the individual accelerometer axes for all ride profiles and both configurations were analyzed. Figure 18 shows an example of the *z*-axis acceleration of one subject's head during the ground vehicle profile for the NB and SB configurations, respectively.

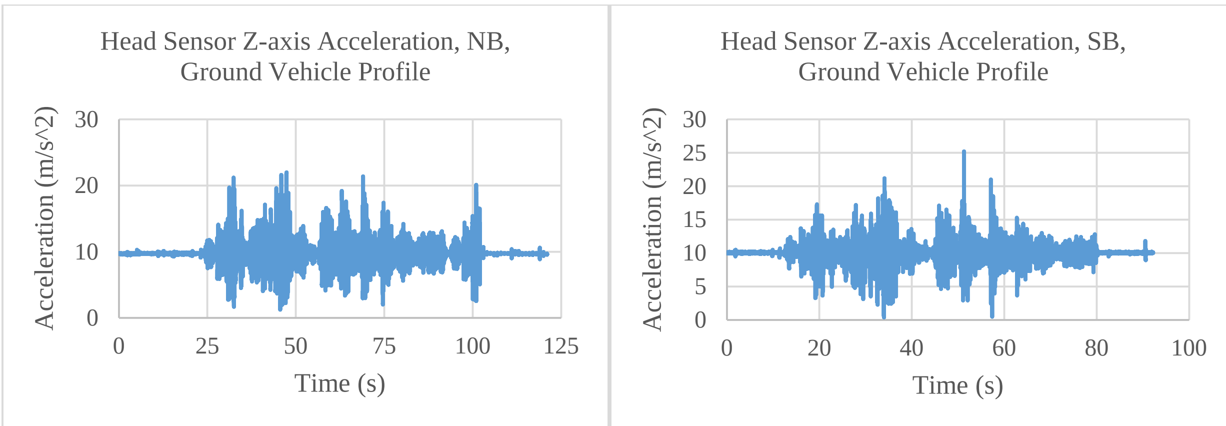

Figure 18. Example *z*-axis acceleration data for both test configurations.

For each sensor, the individual axis acceleration data were analyzed using several methods including RMS, transmissibility, and resonant frequencies.

Figures 19 and 20, show the median transmissibility of the head in only the *z*-axis plotted against the 25th to 75th percentile and the 5th to 95th percentile transmissibilities. Figure 19 compares the two weight groups (LW and HW), and Figure 20 compares the immobilized condition (NB and SB). Every fifth point of each dataset was plotted so that the plots were easier to analyze. The red line represents the subject median transmissibility, the area between the two blue lines represents the 25th to 75th percentile, and the area between the two black lines represents the 5th to 95th percentile. The transmissibility of other body segments can be found in Attachment D.

Figure 19 compares the transmissibility of the head in the *z*-axis for the two weight groups. The median line magnitude (red line) of transmissibility is nearly identical between the LW and HW subjects. The median resonance is where the lines in the graphs peak, the HW group's median resonance was approximately 1.5 Hz lower than the LW group's median resonance. This correlates to the equation to calculate the resonance frequency, which is the square root of stiffness, k, divided by mass, m. The HW subjects have more mass, so the resonance frequency is lower. This relationship can also be seen in the chest and hip sensors when comparing the weight groups. The amplitudes of the frequencies for the HW subjects' 95th percentile transmissibility values at resonance were also higher than the LW group's amplitudes, and featured the same 1.5-Hz shift in resonance frequency from the LW group as the median line. Inertia could play a factor in this. Inertia is a physical property that explains why a stationary object resists motion and why a moving object wants to stay in motion. It is found by multiplying the acceleration by the mass. The HW group would have higher inertia than the LW group because there is more mass moving in the HW group, which would lead to a higher amplitude.

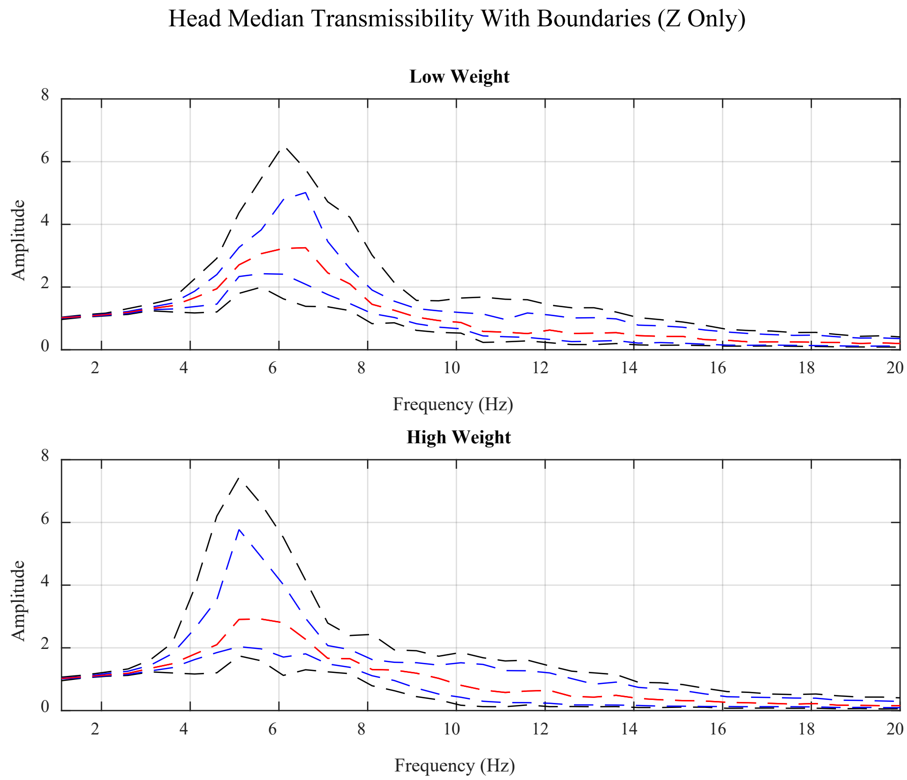

Figure 19. Head median transmissibility compared between the LW and HW categories.

In Figure 20, the median transmissibility of the head was also found when comparing the NB condition to the SB condition. The median transmissibility magnitude (red line) was higher when no board was used, compared to when a spine board was used. The magnitude of the peak transmissibility was reduced by nearly 50 % when a SB was implemented. The SB condition also saw its peak transmissibility shift back by approximately 0.5 Hz when compared to the NB condition; except for the SB 95th percentile in terms of transmissibility amplitude experienced its resonance around 1 Hz after the NB condition. After 10 Hz, the transmissibility magnitude continued towards 0 for the NB condition but remained above 1.0 for much of the frequency content after 10 Hz for the SB condition, meaning the NB condition helps to filter out the higher resonance frequencies.

This space is intentionally blank.

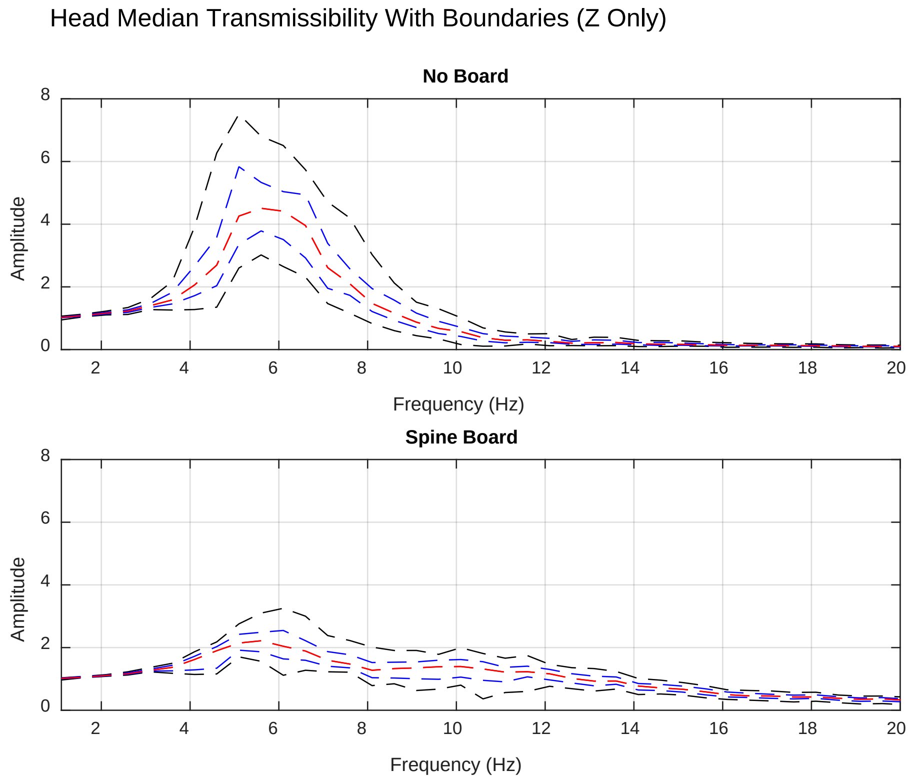

Figure 20. Head median transmissibility compared between the NB and SB categories.

Figure 21 is an example of the box plots in Attachment D. The values represented are the RMS ratios of SB to NB, meaning if the value is greater than one, then the average RMS of the subjects at that value was greater in the SB condition than in the NB condition. The red cross represents the mean RMS value, the red line is the median line, the blue boxes represent the interquartile range (25th to 75th percentiles), the horizontal gray bars represent the 5th and 95th percentiles, and the circles represent outliers in the dataset. The RMS ratios are divided into HW and LW groups, and further subdivided by axis.

This space is intentionally blank.

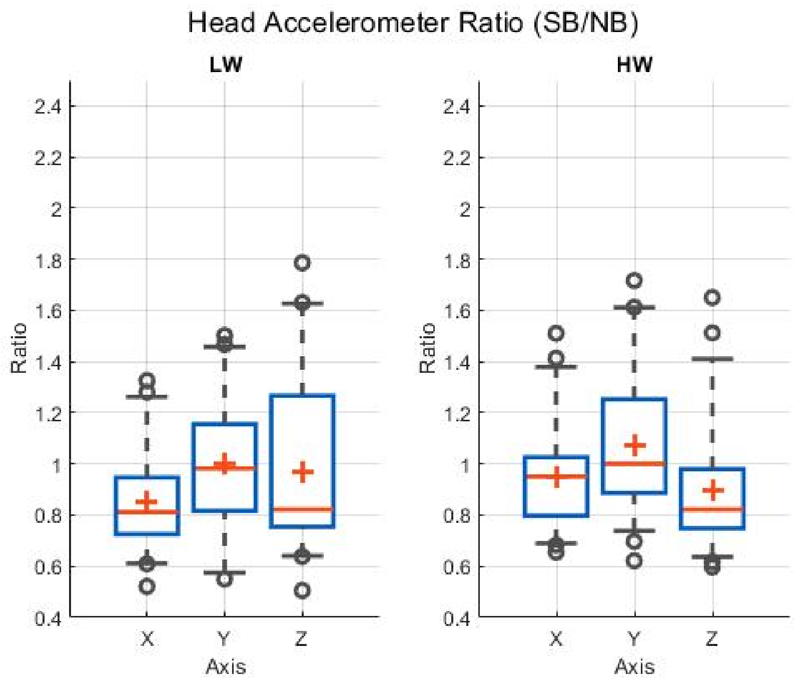

Figure 21. Box plot comparing the SB/NB RMS ratio for HW and LW categories.

Box plots similar to Figure 21 were created to compare the RMS SB/NB acceleration ratios and RMS SB/NB angular velocity ratios for the head, chest, and hip accelerometers. Box plots were also created for the head, chest and pelvis to directly compare the RMS acceleration of all SB and NB subjects divided across axes for each accelerometer, and further subdivided into HW and LW categories. The RMS accelerations of the head, chest, and pelvis for all HW and LW subjects were also represented by boxplots divided by axis, and further subdivided by NB and SB. Similar boxplots were made for RMS rotation.

To provide a statistical analysis of the data, the results were categorized using three factors: weight (HW or LW), immobilization configuration (SB or NB), and ride profile (ground vehicle, helicopter, or white noise). Tables 4 through 7 provide a summary of the data analyses. The columns are divided by SB or NB, and the rows on the side show the ride profiles. The following factors were analyzed: z-axis transmissibility, area under the z-axis transmissibility curve, z-axis resonant frequency, RMS z-axis acceleration, and RMS of the gyroscope.

Tables 4 and Table 5 show the categories that had a statistically significant difference between the immobilization conditions (statistically significant values are highlighted orange). Tables 6 and 7 show the categories that had statistically significant differences between weight groups (statistically significant values are highlighted blue). The gyroscope metric contains all three axes (rather than just the z-axis) because acceleration in the z-axis can cause rotational velocity about all three axes. The metrics were further analyzed for statistical significance using one-way ANOVA. Results were deemed significant if p was less than 0.05.

Table 4. Statistically Significant Difference between Immobilization Conditions LW Category

		Low Weight									
Ride Profile	Segment	Z Transmissibility (Peak)		Area under Z Transmissibility Curve		Z Transmissibility Resonance Frequency (Hz)		RMS Z Acceleration (g)		RMS Gyroscope (deg/s)	
		SB	NB	SB	NB	SB	NB	SB	NB	SB	NB
All	Head	2.74 (±0.45)	5.49 (±1.06)	1.12 (±0.06)	1.19 (±0.08)	5.83 (±0.62)	6.39 (±0.41)	0.16 (±0.04)	0.20 (±0.08)	10.01 (±5.77)	25.91 (±15.61)
	Chest	3.56 (±0.55)	3.72 (±0.54)	1.04 (±0.09)	1.12 (±0.11)	5.73 (±0.50)	5.81 (±0.54)	0.14 (±0.05)	0.15 (±0.05)	9.10 (±5.06)	12.39 (±5.86)
	Pelvis	4.24 (±0.77)	3.72 (±0.71)	1.15 (±0.11)	1.02 (±0.09)	5.75 (±0.45)	5.22 (±0.45)	0.15 (±0.06)	0.14 (±0.05)	14.25 (±8.03)	17.76 (±9.78)
Ground	Head	2.80 (±0.44)	5.75 (±1.15)	1.17 (±0.05)	1.22 (±0.08)	5.88 (±0.40)	6.26 (±0.23)	0.18 (±0.01)	0.22 (±0.01)	7.32 (±1.61)	17.73 (±2.41)
	Chest	3.46 (±0.53)	3.75 (±0.38)	1.07 (±0.08)	1.14 (±0.08)	5.84 (±0.37)	5.82 (±0.48)	0.17 (±0.01)	0.17 (±0.01)	7.42 (±2.80)	10.17 (±2.41)
	Pelvis	3.95 (±0.68)	3.45 (±0.63)	1.13 (±0.11)	1.00 (±0.07)	5.82 (±0.37)	5.15 (±0.45)	0.18 (±0.01)	0.17 (±0.01)	11.84 (±4.16)	13.64 (±4.38)
Air	Head	2.82 (±0.51)	5.52 (±1.19)	1.08 (±0.06)	1.17 (±0.10)	6.30 (±0.68)	6.72 (±0.41)	0.11 (±0.01)	0.09 (±0.05)	5.39 (±1.87)	13.35 (±3.64)
	Chest	3.81 (±0.63)	4.05 (±0.61)	1.07 (±0.10)	1.17 (±0.12)	6.09 (±0.46)	6.06 (±0.65)	0.08 (±0.02)	0.09 (±0.02)	5.48 (±1.99)	8.15 (±2.46)
	Pelvis	4.73 (±0.89)	4.42 (±0.68)	1.20 (±0.12)	1.07 (±0.10)	6.09 (±0.34)	5.42 (±0.51)	0.07 (±0.01)	0.08 (±0.01)	7.33 (±2.29)	9.79 (±1.61)
3D Vibration	Head	2.60 (±0.41)	5.20 (±0.84)	1.11 (±0.04)	1.17 (±0.06)	5.30 (±0.26)	6.18 (±0.36)	0.20 (±0.01)	0.28 (±0.02)	17.41 (±2.97)	46.65 (±6.36)
	Chest	3.41 (±0.45)	3.35 (±0.37)	1.00 (±0.08)	1.05 (±0.09)	5.27 (±0.23)	5.54 (±0.36)	0.17 (±0.01)	0.18 (±0.01)	14.59 (±4.34)	18.85 (±5.17)
	Pelvis	4.03 (±0.49)	3.48 (±0.58)	1.11 (±0.10)	1.01 (±0.07)	5.35 (±0.28)	5.09 (±0.35)	0.20 (±0.02)	0.18 (±0.02)	23.59 (±5.36)	29.85 (±5.91)

Table 5. Statistically Significant Difference between Immobilization Conditions HW Category

		High Weight									
Ride Profile	Segment	Z Transmissibility (Peak)		Area under Z Transmissibility Curve		Z Transmissibility Resonance Frequency (Hz)		RMS Z Acceleration (g)		RMS Gyroscope (deg/s)	
		SB	NB	SB	NB	SB	NB	SB	NB	SB	NB
All	Head	2.31 (±0.27)	6.25 (±1.60)	1.11 (±0.07)	1.13 (±0.09)	5.92 (±1.49)	5.41 (±0.43)	0.16 (±0.04)	0.19 (±0.08)	9.11 (±4.41)	25.87 (±15.98)
	Chest	3.22 (±0.44)	4.33 (±0.76)	0.98 (±0.06)	0.93 (±0.06)	5.38 (±0.50)	4.99 (±0.27)	0.13 (±0.04)	0.14 (±0.04)	9.71 (±5.57)	10.82 (±5.76)
	Pelvis	4.28 (±0.77)	4.00 (±0.92)	1.05 (±0.16)	0.96 (±0.10)	5.36 (±0.43)	4.82 (±0.24)	0.15 (±0.05)	0.14 (±0.04)	20.76 (±11.66)	22.45 (±11.79)
Ground	Head	2.42 (±0.29)	6.43 (±1.42)	1.17 (±0.04)	1.19 (±0.09)	5.38 (±0.61)	5.35 (±0.40)	0.18 (±0.01)	0.21 (±0.01)	6.89 (±1.23)	17.85 (±2.74)
	Chest	3.23 (±0.42)	4.30 (±0.38)	1.00 (±0.08)	0.96 (±0.04)	5.45 (±0.40)	4.97 (±0.33)	0.16 (±0.01)	0.16 (±0.00)	7.39 (±1.96)	8.11 (±1.82)
	Pelvis	4.13 (±0.71)	3.73 (±0.62)	1.04 (±0.16)	0.93 (±0.10)	5.38 (±0.33)	4.82 (±0.22)	0.17 (±0.01)	0.16 (±0.01)	16.37 (±4.88)	16.62 (±3.29)
Air	Head	2.26 (±0.28)	6.50 (±2.22)	1.06 (±0.06)	1.11 (±0.10)	6.96 (±1.58)	5.63 (±0.54)	0.10 (±0.01)	0.09 (±0.01)	5.52 (±1.32)	12.54 (±1.55)
	Chest	3.40 (±0.49)	5.03 (±0.73)	1.00 (±0.07)	0.97 (±0.04)	5.65 (±0.56)	5.12 (±0.24)	0.08 (±0.01)	0.08 (±0.01)	5.82 (±1.84)	6.41 (±1.83)
	Pelvis	4.81 (±0.67)	4.80 (±0.92)	1.10 (±0.18)	0.97 (±0.10)	5.56 (±0.42)	5.01 (±0.18)	0.08 (±0.02)	0.09 (±0.01)	12.05 (±3.50)	13.88 (±3.74)
3D Vibration	Head	2.24 (±0.21)	5.82 (±0.91)	1.10 (±0.04)	1.10 (±0.06)	5.42 (±1.56)	5.24 (±0.22)	0.20 (±0.01)	0.28 (±0.02)	14.91 (±1.66)	47.22 (±6.52)
	Chest	3.04 (±0.36)	3.65 (±0.35)	0.93 (±0.07)	0.87 (±0.03)	5.03 (±0.30)	4.88 (±0.20)	0.16 (±0.01)	0.16 (±0.01)	15.09 (±5.22)	17.92 (±3.82)
	Pelvis	3.89 (±0.66)	3.48 (±0.57)	1.01 (±0.16)	0.89 (±0.10)	5.05 (±0.31)	4.63 (±0.14)	0.17 (±0.01)	0.17 (±0.01)	33.86 (±10.27)	36.83 (±8.64)

Table 6. Statistically Significant Difference between Weight Groups LW Category

		Low Weight									
Ride Profile	Segment	Z Transmissibility (Peak)		Area under Z Transmissibility Curve		Z Transmissibility Resonance Frequency (Hz)		RMS Z Acceleration (g)		RMS Gyroscope (deg/s)	
		SB	NB	SB	NB	SB	NB	SB	NB	SB	NB
All	Head	2.74 (±0.45)	5.49 (±1.06)	1.12 (±0.06)	1.19 (±0.08)	5.83 (±0.62)	6.39 (±0.41)	0.16 (±0.04)	0.20 (±0.08)	10.01 (±5.77)	25.91 (±15.61)
	Chest	3.56 (±0.55)	3.72 (±0.54)	1.04 (±0.09)	1.12 (±0.11)	5.73 (±0.50)	5.81 (±0.54)	0.14 (±0.05)	0.15 (±0.05)	9.10 (±5.06)	12.39 (±5.86)
	Pelvis	4.24 (±0.77)	3.72 (±0.71)	1.15 (±0.11)	1.02 (±0.09)	5.75 (±0.45)	5.22 (±0.45)	0.15 (±0.06)	0.14 (±0.05)	14.25 (±8.03)	17.76 (±9.78)
Ground	Head	2.80 (±0.44)	5.75 (±1.15)	1.17 (±0.05)	1.22 (±0.08)	5.88 (±0.40)	6.26 (±0.23)	0.18 (±0.01)	0.22 (±0.01)	7.32 (±1.61)	17.73 (±2.41)
	Chest	3.46 (±0.53)	3.75 (±0.38)	1.07 (±0.08)	1.14 (±0.08)	5.84 (±0.37)	5.82 (±0.48)	0.17 (±0.01)	0.17 (±0.01)	7.42 (±2.80)	10.17 (±2.41)
	Pelvis	3.95 (±0.68)	3.45 (±0.63)	1.13 (±0.11)	1.00 (±0.07)	5.82 (±0.37)	5.15 (±0.45)	0.18 (±0.01)	0.17 (±0.01)	11.84 (±4.16)	13.64 (±4.38)
Air	Head	2.82 (±0.51)	5.52 (±1.19)	1.08 (±0.06)	1.17 (±0.10)	6.30 (±0.68)	6.72 (±0.41)	0.11 (±0.01)	0.09 (±0.05)	5.39 (±1.87)	13.35 (±3.64)
	Chest	3.81 (±0.63)	4.05 (±0.61)	1.07 (±0.10)	1.17 (±0.12)	6.09 (±0.46)	6.06 (±0.65)	0.08 (±0.02)	0.09 (±0.02)	5.48 (±1.99)	8.15 (±2.46)
	Pelvis	4.73 (±0.89)	4.42 (±0.68)	1.20 (±0.12)	1.07 (±0.10)	6.09 (±0.34)	5.42 (±0.51)	0.07 (±0.01)	0.08 (±0.01)	7.33 (±2.29)	9.79 (±1.61)
3D Vibration	Head	2.60 (±0.41)	5.20 (±0.84)	1.11 (±0.04)	1.17 (±0.06)	5.30 (±0.26)	6.18 (±0.36)	0.20 (±0.01)	0.28 (±0.02)	17.41 (±2.97)	46.65 (±6.36)
	Chest	3.41 (±0.45)	3.35 (±0.37)	1.00 (±0.08)	1.05 (±0.09)	5.27 (±0.23)	5.54 (±0.36)	0.17 (±0.01)	0.18 (±0.01)	14.59 (±4.34)	18.85 (±5.17)
	Pelvis	4.03 (±0.49)	3.48 (±0.58)	1.11 (±0.10)	1.01 (±0.07)	5.35 (±0.28)	5.09 (±0.35)	0.20 (±0.02)	0.18 (±0.02)	23.59 (±5.36)	29.85 (±5.91)

Table 7. Statistically Significant Difference between Weight Groups HW Category

		High Weight									
Ride Profile	Segment	Z Transmissibility (Peak)		Area under Z Transmissibility Curve		Z Transmissibility Resonance Frequency (Hz)		RMS Z Acceleration (g)		RMS Gyroscope (deg/s)	
		SB	NB	SB	NB	SB	NB	SB	NB	SB	NB
All	Head	2.31 (±0.27)	6.25 (±1.60)	1.11 (±0.07)	1.13 (±0.09)	5.92 (±1.49)	5.41 (±0.43)	0.16 (±0.04)	0.19 (±0.08)	9.11 (±4.41)	25.87 (±15.98)
	Chest	3.22 (±0.44)	4.33 (±0.76)	0.98 (±0.06)	0.93 (±0.06)	5.38 (±0.50)	4.99 (±0.27)	0.13 (±0.04)	0.14 (±0.04)	9.71 (±5.57)	10.82 (±5.76)
	Pelvis	4.28 (±0.77)	4.00 (±0.92)	1.05 (±0.16)	0.96 (±0.10)	5.36 (±0.43)	4.82 (±0.24)	0.15 (±0.05)	0.14 (±0.04)	20.76 (±11.66)	22.45 (±11.79)
Ground	Head	2.42 (±0.29)	6.43 (±1.42)	1.17 (±0.04)	1.19 (±0.09)	5.38 (±0.61)	5.35 (±0.40)	0.18 (±0.01)	0.21 (±0.01)	6.89 (±1.23)	17.85 (±2.74)
	Chest	3.23 (±0.42)	4.30 (±0.38)	1.00 (±0.08)	0.96 (±0.04)	5.45 (±0.40)	4.97 (±0.33)	0.16 (±0.01)	0.16 (±0.00)	7.39 (±1.96)	8.11 (±1.82)
	Pelvis	4.13 (±0.71)	3.73 (±0.62)	1.04 (±0.16)	0.93 (±0.10)	5.38 (±0.33)	4.82 (±0.22)	0.17 (±0.01)	0.16 (±0.01)	16.37 (±4.88)	16.62 (±3.29)
Air	Head	2.26 (±0.28)	6.50 (±2.22)	1.06 (±0.06)	1.11 (±0.10)	6.96 (±1.58)	5.63 (±0.54)	0.10 (±0.01)	0.09 (±0.01)	5.52 (±1.32)	12.54 (±1.55)
	Chest	3.40 (±0.49)	5.03 (±0.73)	1.00 (±0.07)	0.97 (±0.04)	5.65 (±0.56)	5.12 (±0.24)	0.08 (±0.01)	0.08 (±0.01)	5.82 (±1.84)	6.41 (±1.83)
	Pelvis	4.81 (±0.67)	4.80 (±0.92)	1.10 (±0.18)	0.97 (±0.10)	5.56 (±0.42)	5.01 (±0.18)	0.08 (±0.02)	0.09 (±0.01)	12.05 (±3.50)	13.88 (±3.74)
3D Vibration	Head	2.24 (±0.21)	5.82 (±0.91)	1.10 (±0.04)	1.10 (±0.06)	5.42 (±1.56)	5.24 (±0.22)	0.20 (±0.01)	0.28 (±0.02)	14.91 (±1.66)	47.22 (±6.52)
	Chest	3.04 (±0.36)	3.65 (±0.35)	0.93 (±0.07)	0.87 (±0.03)	5.03 (±0.30)	4.88 (±0.20)	0.16 (±0.01)	0.16 (±0.01)	15.09 (±5.22)	17.92 (±3.82)
	Pelvis	3.89 (±0.66)	3.48 (±0.57)	1.01 (±0.16)	0.89 (±0.10)	5.05 (±0.31)	4.63 (±0.14)	0.17 (±0.01)	0.17 (±0.01)	33.86 (±10.27)	36.83 (±8.64)

From Tables 4 and 5, SB use had a significant impact on head motion (as compared to the NB condition) in the HW and LW conditions. This significance was present in all ride profiles. The impact was most readily seen as a large (often more than 50%) reduction in the peak *z*-axis transmissibility, though significant reduction in most of the other metrics was also apparent. This reduction with respect to the NB condition is logical given that in the SB condition the head was constrained to the board via a foam block that greatly restricted any motion of the head with respect to the board.

From Tables 6 and 7, the resonant frequency was significantly impacted by weight. Specifically, the resonant frequencies of the HW subjects were lower than the resonant frequencies of the LW subjects by a range of 0.5 to 1.5 Hz. This decrease was statistically significant in every NB condition and in most SB conditions. Given the direct relationship between mass and resonant frequency, this reduction in frequency for higher weight subjects was expected. Furthermore, though the magnitude of the reduction may seem small, the potential for vibration mitigation should not be underestimated. Offsetting a subject's resonant frequency from the vibration frequency of the transport vehicle or aircraft by even 0.5 Hz can reduce vibration magnitude compared to a scenario where the resonant frequency matches the ambient frequency of the transport platform.

Discussion

The data were analyzed by ABM and the following characterizations were noted:

1. The average RMS acceleration of the head was lower when immobilized by head blocks compared to NB.
2. When comparing the mean RMS acceleration between all SB versus NB subjects, the chest acceleration was unaffected by immobilization conditions.
3. Across all the ride profiles, subjects experienced 5% more RMS acceleration at the hips when immobilized.
4. HW subjects have lower vertical RMS acceleration across the whole body in comparison to the LW subjects.
5. The interquartile range was the range that the 25th to 75th percentile of subjects fell within. HW subjects have a smaller interquartile range for acceleration at the head and pelvis than LW subjects.
6. HW subjects have a larger interquartile range for acceleration at the chest than LW subjects.
7. Subjects' heads in both weight groups experienced less *z*-axis rotational velocity in the SB condition.
8. HW subjects' heads have lower resonant frequencies than LW subjects.
9. According to ANOVA analysis, the SB significantly reduced head motion.
10. According to ANOVA analysis, weight significantly impacted the subjects' resonant frequencies.

A previous USAARL study used motion capture to analyze the movement of subjects while testing eight different pieces of immobilization equipment on the MARS platform (Kinsler, Khouri, Squire, Conti, & Wurzbach, 2018). When comparing the ABM data to the previous study, both datasets revealed that a SB subject's head often experienced different movements than their chest and pelvis while immobilized (Attachment D, Figure 11). The mismatched movement of the head and chest could be detrimental to patients with neck injuries, as the relative motion between the head and torso could exacerbate their injuries. The same principle can be applied to movement differences between the chest and pelvis, which could exacerbate spinal injuries.

In Attachment D, Figures 7 through 9 show the SB:NB ratio of RMS acceleration in the LW and HW categories and Figures 10 through 12 show the SB:NB ratio of RMS rotation in LW and HW categories. The following observations are based on interquartile range values, and exclude other data:

- Attachment D, Figure 7: immobilization sometimes caused greater acceleration of the head in the *x*-, *y*-, and *z*-axes.
- Attachment D, Figure 8: immobilization sometimes caused greater acceleration of the chest in the *y*- and *z*-axes.
- Attachment D, Figure 9: immobilization sometimes caused greater acceleration of the pelvis in the *x*-, *y*-, and *z*-axes.
- Attachment D, Figure 10: immobilization always lowered the angular velocity of the head in the *x*-, *y*-, and *z*-axes.
- Attachment D, Figure 11: immobilization sometimes increased the angular velocity of the chest in the *x*-, *y*-, and *z*-axes.
- Attachment D, Figure 12: immobilization sometimes increased the angular velocity of the pelvis for *x*- and *y*-axes.

Conclusions

Because of the lower resonance frequencies of HW subjects when compared to LW subjects, it is necessary to consider both groups when developing mitigation technologies, as certain frequencies will potentially be more harmful to one group than to the other.

The bare litter is better at filtering out frequencies over 10 Hz than the litter used with an immobilization system. This may be of particular interest in air ambulances, since the predominant driving frequency in a UH-60 model is centered around 17.2 Hz (Department of Defense, 2008).

The SB configuration greatly reduced head motion, but caused it to move at different frequencies than the chest, and the chest often moved at different frequencies than the pelvis. Due to the disparity of motion between body segments, it is possible that a patient could suffer further injury when immobilized, depending on the nature of their injuries. Further investigation may be needed to determine if the head, chest, and pelvis moving at different frequencies has caused injury exacerbation in patients with spinal injuries.

The use of restraints on study subjects often caused the energy input from the litter to escape in areas of the body that were not restrained, which could cause further discomfort or exacerbation of limb injuries. These results may point toward the importance of vibration mitigation, instead of using only restraints to secure transport patients.

This page is intentionally left blank.

References

Ben-Galim P., Dreiangel N. Mattox K., Reitman C., Kalantar S., & Hipp J., (2010). Extrication collars can result in abnormal separation between vertebrae in the presence of a dissociative injury. *Journal of Trauma and Acute Injury Care*, 69(2), 447-450.

Department of Defense, *Environmental Engineering Considerations and Laboratory Tests.* Department of Defense MIL-STD-810G. Washington, DC: U.S. Department of Defense, October 31, 2008.

DeShaw, J., & Rahmatalla, S. (2012). Comprehensive Measurement in Whole-Body Vibration. *Journal of Low Frequency Noise, Vibration and Active Control*, 31(2), 63-74.

DeShaw, J., & Rahmatalla, S. (2014a). Predictive discomfort in single-and combined-axis whole-body vibration considering different seated postures. *Human Factors: The Journal of the Human Factors and Ergonomics Society*, 56(5), 850-863.

DeShaw, J., & Rahmatalla, S. (2014b). Effective seat-to-head transmissibility under combined-axis vibration and multiple postures. *International Journal of Vehicle Performance,* 1(3-4), 235-253.

DeShaw, J., Rahmatalla, S. (2016). Predictive discomfort of supine humans in whole-body vibration and shock environments. *Ergonomics*, 59(4), 568-581.

Hinz, B., Menzel, G., Bluthner, R., & Seidel, H. (2010). Seat-to-head transfer function of seated men--determination with single and three axis excitations at different magnitudes. Industrial Health. 48(5), 565-583.

Kinsler, R., Barazanji, K., Lee, J., Fulton, L., & Hatzfeld, J. (2015). *Analysis of Two Surveys Examining Enroute Care Technologies, Platforms, and Space Requirements.* Poster Presentation at Military Health System Research Symposium, August 2015.

Kinsler, R., Khouri, R., Squire, C., Conti, S., & Wurzbach, J. (2018). [Immobilization and Vibration Mitigation Systems: Test and Evaluation of Current and Developmental Products]. Unpublished report. Fort Rucker, AL: U.S. Army Aeromedical Research Laboratory.

Meusch, J. (2012). *Supine human response and vibration-suppression during whole-body vibration.* Master's Thesis, University of Iowa, Iowa City, IA.

Meusch, J., & Rahmatalla, S. (2014a). 3D Transmissibility and Relative Transmissibility of Immobilized Supine Humans during Transportation. *Journal of Low Frequency Noise, Vibration and Active Control*, 33(2), 125-138.

Meusch, J., & Rahmatalla, S. (2014b). Whole-body vibration transmissibility in supine humans: effects of board litter and neck collar. *Applied Ergonomics,* 45 (3), 677–685.

Paddan, G.S., &Griffin, M.J. (1998). A Review of the Transmission of Translational Seat Vibration to the Head. *Journal of Sound and Vibration*, 215, 863-882.

Rahmatalla, S., DeShaw, J., & Barazanji, K. (2017). Biodynamics of supine humans and interaction with transport systems during vibration and shocks. *Journal of Low Frequency Noise, Vibration and Active Control*, 38(2), 808-816.

Ratanalert, S., Phuenpathom, N., Saeheng, S., Oearsakul, T., Sripairojkul, B., & Hirunpat, S. (2004). ICP Threshold in CPP Management of Severe Head Injury Patients. *Surgical Neurology*, 61(5), 429-434.

Reno, J. (2010). Military aeromedical evacuation, with special emphasis on craniospinal trauma. *Neurosurgical Focus*, 28 (5), E12.

Wang Y., & Rahmatalla, S. (2013a). Three-dimensional modeling of supine human and transport system under whole-body vibration. *Journal of Biomechanical Engineering*, 135(6), 61010-61013.

Wang, Y., & Rahmatalla, S. (2013b). Human head-neck models in whole-body vibration: effect of posture. *Journal of Biomechanics*, 46(4), 702-710.

Wanner, I., Mayer, A., Kinsler, R., DeShaw, J., & Rahmatalla, S. (2016). *Improved Field Management and Safe Ground Transport of Patients with Head and Spine Injuries.* Fort Rucker, AL: U.S. Army Aeromedical Research Laboratory. Annual report, 29 Oct 2016.

Attachment A. Medical History Questionnaire

This page is intentionally blank.

Medical History Questionnaire

GENERAL HEALTH:

Date of last physical examination: ____

Date last consulted a doctor: ____

Nature of consult: ____
____
____

Are you in good health currently?	YES	NO - If no, why not? ____ ____ ____
Do you have any medical waivers (military only)?	N/A	NO YES – If yes, please describe ____ ____ ____
Do you have any profiles (military only)?	N/A	NO YES – If yes, please describe ____ ____ ____
Have you taken any medication within the past 7 days?	NO	YES - If yes, please describe ____ ____ ____
Have you ever had any neck pain or injuries? (whiplash, compression injuries, etc.)	NO	YES - If yes, please describe ____ ____ ____
Have you ever had any back pain or injuries?	NO	YES - If yes, please describe ____ ____ ____
Have you ever had any head injuries? (TBI, concussion, etc.)	NO	YES - If yes, please describe ____ ____ ____
Have you ever had unusual pain or injuries in your upper or lower limbs?	NO	YES - If yes, please describe ____ ____ ____
Have you ever had circulatory problems, including deep vein thrombosis?	NO	YES - If yes, please describe ____ ____ ____
Have you been diagnosed with diabetes?	NO	YES – If yes, please describe ____ ____ ____
Do you have any known severe skin sensitivities	NO	YES – If yes, please describe

or allergies to adhesives? (glues, surgical tape, etc.) ____________________

Are you prone to motion sickness? NO YES – If yes, please describe ____________________

Are you prone to claustrophobia? NO YES – If yes, please describe ____________________

Are you currently pregnant or trying to get pregnant? N/A NO YES

Have you had unprotected intercourse within the last 3 weeks? N/A NO YES

Pregnancy Test Result: Negative Positive

Date of Test ____________________

Signature of Verifying Physician ____________________

Qualified for study? **NO** **YES** Reason for disqualification: ____________________

____
Principal Investigator's Signature & Date

____
Study Physician’s Signature & Date

____
Volunteer’s Signature & Date

STUDY PHYSICIAN POST-TEST ASSESSMENT

Is the subject suffering any ill effects from participation in the study? NO YES – If yes, please describe

____
____
____

If answer to first question is YES, is medical intervention recommended? N/A NO YES – If yes, please describe

____
____
____

____
Study Physician's Signature & Date

This page is intentionally blank.

Attachment B. Ride Comfort Survey

This page is intentionally blank.

Ride Comfort Survey

Subject code: ________________

Profile: ______________________

Configuration: ________________

For this testing configuration and profile, how would you rate the comfort of the system on a scale of 1 to 10, with 1 being very comfortable and 10 being extremely uncomfortable?
(Note: call study physician if rated 7 or higher)

1 2 3 4 5 6 7 8 9 10

Are there any places in the system that feel uncomfortable to you? Yes No

If yes, please describe where and the sensation you feel (such as discomfort, pressure, pain, numbness, pins and needles, etc)

____
____
____
____

If you are having pain, how would you rate the severity of the pain on a scale of 1 to 10, with 0 being no pain, 1 being very minor pain and 10 being the worst pain you have ever experienced?
(Note: call study physician if rated 3 or higher)

0 1 2 3 4 5 6 7 8 9 10

If you are having pain, where is the pain located (head, neck, back, shoulders, torso, arms, legs, other)?

____
____
____
____

This page is intentionally blank.

Attachment C. Sensor Placement

This page is intentionally blank.

Table C1. Sensor Placement Chart for Subjects 1 and 2 with No Board

Data Acquisition System	Channel	Axis	Sensor Type	Sensitivity	Range	Sensor Location
COCO-90 #1 SN#53542	1	AX	6 DOF (combined accelerometer and gyroscope)	209.390 mV/g	±6 unit of gravity (g)	Subject's head SN:163
	2	AY		207.723 mV/g	±6 g	
	3	AZ		208.539 mV/g	±6 g	
	4	GX		0.9863 mV/°/s	±1000 degree per second (deg/s)	
	5	GY		1.0225 mV/°/s	±1000 deg/s	
	6	GZ		1.0513 mV/°/s	±1000 deg/s	
	7	AX	6 DOF (combined accelerometer and gyroscope)	211.755 mV/g	±6 g	Subject's sternum SN:164
	8	AY		198.013 mV/g	±6 g	
	9	AZ		205.533 mV/g	±6 g	
	10	GX		0.9415 mV/°/s	±1000 deg/s	
	11	GY		1.0125 mV/°/s	±1000 deg/s	
	12	GZ		1.0753 mV/°/s	±1000 deg/s	
	13	X	Triaxial accelerometer	187.1 mV/g	±5 g	Subject's leg SN:159
	14	Y		187.0 mV/g	±5 g	
	15	Z		188.1 mV/g	±5 g	
	16	n/a	n/a	1000 mV/V	±5 volt (V)	Synchronization pulse (square wave CoCo-90 output)
COCO-90 #2 SN#58967	1	AX	6 DOF (combined accelerometer and gyroscope)	210.130	±6 g	Litter Surface SN: 167
	2	AY		215.170	±6 g	
	3	AZ		208.230	±6 g	
	4	GX		1.0257	±1000 deg/s	
	5	GY		0.9955	±1000 deg/s	
	6	GZ		0.9919	±1000 deg/s	
	7	X	Triaxial accelerometer	185.4 mV/g	±5 g	MARS platform surface SN:157
	8	Y		186.2 mV/g	±5 g	
	9	Z		186.6 mV/g	±5 g	
	10	AX	6 DOF (combined accelerometer and gyroscope)	212.146 mV/g	±6 g	Subject's pelvis SN:166
	11	AY		211.186 mV/g	±6 g	
	12	AZ		208.596 mV/g	±6 g	
	13	GX		1.0225 mV/°/s	±1000 deg/s	
	14	GY		1.0381 mV/°/s	±1000 deg/s	
	15	GZ		0.9918 mV/°/s	±1000 deg/s	
	16	n/a	n/a	1000 mV/V	±5 V	Synchronization pulse (square wave CoCo-90 output)

Table C2. Sensor Placement Chart for Subjects 1 and 2 with Spine Board

Data Acquisition System	Channel	Axis	Sensor Type	Sensitivity	Range	Sensor Location
COCO-90 #1 SN#53542	1	AX	6 DOF (combined accelerometer and gyroscope)	209.390 mV/g	±6 unit of gravity (g)	Subject’s head SN:163
	2	AY		207.723 mV/g	±6 g	
	3	AZ		208.539 mV/g	±6 g	
	4	GX		0.9863 mV/°/s	±1000 degree per second (deg/s)	
	5	GY		1.0225 mV/°/s	±1000 deg/s	
	6	GZ		1.0513 mV/°/s	±1000 deg/s	
	7	AX	6 DOF (combined accelerometer and gyroscope)	211.755 mV/g	±6 g	Subject’s sternum SN:164
	8	AY		198.013 mV/g	±6 g	
	9	AZ		205.533 mV/g	±6 g	
	10	GX		0.9415 mV/°/s	±1000 deg/s	
	11	GY		1.0125 mV/°/s	±1000 deg/s	
	12	GZ		1.0753 mV/°/s	±1000 deg/s	
	13	X	Triaxial accelerometer	187.1 mV/g	±5 g	Subject’s leg SN:159
	14	Y		187.0 mV/g	±5 g	
	15	Z		188.1 mV/g	±5 g	
	16	n/a	n/a	1000 mV/V	±5 volt (V)	Synchronization pulse (square wave CoCo-90 output)
COCO-90 #2 SN#58967	1	AX	6 DOF (combined accelerometer and gyroscope)	214.97	±6 g	Spine Board SN: 315
	2	AY		204.09	±6 g	
	3	AZ		199.77	±6 g	
	4	GX		1.033	±1000 deg/s	
	5	GY		1.082	±1000 deg/s	
	6	GZ		1.072	±1000 deg/s	
	7	X	Triaxial accelerometer	185.4 mV/g	±5 g	MARS platform surface SN:157
	8	Y		186.2 mV/g	±5 g	
	9	Z		186.6 mV/g	±5 g	
	10	AX	6 DOF (combined accelerometer and gyroscope)	212.146 mV/g	±6 g	Subject’s pelvis SN:166
	11	AY		211.186 mV/g	±6 g	
	12	AZ		208.596 mV/g	±6 g	
	13	GX		1.0225 mV/°/s	±1000 deg/s	
	14	GY		1.0381 mV/°/s	±1000 deg/s	
	15	GZ		0.9918 mV/°/s	±1000 deg/s	
	16	n/a	n/a	1000 mV/V	±5 V	Synchronization pulse (square wave CoCo-90 output)

Table C3. Sensor Placement Chart for Subjects 3-6 with No Board

Data Acquisition System	**Channel**	**Axis**	**Sensor Type**	**Sensitivity**	**Range**	**Sensor Location**
COCO-90 #1 SN#53542	1	AX	6 DOF (combined accelerometer and gyroscope)	1000 mV/V	±6 unit of gravity (g)	Subject's head SN:163
	2	AY		1000 mV/V	±6 g	
	3	AZ		1000 mV/V	±6 g	
	4	GX		1000 mV/V	±1000 degree per second (deg/s)	
	5	GY		1000 mV/V	±1000 deg/s	
	6	GZ		1000 mV/V	±1000 deg/s	
	7	AX	6 DOF (combined accelerometer and gyroscope)	1000 mV/V	±6 g	Subject's sternum SN:164
	8	AY		1000 mV/V	±6 g	
	9	AZ		1000 mV/V	±6 g	
	10	GX		1000 mV/V	±1000 deg/s	
	11	GY		1000 mV/V	±1000 deg/s	
	12	GZ		1000 mV/V	±1000 deg/s	
	13	X	Triaxial accelerometer	1000 mV/V	±5 g	Subject's leg SN:159
	14	Y		1000 mV/V	±5 g	
	15	Z		1000 mV/V	±5 g	
	16	n/a	n/a	1000 mV/V	±5 volt (V)	Synchronization pulse (square wave CoCo-90 output)
COCO-90 #2 SN#58967	1	AX	6 DOF (combined accelerometer and gyroscope)	1000 mV/V	±6 g	Litter Surface SN: 167
	2	AY		1000 mV/V	±6 g	
	3	AZ		1000 mV/V	±6 g	
	4	GX		1000 mV/V	±1000 deg/s	
	5	GY		1000 mV/V	±1000 deg/s	
	6	GZ		1000 mV/V	±1000 deg/s	
	7	X	Triaxial accelerometer	1000 mV/V	±5 g	MARS platform surface SN:157
	8	Y		1000 mV/V	±5 g	
	9	Z		1000 mV/V	±5 g	
	10	AX	6 DOF (combined accelerometer and gyroscope)	1000 mV/V	±6 g	Subject's pelvis SN:166
	11	AY		1000 mV/V	±6 g	
	12	AZ		1000 mV/V	±6 g	
	13	GX		1000 mV/V	±1000 deg/s	
	14	GY		1000 mV/V	±1000 deg/s	
	15	GZ		1000 mV/V	±1000 deg/s	
	16	n/a	n/a	1000 mV/V	±5 V	Synchronization pulse (square wave CoCo-90 output)

Table C4. Sensor Placement Chart for Subjects 3-6 with Spine Board

Data Acquisition System	Channel	Axis	Sensor Type	Sensitivity	Range	Sensor Location
COCO-90 #1 SN#53542	1	AX	6 DOF (combined accelerometer and gyroscope)	1000 mV/V	±6 unit of gravity (g)	Subject's head SN:163
	2	AY		1000 mV/V	±6 g	
	3	AZ		1000 mV/V	±6 g	
	4	GX		1000 mV/V	±1000 degree per second (deg/s)	
	5	GY		1000 mV/V	±1000 deg/s	
	6	GZ		1000 mV/V	±1000 deg/s	
	7	AX	6 DOF (combined accelerometer and gyroscope)	1000 mV/V	±6 g	Subject's sternum SN:164
	8	AY		1000 mV/V	±6 g	
	9	AZ		1000 mV/V	±6 g	
	10	GX		1000 mV/V	±1000 deg/s	
	11	GY		1000 mV/V	±1000 deg/s	
	12	GZ		1000 mV/V	±1000 deg/s	
	13	X	Triaxial accelerometer	1000 mV/V	±5 g	Subject's leg SN:159
	14	Y		1000 mV/V	±5 g	
	15	Z		1000 mV/V	±5 g	
	16	n/a	n/a	1000 mV/V	±5 volt (V)	Synchronization pulse (square wave CoCo-90 output)
COCO-90 #2 SN#58967	1	AX	6 DOF (combined accelerometer and gyroscope)	1000 mV/V	±6 g	Spine Board SN: 315
	2	AY		1000 mV/V	±6 g	
	3	AZ		1000 mV/V	±6 g	
	4	GX		1000 mV/V	±1000 deg/s	
	5	GY		1000 mV/V	±1000 deg/s	
	6	GZ		1000 mV/V	±1000 deg/s	
	7	X	Triaxial accelerometer	1000 mV/V	±5 g	MARS platform surface SN:157
	8	Y		1000 mV/V	±5 g	
	9	Z		1000 mV/V	±5 g	
	10	AX	6 DOF (combined accelerometer and gyroscope)	1000 mV/V	±6 g	Subject's pelvis SN:166
	11	AY		1000 mV/V	±6 g	
	12	AZ		1000 mV/V	±6 g	
	13	GX		1000 mV/V	±1000 deg/s	
	14	GY		1000 mV/V	±1000 deg/s	
	15	GZ		1000 mV/V	±1000 deg/s	
	16	n/a	n/a	1000 mV/V	±5 V	Synchronization pulse (square wave CoCo-90 output)

Table C5. Sensor Placement Chart for Subjects 7-26 with No Board

Data Acquisition System	**Channel**	**Axis**	**Sensor Type**	**Sensitivity**	**Range**	**Sensor Location**
COCO-90 #3 SN#35066	1	AX	6 DOF (combined accelerometer and gyroscope)	1000 mV/V	±6 unit of gravity (g)	Subject's head SN:163
	2	AY		1000 mV/V	±6 g	
	3	AZ		1000 mV/V	±6 g	
	4	GX		1000 mV/V	±1000 degree per second (deg/s)	
	5	GY		1000 mV/V	±1000 deg/s	
	6	GZ		1000 mV/V	±1000 deg/s	
	7	AX	6 DOF (combined accelerometer and gyroscope)	1000 mV/V	±6 g	Subject's sternum SN:164
	8	AY		1000 mV/V	±6 g	
	9	AZ		1000 mV/V	±6 g	
	10	GX		1000 mV/V	±1000 deg/s	
	11	GY		1000 mV/V	±1000 deg/s	
	12	GZ		1000 mV/V	±1000 deg/s	
	13	X	Triaxial accelerometer	1000 mV/V	±5 g	Subject's leg SN:159
	14	Y		1000 mV/V	±5 g	
	15	Z		1000 mV/V	±5 g	
	16	n/a	n/a	1000 mV/V	±5 volt (V)	Synchronization pulse (square wave CoCo-90 output)
COCO-90 #2 SN#58967	1	AX	6 DOF (combined accelerometer and gyroscope)	1000 mV/V	±6 g	Litter Surface SN: 167
	2	AY		1000 mV/V	±6 g	
	3	AZ		1000 mV/V	±6 g	
	4	GX		1000 mV/V	±1000 deg/s	
	5	GY		1000 mV/V	±1000 deg/s	
	6	GZ		1000 mV/V	±1000 deg/s	
	7	X	Triaxial accelerometer	1000 mV/V	±5 g	MARS platform surface SN:157
	8	Y		1000 mV/V	±5 g	
	9	Z		1000 mV/V	±5 g	
	10	AX	6 DOF (combined accelerometer and gyroscope)	1000 mV/V	±6 g	Subject's pelvis SN:166
	11	AY		1000 mV/V	±6 g	
	12	AZ		1000 mV/V	±6 g	
	13	GX		1000 mV/V	±1000 deg/s	
	14	GY		1000 mV/V	±1000 deg/s	
	15	GZ		1000 mV/V	±1000 deg/s	
	16	n/a	n/a	1000 mV/V	±5 V	Synchronization pulse (square wave CoCo-90 output)

Table C6. Sensor Placement Chart for Subjects 7-26 with Spine Board

Data Acquisition System	**Channel**	**Axis**	**Sensor Type**	**Sensitivity**	**Range**	**Sensor Location**
COCO-90 #3 SN#35066	1	AX	6 DOF (combined accelerometer and gyroscope)	1000 mV/V	±6 unit of gravity (g)	Subject's head SN:163
	2	AY		1000 mV/V	±6 g	
	3	AZ		1000 mV/V	±6 g	
	4	GX		1000 mV/V	±1000 degree per second (deg/s)	
	5	GY		1000 mV/V	±1000 deg/s	
	6	GZ		1000 mV/V	±1000 deg/s	
	7	AX	6 DOF (combined accelerometer and gyroscope)	1000 mV/V	±6 g	Subject's sternum SN:164
	8	AY		1000 mV/V	±6 g	
	9	AZ		1000 mV/V	±6 g	
	10	GX		1000 mV/V	±1000 deg/s	
	11	GY		1000 mV/V	±1000 deg/s	
	12	GZ		1000 mV/V	±1000 deg/s	
	13	X	Triaxial accelerometer	1000 mV/V	±5 g	Subject's leg SN:159
	14	Y		1000 mV/V	±5 g	
	15	Z		1000 mV/V	±5 g	
	16	n/a	n/a	1000 mV/V	±5 volt (V)	Synchronization pulse (square wave CoCo-90 output)
COCO-90 #2 SN#58967	1	AX	6 DOF (combined accelerometer and gyroscope)	1000 mV/V	±6 g	Spine Board SN: 315
	2	AY		1000 mV/V	±6 g	
	3	AZ		1000 mV/V	±6 g	
	4	GX		1000 mV/V	±1000 deg/s	
	5	GY		1000 mV/V	±1000 deg/s	
	6	GZ		1000 mV/V	±1000 deg/s	
	7	X	Triaxial accelerometer	1000 mV/V	±5 g	MARS platform surface SN:157
	8	Y		1000 mV/V	±5 g	
	9	Z		1000 mV/V	±5 g	
	10	AX	6 DOF (combined accelerometer and gyroscope)	1000 mV/V	±6 g	Subject's pelvis SN:166
	11	AY		1000 mV/V	±6 g	
	12	AZ		1000 mV/V	±6 g	
	13	GX		1000 mV/V	±1000 deg/s	
	14	GY		1000 mV/V	±1000 deg/s	
	15	GZ		1000 mV/V	±1000 deg/s	
	16	n/a	n/a	1000 mV/V	±5 V	Synchronization pulse (square wave CoCo-90 output)

Attachment D. ActiBioMotion Data Analysis Report

This page is intentionally blank.

This work was performed under Contract No. W81XWH-17-P-0315.

Data Analysis for:

Effect of Patient Weight as a Factor During Use of an Immobilization System Versus No Immobilization System

By

Chuck Harris, B.S. and Eric Frick, Ph.D.

ActiBioMotion, LLC

2500 Crosspark Rd, Suite W150A

Coralville, IA 52241

214-287-0157; eric@actibiomotion.com

for

U.S. Army Aeromedical Research Laboratory

6901 Farrel Road

Fort Rucker, AL 36362-0577

Rachel Kinsler, M.S.

334-255-6982, rachel.e.kinsler.civ@mail.mil

25 September 2019

Contents

INTRODUCTION

Recent surveys on health care providers in the field have reported severe discomfort and pain experienced by casualties during military ground and air transport and attributed the pain to vibration and repeated shock associated with the transport (Kinsler, Barazanji, Lee, Fulton, and Hatzfeld, 2015). The transmitted forces and vibrations to the patient's body through the transport system can have severe consequences, especially for those neurotrauma patients sensitive to increased intracranial pressure (ICP) (Ratanalert, 2004; Reno, 2010). Litters and immobilization systems can also cause exacerbation of vibration stresses (Kinsler et al, 2018). Prior to transport, casualties with serious injuries such as head and back injuries are required to be immobilized to prevent movement that may lead to further complications. In other circumstances, patients may get transported using only litters with no backboard.

Besides the transmitted forces to the human body, patients may also suffer from discomfort/pain resulting from the formation of pressure sores at the contact points between the patient's body and the transport system. Previous studies have indicated association between the formation of the pressure sores and immobilization during transport (Linares et al, 1987). Strapping the patient and the degree of strapping tension varies dependent on patient condition and injuries, and that may play an effective role in the formation of pressure sores. It may also affect the severity of the motion transmitted to the patient's neck and lower back areas. Due to the inertial effect, it is expected that the severity of the resulting motion will be proportional to the patient's body mass.

The objective of this work was to investigate the effect of immobilization systems and body weight on the biodynamics response of supine humans during medical transport.

METHODS

This study was performed to investigate the interaction of patient weight with immobilization condition on relative body segment motion and magnitude of transmitted motion of supine humans. The hypothesis that the human weight has significant effect on the characteristics of the transfer functions was tested using 26 human subjects with different body weights. Two groups were selected based on weight: (1) 13 subjects with low weight (110 to 150 lbs.) (LW group), and (2) 13 subjects with high weight (185 to 245 lbs.) (HW group), were tested under the two different support conditions. Due to data corruption, however, data from two LW subjects could not be used in the analysis. As a result, only 24 subjects were tested, with 11 subjects in the LW group and 13 subjects in the HW group. This group selection allowed comparison of vibration transmissibility due to weight. The goal of the study is to determine whether different body weights produce different biodynamical responses with and without the immobilization system. The transmitted vibration of LW and HW human subject groups under the conditions of board verses no-board was measured using a man-rated shaking table. The subjects were secured to the litter and/or immobilization system on the Multi-axis Ride Simulator (MARS) at the U.S. Army Aeromedical Research Laboratory (USAARL) and subjected to different vibration profiles that included vibration of different magnitudes and directions as well as repeated shocks. The effect of the interactions between the body's weight and two immobilization conditions on the magnitude of the transmitted motion to the different body segments were evaluated. Appropriate transfer functions were calculated between the input/output motions to identify the critical frequencies where the transfer functions have large magnitudes, i.e., where the input motion is magnified as it reaches the human body.

For the litter with no immobilization board (NB), the subjects were restrained on the litter using two straps across the body as shown in Figure 1. For the litter with full immobilization set-up, where the spinal-board is used (SB) a full immobilization system complete with a head brace, spine board, and spider straps is shown in Figure 2. The coordinate system showing the direction of the translational and rotational accelerations is illustrated in Figures 1 and 2.

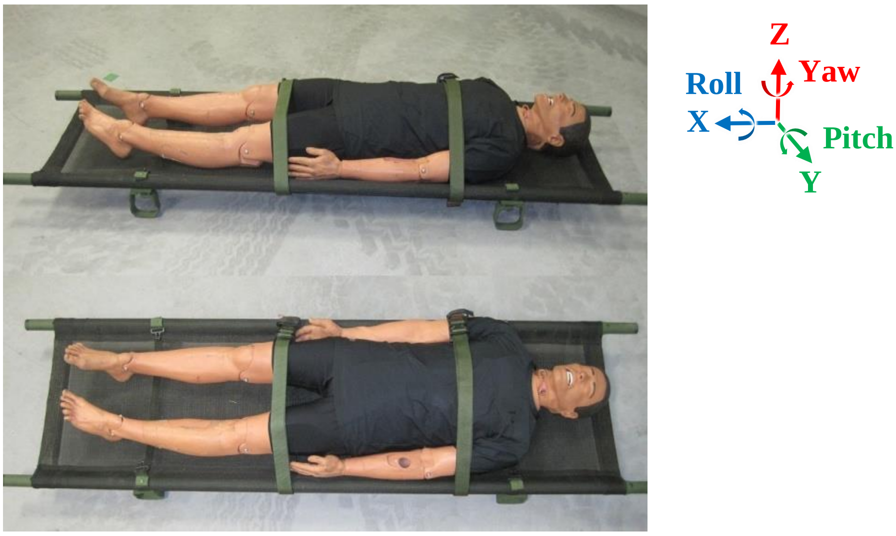

Figure 1: Litter with no immobilization system.

Figure 2: Litter with full immobilization set up.

While secured in the testing configuration, each subject was exposed to three ride profiles: (1) ground vehicle (~60 seconds), (2) air vehicle (~60 seconds), and (3) white noise shocks/vibration random vibration (~60 seconds). The ground vehicle profile is a recorded ride signature from a ground ambulance that was driven over a rough road with bumps. This profile contains a predominant low frequency vibration of 2 Hz associated with the vehicle suspension and some higher frequencies elements associated with the engine operation, along with some jolts from the bumps in the road. The air vehicle profile is a compilation of recorded signatures from an H-60 series MEDEVAC helicopter that was performing standard flight maneuvers. This profile contains energy associated with a predominant frequency of approximately 17 Hz that is associated with the operation of the main rotor. There are also some minor jolts in the profile from landing maneuvers. The shocks/random vibration profile is a Gaussian white noise signal with mixed frequencies at multiple amplitudes. The maximum amplitudes in each ride profile fall within the safety standards described in the ISO 2631 series (USAARL, 2019).

Motion sensors were placed on the head, chest, pelvis, and leg to gather data at each major body segment. The motion sensors used, except for the leg, were 6DOF to allow for the recording of both acceleration and rotational data. Another 6DOF sensor was mounted to the litter and was moved onto the spine board when the subject was immobilized. A 3DOF sensor was placed on the MARS platform. By placing sensors on both the litter and the MARS platform (both considered as input vibration), the biodynamic response of each subject could be measured relative to either input.

Before testing, each subject had their anthropometric data collected. Properties such as weight, height, and certain anthropometric measurements were measured. The subjects rated the comfort/discomfort of the system on a scale of 1 to 10 on the Borg CR-10 scale with higher numbers representing more discomfort, after each ride profile (Borg, 1982). They were also asked to report any pain being experienced. No subject reported a discomfort level of 7 or higher, or a pain level of 3 or higher. Those levels were the maximum allowed before the experiment was discontinued until the study physician examined the subject.

Transmissibility represents the ratio of output motion to input motion. When the transmissibility is above unity, the output is moving more than the input, and amplification occurs. When the driving frequency matches the natural frequency of the system, the output amplification is maximized. Likewise, when the transmissibility is below unity, the output is moving less than the input, and attenuation occurs. A more thorough way to calculate transmissibility is to use the *spa* function in MATLAB, which estimates frequency response using the Blackman-Tukey spectral analysis method. This method computes the covariances and cross-covariance from the input and output signals and computes the Fourier transforms of these values. The frequency-response function is calculated next by taking the ratio of the transformed cross-covariance to the transformed input covariance. In this study, transmissibility was calculated in 3D space (3 input/ 3 output).

The root mean square acceleration (RMS) was used in this analysis to quantify how much acceleration and rotation each subject received, on average, over the course of the entire ride profile. The acceleration and rotation that each subject received, in each direction over the course of the entire ride was converted to one RMS value per degree of freedom using Equation 1. All subjects' RMS values were averaged per each degree of freedom.

$$\textbf{Equation 1: } X_{RMS} = \sqrt{\frac{(x_1^2+x_2^2+x_3^2+\cdots+x_n^2)}{n}}$$

The concept of resonance was referenced and mentioned often when analyzing data in this investigation. An object will resonate, or store energy and increase the amplitude of its motion, when the driving frequency matches the natural frequency of the object. When referenced in simple harmonic motion, resonant frequency is determined by only two parameters. These parameters are the stiffness of the system k, and the mass of the system m. Equation 2 was used frequently when identifying key differences between the LW and HW groups.

$$\textbf{Equation 2: } \boldsymbol{\omega_n = \sqrt{\frac{k}{m}}}$$

Many of the data collected between testing conditions were converted to ratios comparing the differences between each testing condition. When considering the effect of immobilization condition, the output at the spine board (SB) test was divided by the output at the litter only (NB) test for each subject, then averaged among the LW and HW groups (i.e., SB/NB). When analyzing the effect of subject weight, the output metric of the LW subject was divided by the output metric of the HW subject. Ratios allow intra-subject comparison and a comparison between testing conditions that is easily visualized.

The two conditions being tested, immobilization and weight, are different in nature. For the immobilization factor, there is data on every subject from both conditions (spine board and no board). This allows for an intra-subject comparison to be applied to all subjects. Specifically, spine board metrics could be normalized against the no board metrics (through division), yielding a normalized ratio that could be fairly compared between subjects. For the weight factor, however, no subject could be both high and low weight. Therefore, no intra-subject comparison can be done; it must be inter-subject. Therefore, the output metrics for the high and low weight subjects were compared directly, without any normalization.

To reduce unwanted noise within each subject's data, a bidirectional, 4^{th} order lowpass Butterworth filter was utilized to cut off unwanted data above 30Hz.

The power spectral density was also analyzed for each body segment, immobilization condition, and ride profile. A power spectral density, or PSD, describes the distribution of power inside a signal by decomposing the signal into discrete frequencies over a continuous range (Stoica & Moses, 2004). The mean of all subjects' PSDs was used to identify where the most power was being transmitted to the subject. In addition, the PSD was generated at the MARS platform and at the litter in order to analyze the frequency content of each ride profile.

The coherence of each subject was used to determine the degree of causality between the input vibration and the subject. A higher coherence implies direct causality between the input vibration and the output.

Boxplots were used to further investigate the distribution of data for each testing condition, since the data followed a non-gaussian distribution. The boxed region represents data points contained inside 25 to 75 percent of the data range, and the plot whiskers expand out to include data points within 5 to 95 percent of the data range. The median and mean of the data is also provided. In some cases, outliers are also represented on the plot as circular regions outside of the 5th to 95th percentile. A sample plot can be found in Figure 3.

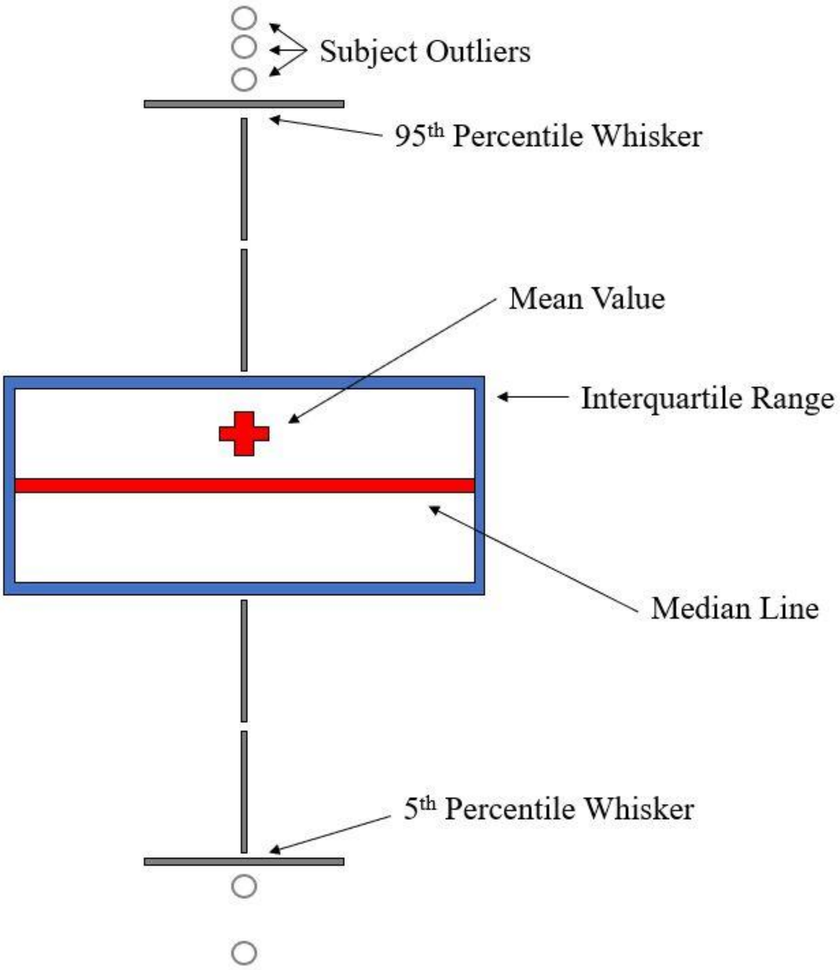

Figure 3: A sample box plot. The interquartile range is represented by the blue box, while the whiskers represent all data points within 5 to 95 percent of the data range. The red line represents the median of the data, while the red plus represents the mean. Outliers are located outside of the 5th to 95th percentile range and are indicated by hollow circles. Each circle represents one outlier.

The input power to the system was analyzed for all three axes. Data was broken out into each axis of motion, which can be found in Figure 4-Figure 6.

Figure 4 describes the input power for all ride profiles, analyzed at the X axis. Profile 1 shows a steady increase in power as frequency increases. Profile 2 features a smaller peak centered around 5 Hz, with lower power until 15 Hz. After this, power rises quickly to a large peak at 17 Hz. Power is centered around 12 Hz in Profile 3 but decreases more slowly after the resonance.

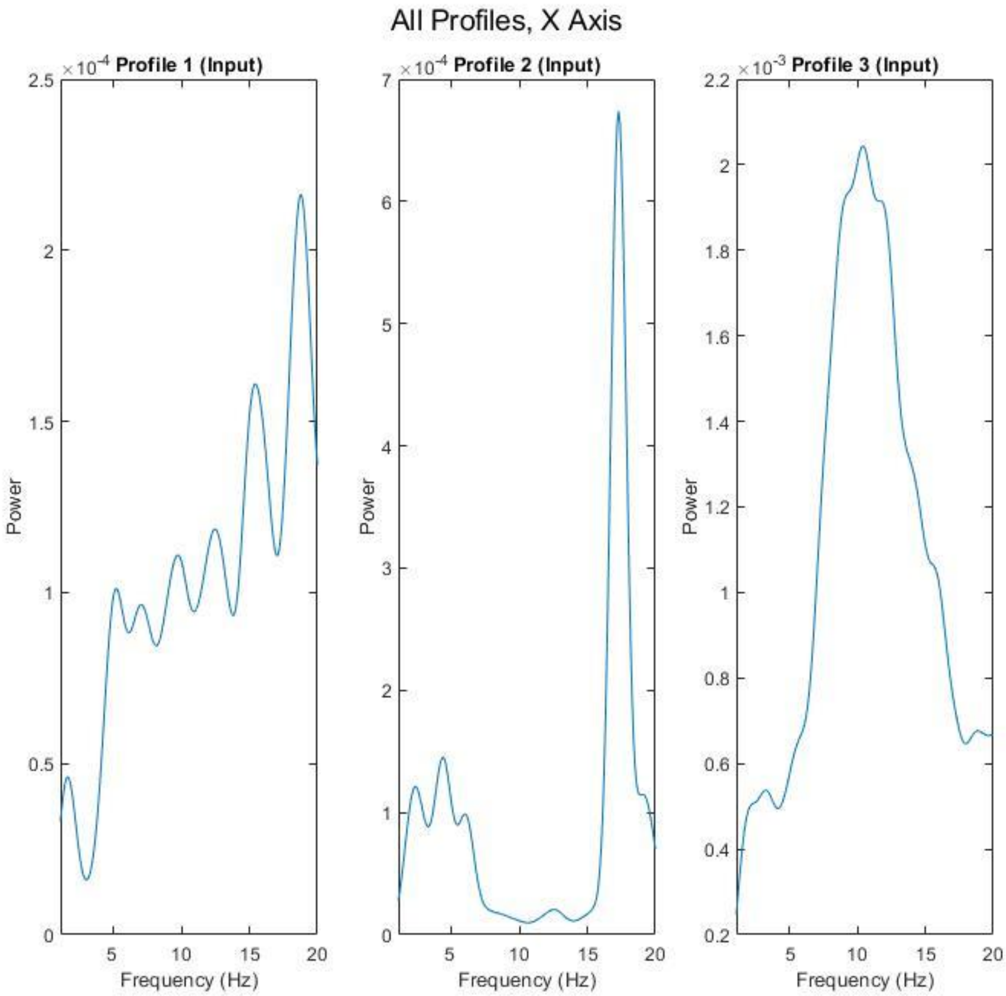

Figure 4: The input PSD power from the ground vehicle (Profile 1), helicopter ride (Profile 2) and the random 3D motion (Profile 3). Each PSD contains data from the X axis.

The input power analyzed at the Y axis can be described in Figure 5. All ride profiles exhibit one large peak. Profile 1 shows a large peak at 8 Hz, while Profile 2 features a large peak near 17 Hz. Profile 1 contains some power after its resonance, but at only 35% of the peak value. Profile 2 contains power almost exclusively at its resonance. 3 contains most of its power around 9 Hz, but still has power roughly 40% that of the peak across all frequencies.

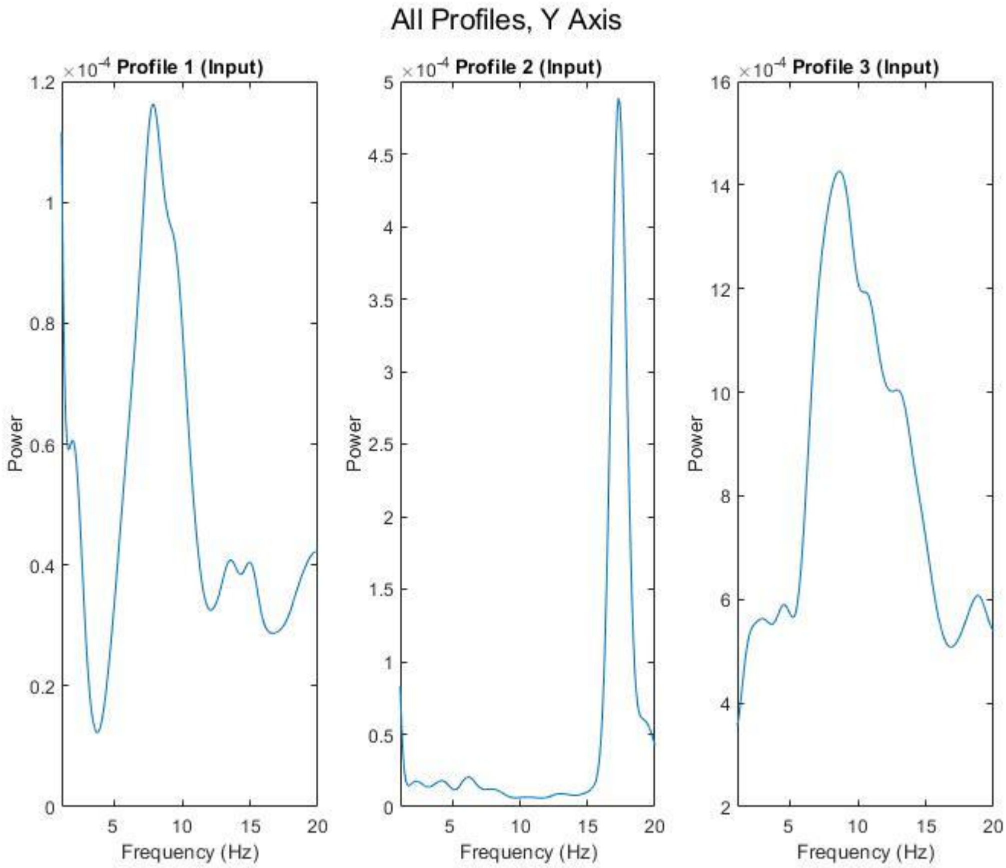

Figure 5: The input PSD power from the ground vehicle (Profile 1), helicopter ride (Profile 2), and the random 3D motion (Profile 3). Data pertains to the Y axis.

The input power analyzed at the Z axis can be described in Figure 6. Both Profiles 1 and 2 contain nearly all their power at their peaks. Profile 1 exhibits maximum power near 2 Hz, and Profile 2 reaches full power at 17 Hz. Profile 3 contains power throughout all frequencies but exhibits its maximum power near 2 Hz. A second, smaller peak is present near 16 Hz, at approximately 80% the power of the larger peak.

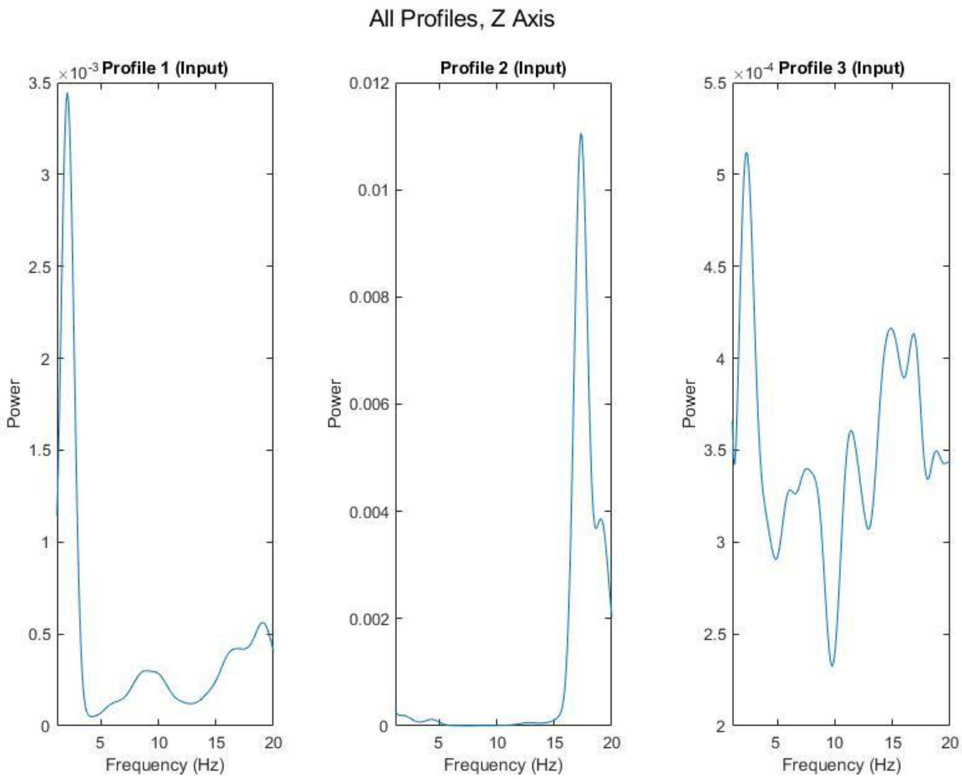

Figure 6: The input PSD power from the ground vehicle (Profile 1), helicopter ride (Profile 2), and the random 3D motion (Profile 3). Data pertains to the Z axis.

RESULTS

RMS Acceleration Ratio

The ratio of the RMS acceleration at the head when immobilized to when not immobilized (SB/NB) can be found in Figure 7. Along the Z axis, median acceleration was reduced by nearly 20 percent for both LW and HW subjects. The mean RMS acceleration for the LW group is slightly higher than that for the HW group. The interquartile range for the LW group was larger than that for the HW group. The 5th percentile was nearly the same for both groups, but the 95th percentile was larger for LW group.

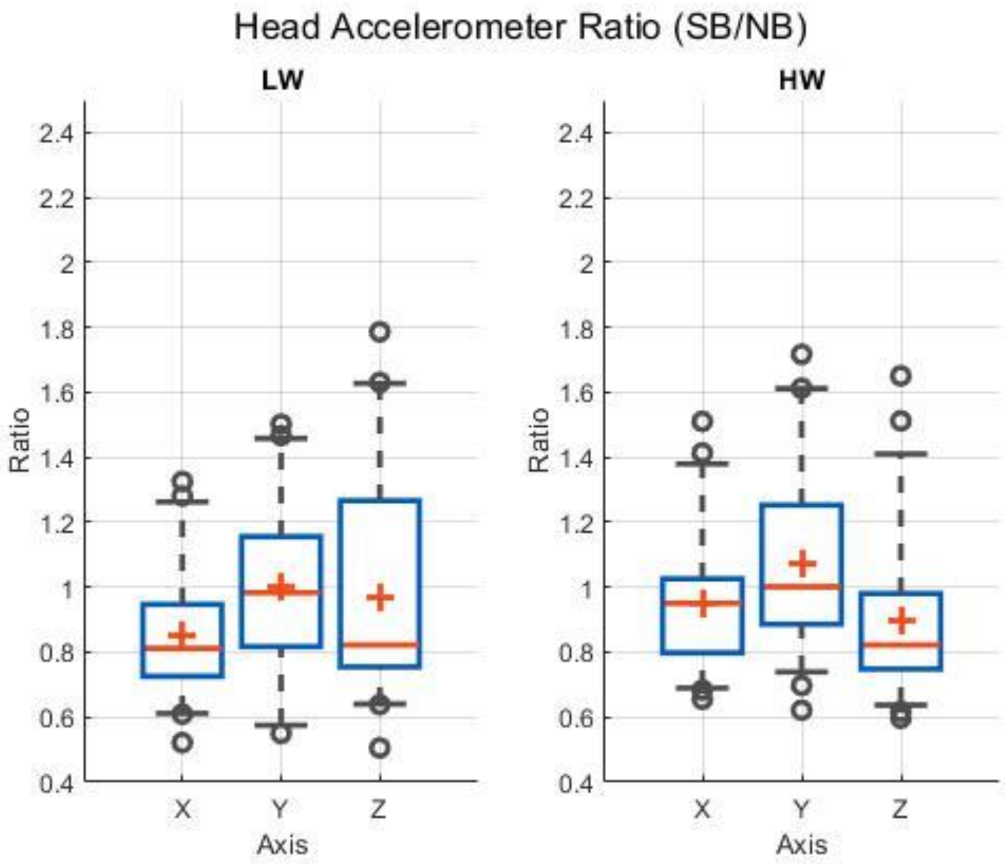

Figure 7: The ratio of the RMS acceleration experienced while immobilized to when not immobilized, measured at the head.

The ratio of the RMS acceleration at the chest when immobilized to when not immobilized (SB/NB) can be found in Figure 8. When looking to the Z axis, the median acceleration was largely unchanged when implementing a spine board versus when no spine board was used. The interquartile for the LW group, and both the interquartile range and the 5th to 95th percentile on the HW subjects are tightly grouped. The mean RMS acceleration remains close to the median in both weight groups.

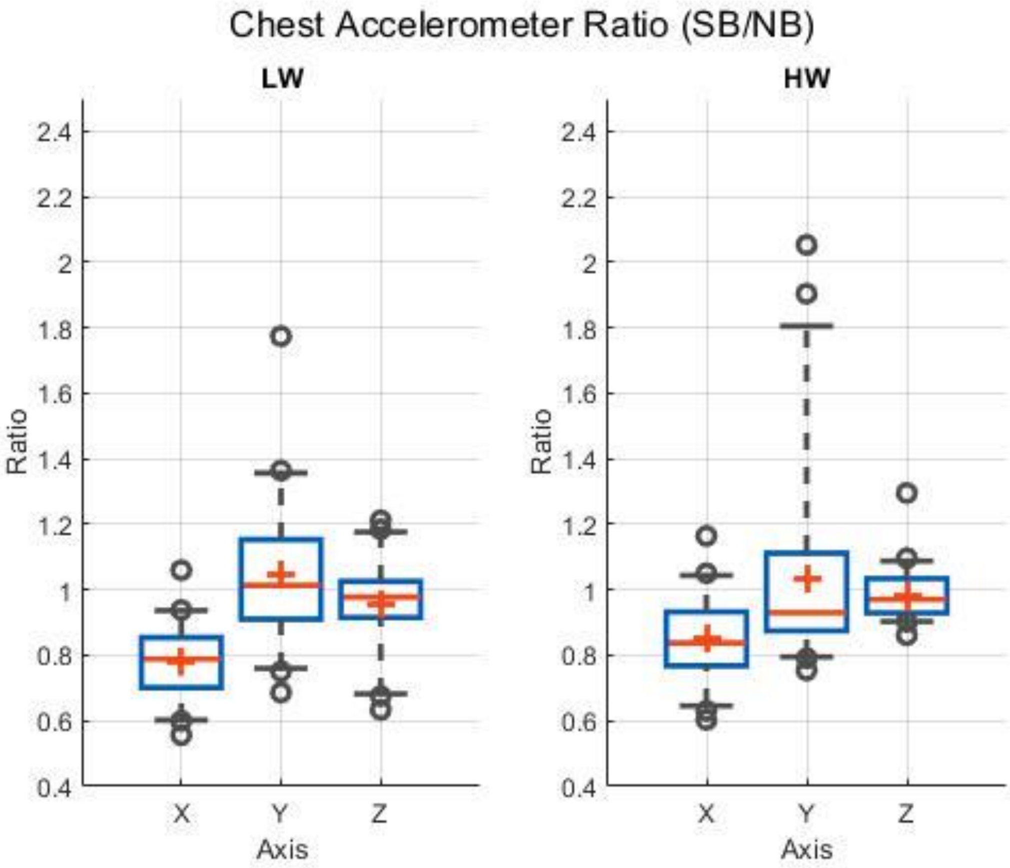

Figure 8: The ratio of the RMS acceleration experienced while immobilized to when not immobilized, measured at the chest.

The RMS acceleration ratio at the hip when immobilized to when not immobilized can be found in Figure 9. Both the median and mean acceleration along the Z axis increased when implementing a spine board. The interquartile range for both weight groups were closely grouped. The 5th percentile for both weight groups were similar, although the 95th percentile for the LW subjects was slightly higher than the HW subjects.

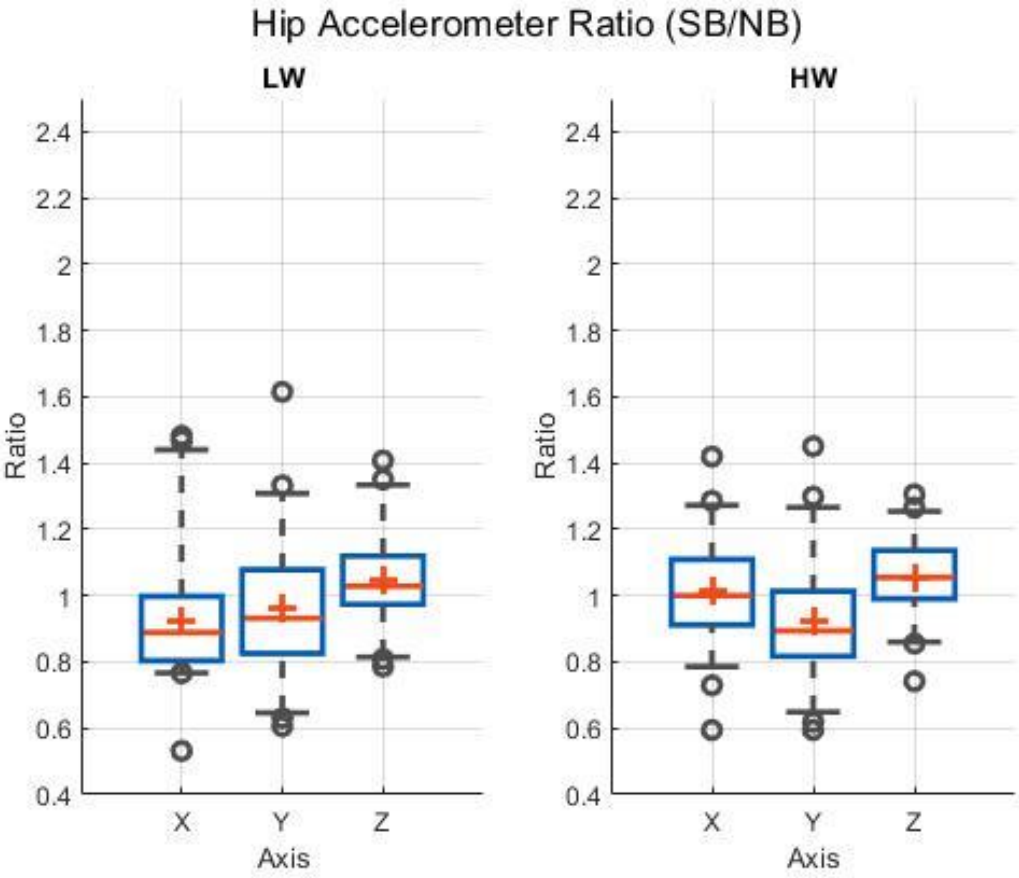

Figure 9: The ratio of the RMS acceleration experienced while immobilized to when not immobilized, measured at the hip.

RMS Angular Velocity Ratio

Figure 10 describes the ratio between the gyroscope measurements when using a spine board to when no spine board was used. These measurements were taken at the subject's head. A reduction in median and mean RMS rotational velocity was observed when rotating around the Z axis. Both the LW and HW groups saw an ~50 percent reduction in the median RMS rotation at the head. The interquartile range for the HW subjects was lower than that of the LW subjects. The 5th percentile was similar between the two weight groups, but the 95th percentile was higher for the LW group.

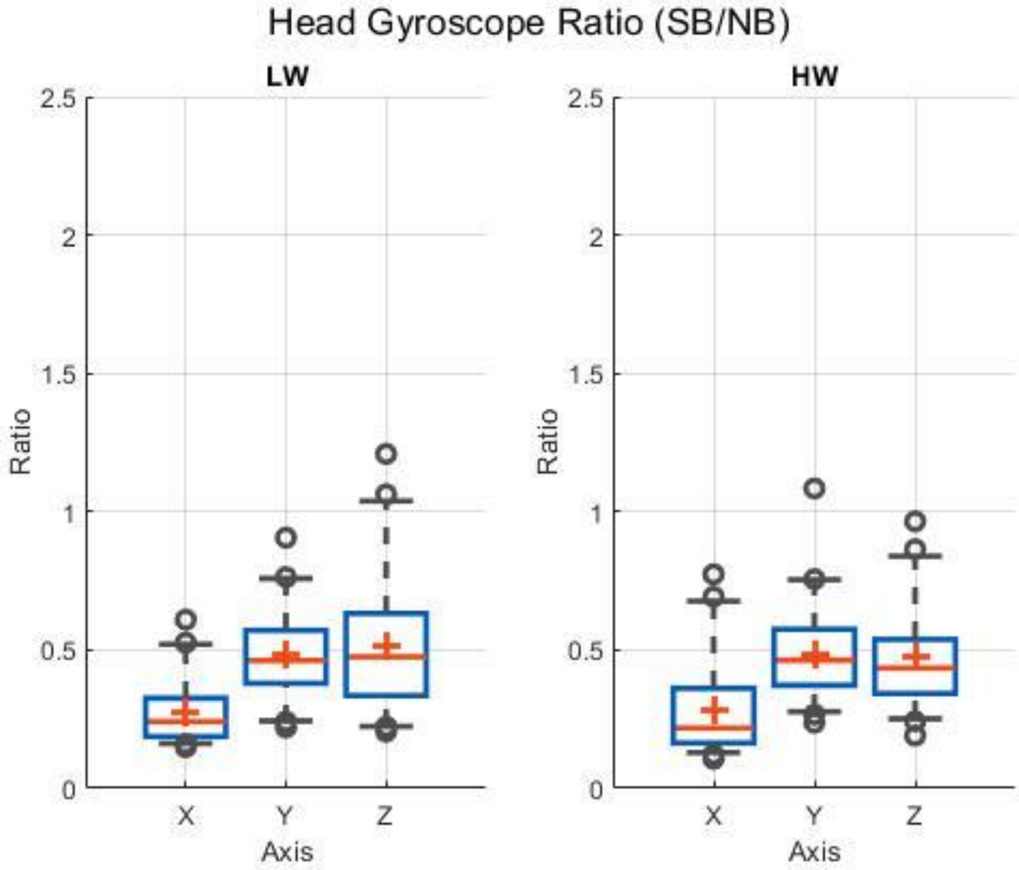

Figure 10: The ratio of the RMS rotation experienced while immobilized to when not immobilized, measured at the head.

The ratio of RMS rotational velocity experienced by each subject at the chest while using a spine board to without using a spine board can be found in Figure 11. For rotation around the Z axis, the median and mean RMS rotation was reduced by more than 25 percent when using a spine board (as compared to no spine board). The interquartile range for the LW subjects was lower than the HW subjects, and the 5th to 95th percentile ranges for both weight groups were similar.

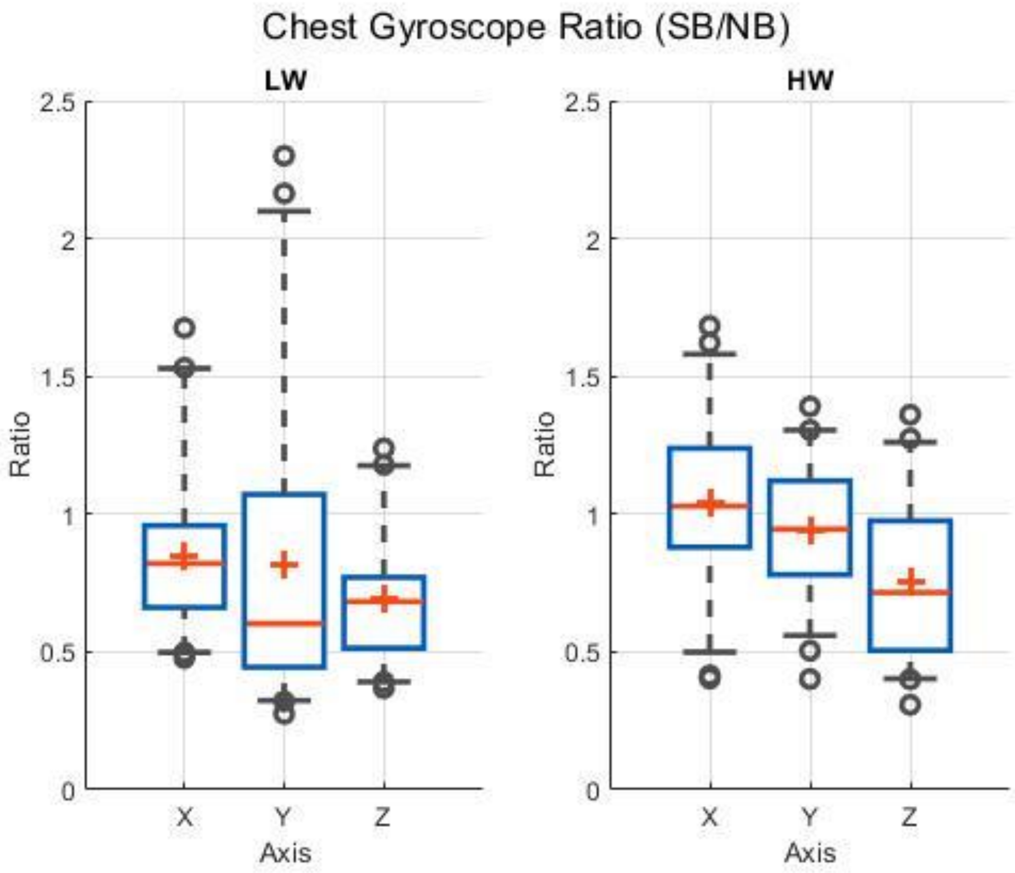

Figure 11: The ratio of the RMS rotation experienced while immobilized to when not immobilized, measured at the chest.

The ratio of the gyroscope measurements at the hip when using a spine board to when not using a spine board can be found in Figure 12. The median acceleration for the HW subjects was lower than the LW subjects; however, the mean acceleration was similar between the two weight groups. The interquartile ranges were similar between the two weight groups. The 5th and 95th percentiles for the HW subjects were higher than LW subjects.

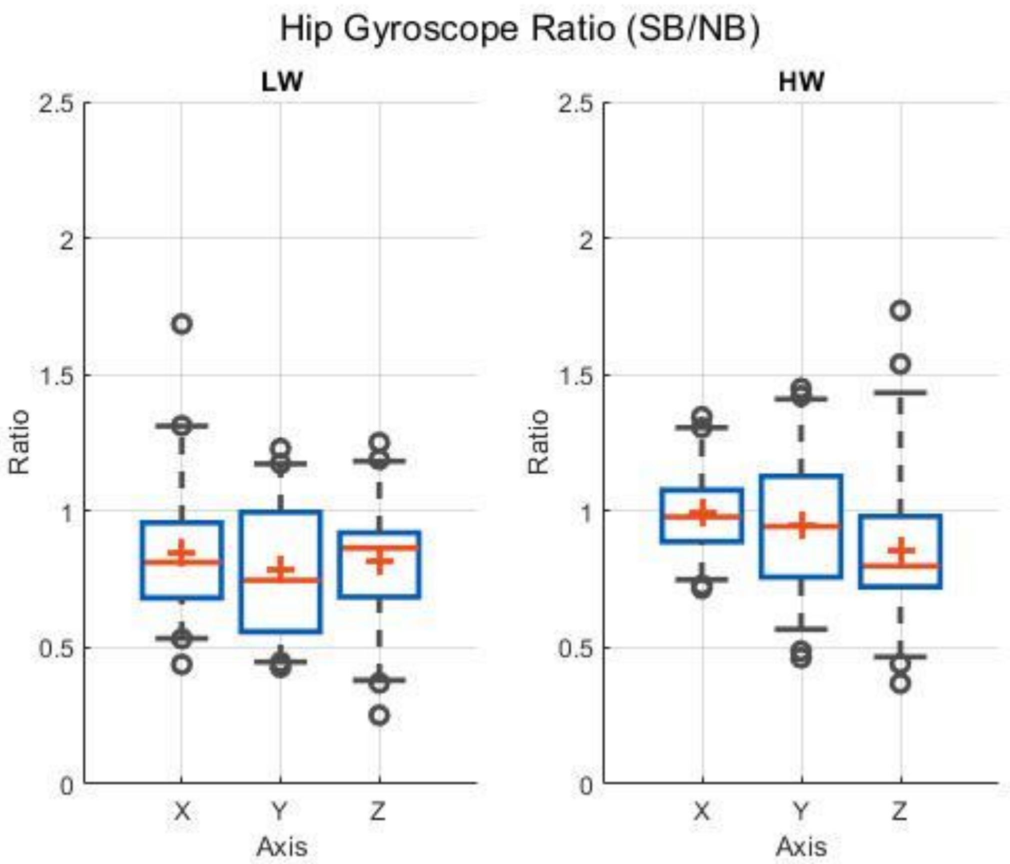

Figure 12: The ratio of the RMS rotation experienced while immobilized to when not immobilized, measured at the hip.

RMS Acceleration Ratio of All Subjects

Effect of Weight

For Figure 13-Figure 18, boxplots were used to describe the median, mean, interquartile range, and 5th to 95th percentile range of RMS acceleration experienced by all subjects. Figure 13-Figure 15 represent statistical data pertaining to the two weight groups, while Figure 16Figure 18 represent statistical data pertaining to the two immobilization conditions.

The RMS acceleration experienced by each weight group can be found in Figure 13. Each weight group represents both immobilized and non-immobilized subjects. When analyzing RMS acceleration along the Z axis, both the median and mean accelerations were similar between the LW subjects and HW subjects. The interquartile ranges were also similar, with the HW group having an interquartile range shifted lower than the LW group. The 5th percentile acceleration was higher in the HW group subjects, and the 95th percentile was very similar between the two weight groups.

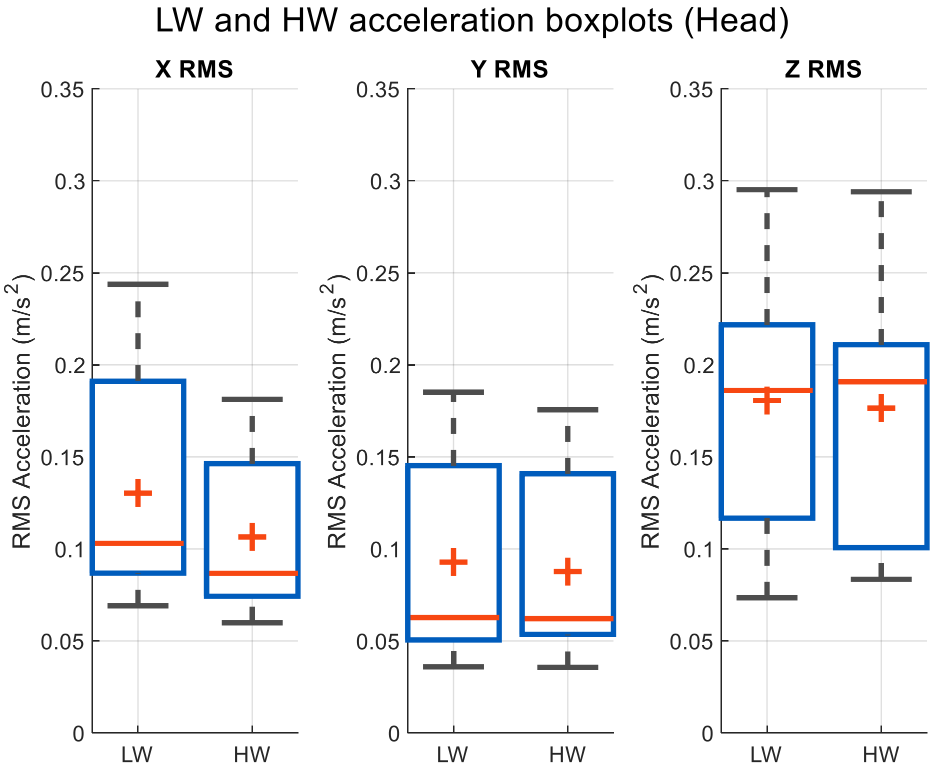

Figure 13: The RMS acceleration experienced at the head for each weight group.

A comparison of the RMS acceleration at the chest between LW and HW groups can be found in Figure 14. Both non-immobilized and immobilized conditions are represented by the boxplots. The median and mean RMS acceleration of the HW subjects along the Z axis is lower than the LW subjects, and also has a smaller 5th to 95th percentile. The interquartile range between the two weight groups is similar, although the range is shifted lower for the HW group.

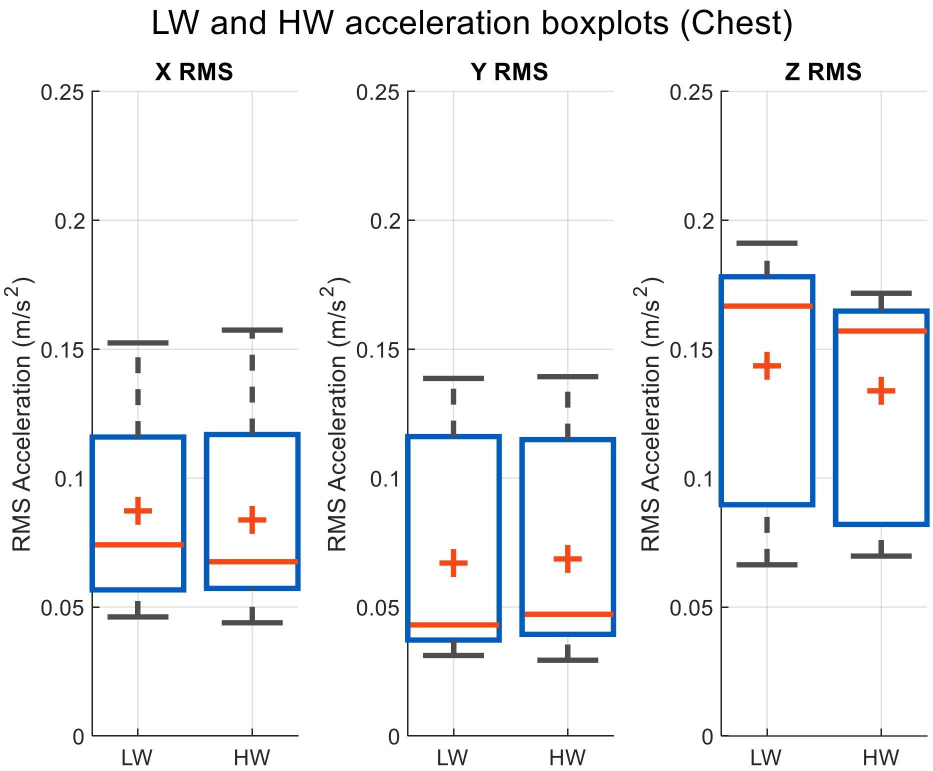

Figure 14: The RMS acceleration experienced at the chest for each weight group.

Figure 15 compares the RMS acceleration of the LW subjects to the HW subjects, with both immobilization conditions represented. The mean RMS acceleration along the Z axis was very similar between the two weight groups, but the median acceleration was higher in the LW group. The HW subjects also featured a smaller interquartile range, as well as a smaller 5th to 95th percentile range.

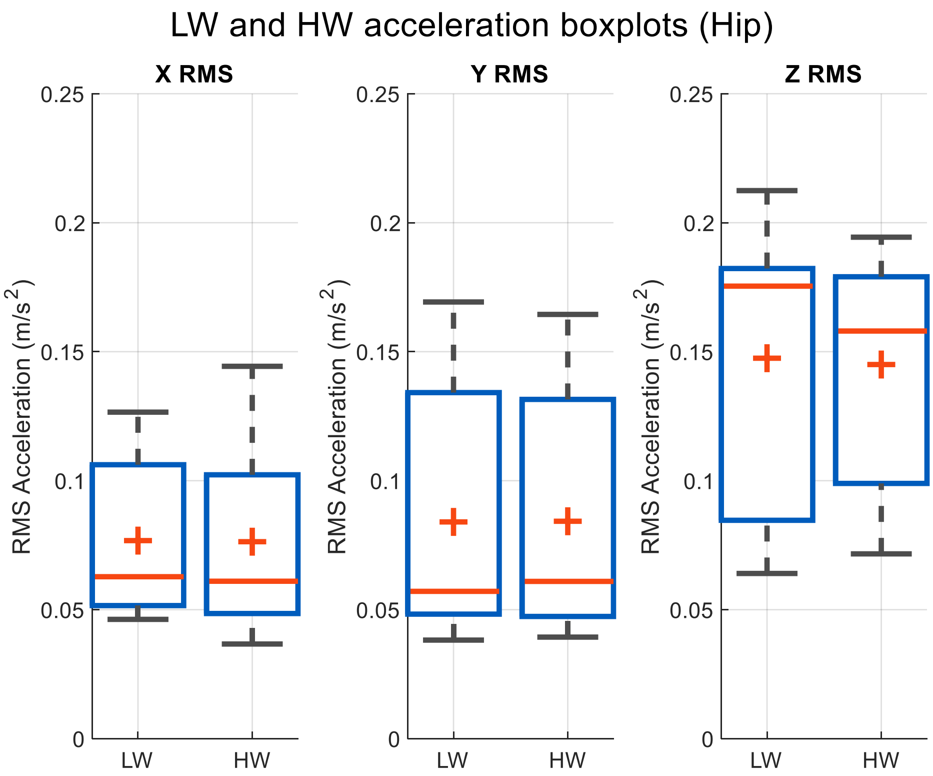

Figure 15: The RMS acceleration experienced at the hip for each weight group.

Effect of Immobilization

The RMS acceleration at the head is shown in Figure 16. Figure 16 compares the RMS acceleration when no immobilization system was used versus when a full immobilization system was used. Both weight groups were represented. Along the Z axis, the immobilized subjects had a lower median and mean RMS acceleration. The immobilized subjects also had a smaller interquartile range, as well as a smaller 5th to 95th percentile range.

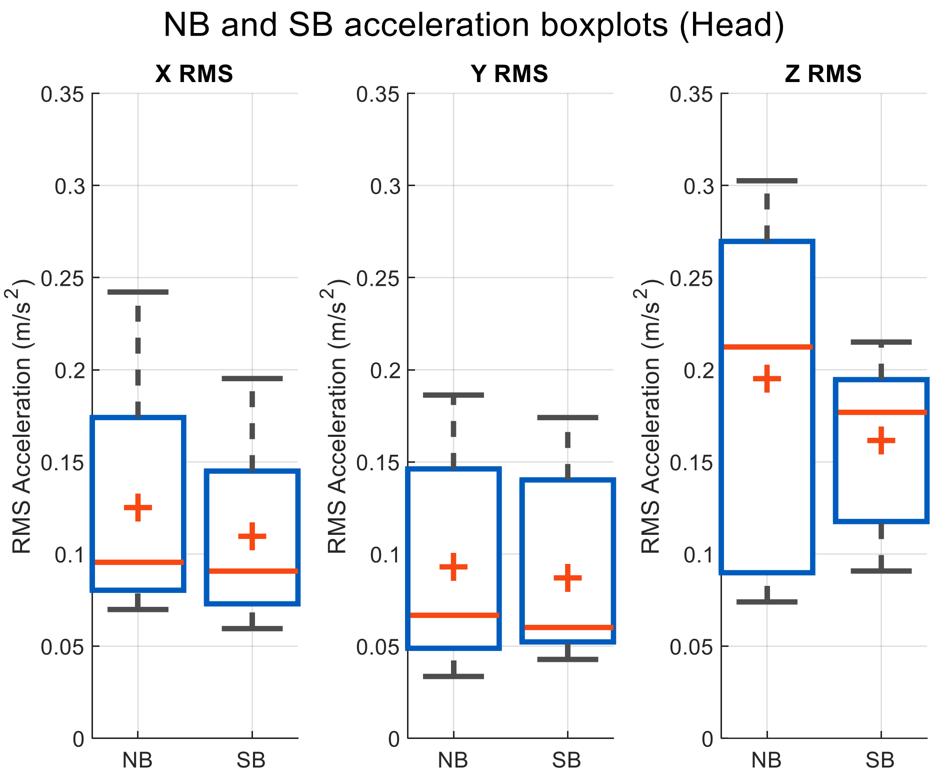

Figure 16: The RMS acceleration experienced for each immobilization condition, measured at the head.

A comparison between the RMS acceleration when immobilized and when not immobilized can be found in Figure 17. These accelerations were measured at the chest and analyzed along the Z axis. The mean and median acceleration of the immobilized subjects was slightly lower than the non-immobilized subjects. Both immobilization conditions had very similar interquartile ranges and 5th to 95th percentile ranges.

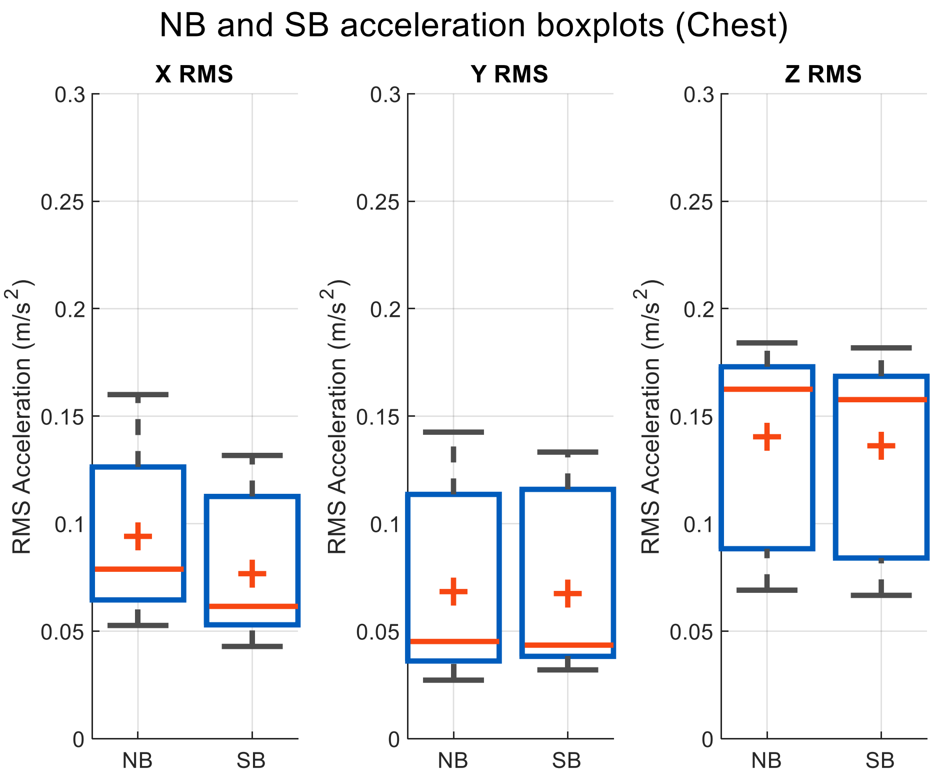

Figure 17: The RMS acceleration experienced for each immobilization condition, measured at the chest.

Figure 18 describes the RMS acceleration at the hip for each immobilization condition. Both weight groups were represented in each immobilization condition. Along the Z axis, the mean and median RMS acceleration for the immobilized subjects were higher than the non-immobilized subjects. The immobilized subjects had a wider 5th to 95th percentile, as well as a wider interquartile range.

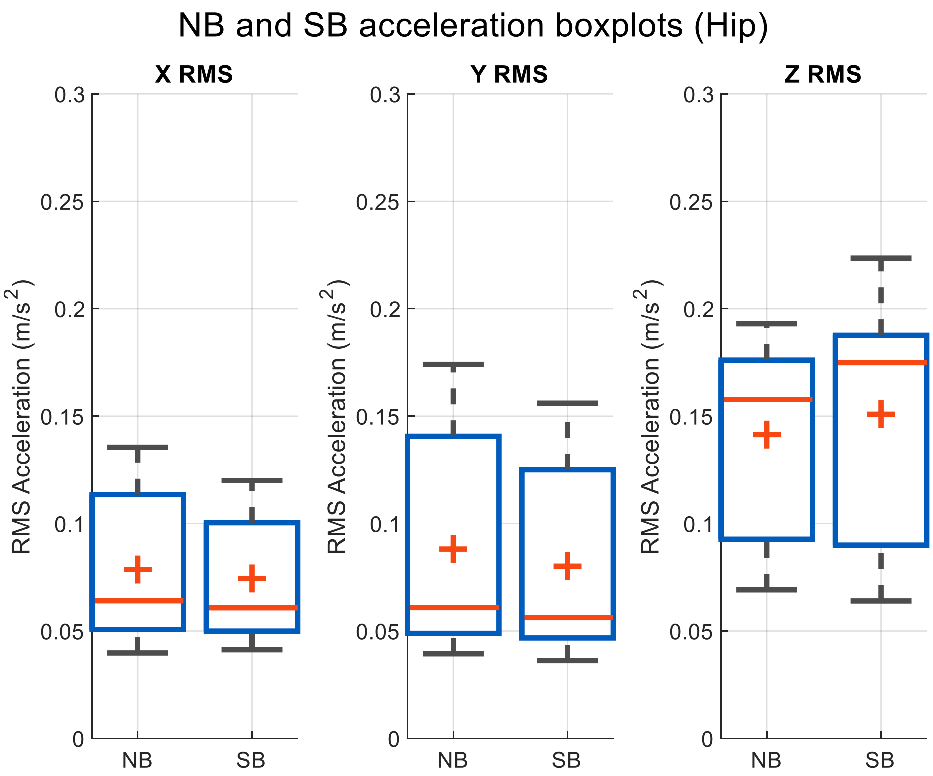

Figure 18: The RMS acceleration experienced for each immobilization condition, measured at the hip.

RMS Rotation

Effect of Weight

The RMS rotation experienced by each subject is described in Figure 19-Figure 24. Boxplots were used to display the median, mean, interquartile range, and the 5th to 95th percentile of RMS rotation. Figure 19-Figure 21 compare the effect of subject weight on RMS rotation. Figure 22-Figure 24 compare the effect of immobilization condition on RMS rotation.

The RMS rotation by each subject at the head can be described in Figure 19. Each weight group also represented both immobilization conditions. The median and mean RMS rotation around the Z axis was higher in the HW subjects than in the LW group. The HW group also had a slightly higher interquartile range, and a higher 95th percentile.

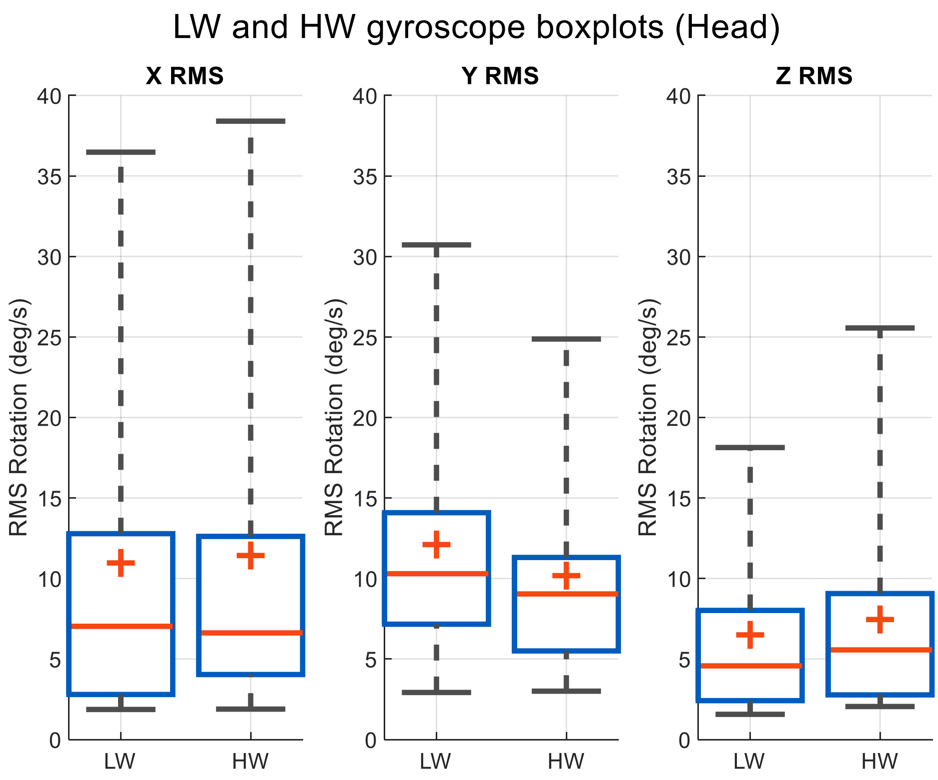

Figure 19: The RMS rotation for each weight group, measured at the head.

Figure 20 compares the effect of subject weight on RMS rotation, analyzed at the chest. For rotation around the Z axis, the HW subjects had a lower median and mean RMS rotation. Both weight groups had a very similar 5th to 95th percentile, but the HW subjects had a smaller interquartile range.

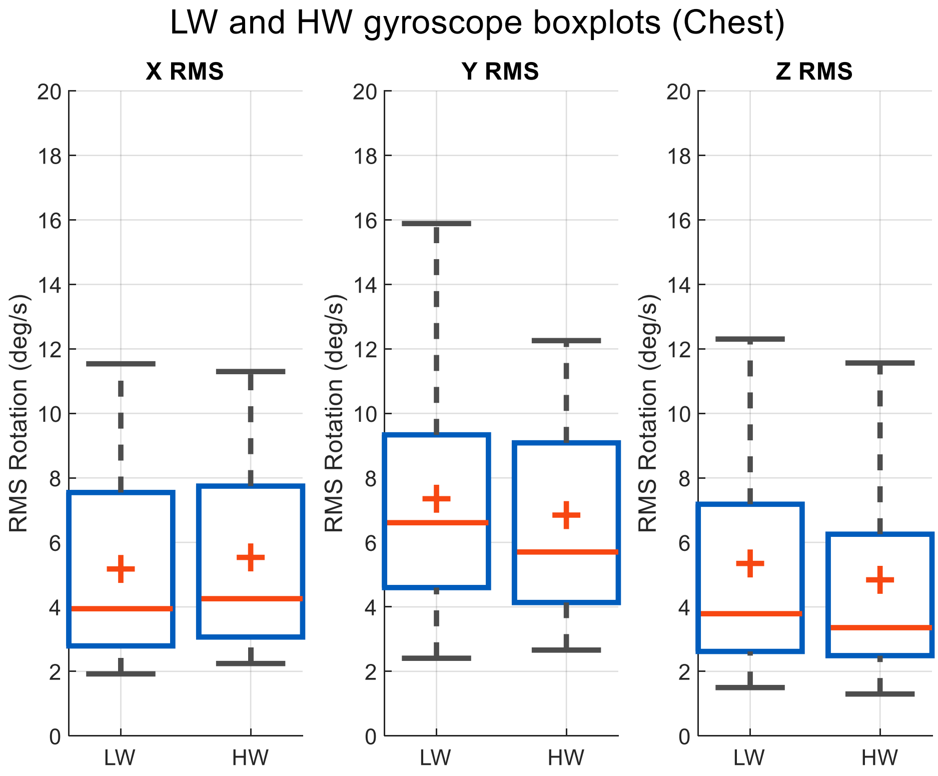

Figure 20: The RMS rotation for each weight group, measured at the chest.

An analysis was performed on the RMS rotation experienced at the hip for all subjects and compared the results between both weight groups. Figure 21 describes this analysis. The HW subjects experienced a higher mean and median RMS rotation around the Z axis than the LW subjects. The interquartile range was similar between the two weight groups, with the HW group having a slightly larger range but shifted higher than the LW group. The HW group also has a wider 5th to 95th percentile.

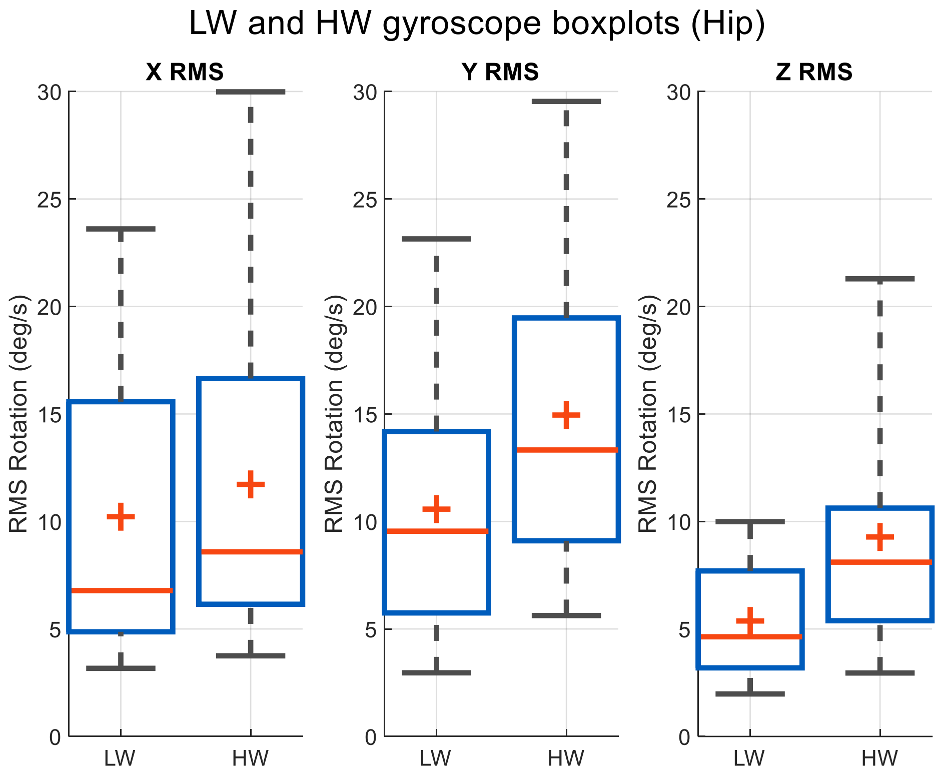

Figure 21: The RMS rotation for each weight group, measured at the hip.

Effect of Immobilization

Figure 22 compares the effect of immobilization condition on RMS rotation experienced by each subject at the head. Both weight groups were represented in each immobilization condition. The immobilized subjects had a lower median and mean RMS rotation, as well as a smaller interquartile range. This interquartile range is also shifted downwards in the immobilized subjects. The immobilized subjects also had a smaller 5th to 95th percentile than the non-immobilized subjects.

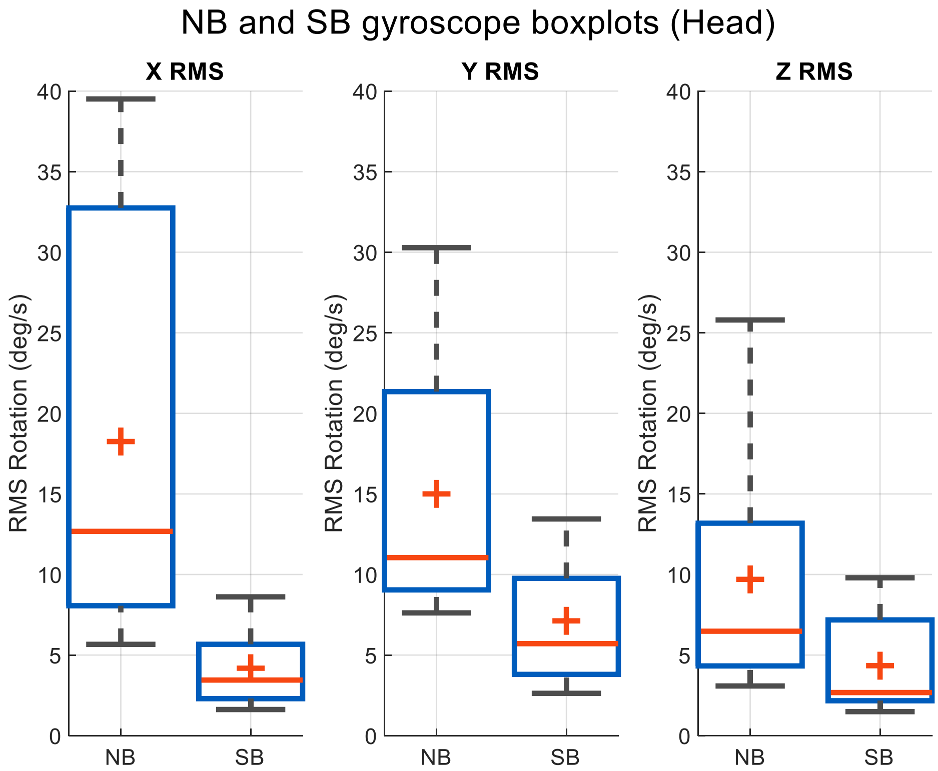

Figure 22: The RMS rotation experienced for each immobilization condition, measured at the head.

An analysis was performed on the RMS rotation experienced by each subject at the chest and compared between each immobilization condition. Both weight groups were represented in each immobilization condition. Figure 23 displays this analysis. The immobilized subjects had a lower mean and median RMS rotation, and had a smaller interquartile range. The 5th percentile was lower in the immobilized subjects, but the 95th percentile was similar between the two weight groups.

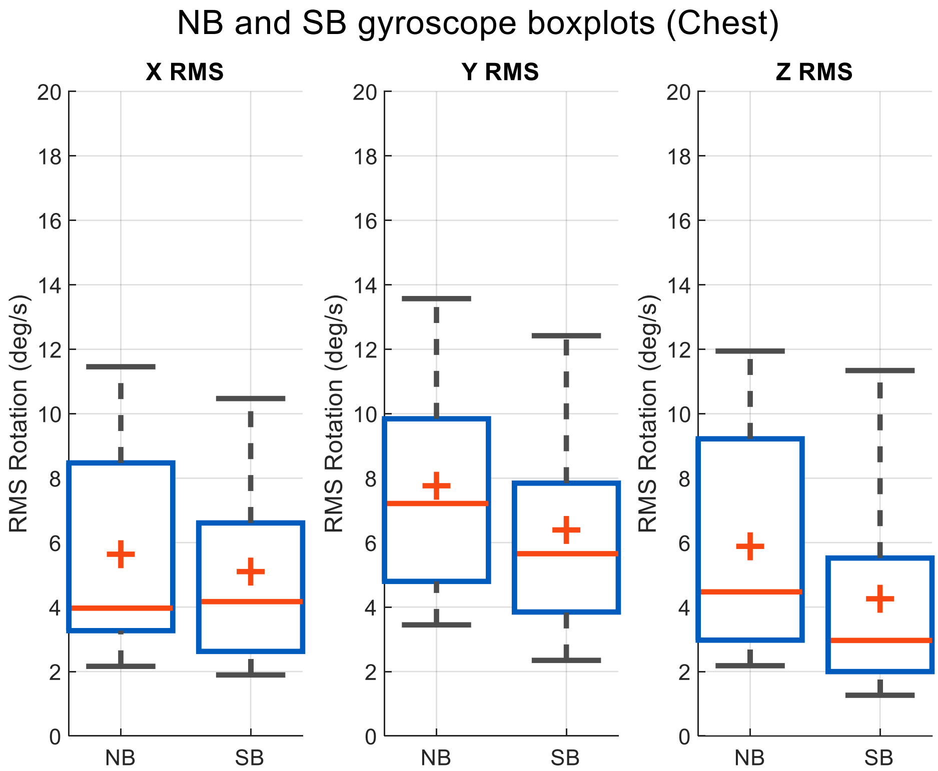

Figure 23: The RMS rotation experienced for each immobilization condition, measured at the chest.

Figure 24 depicts a comparison of the RMS rotation each subject experienced at the hip when immobilized versus not immobilized. The median and mean RMS rotation was lower for the immobilized subjects, and the interquartile range was shifted lower for the immobilized subjects. In addition, the 5th to 95th percentile was smaller in the immobilized subjects.

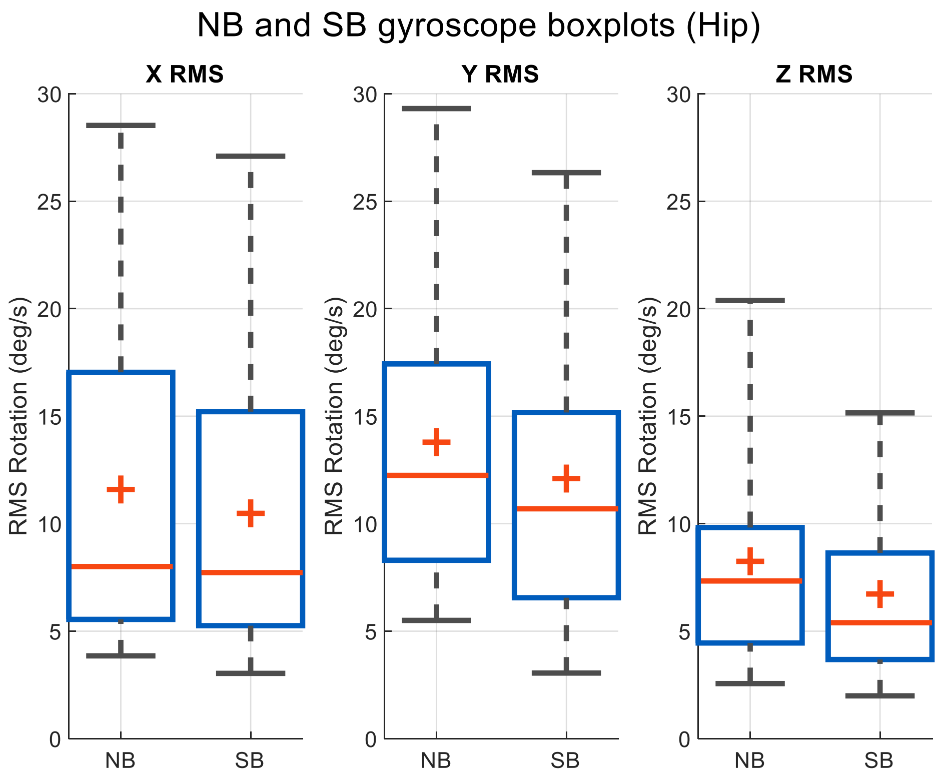

Figure 24: The RMS rotation experienced for each immobilization condition, measured at the hip.

Transmissibility

In Figure 25-Figure 30, the median transmissibility plot is plotted against the 25th to 75th percentile, and the 5th to 95th percentile. The fifth point of each data set was plotted so that the plots were easier to analyze. Figure 25, Figure 26, and Figure 27 separate the data into LW and HW categories, while Figure 28, Figure 29, and Figure 30 separate the data into non-immobilized and immobilized categories.

The median transmissibility for each weight group at the head was analyzed in Figure 25. Only transmissibility along the Z axis was analyzed. When looking to the median line, the magnitude of transmissibility is nearly identical between the LW and HW subjects. The HW group's resonance has been shifted back by approximately 1.5 Hz, however. The HW subjects' 95th percentile was also higher than the LW group, and also featured the same shift in frequency as the median line.

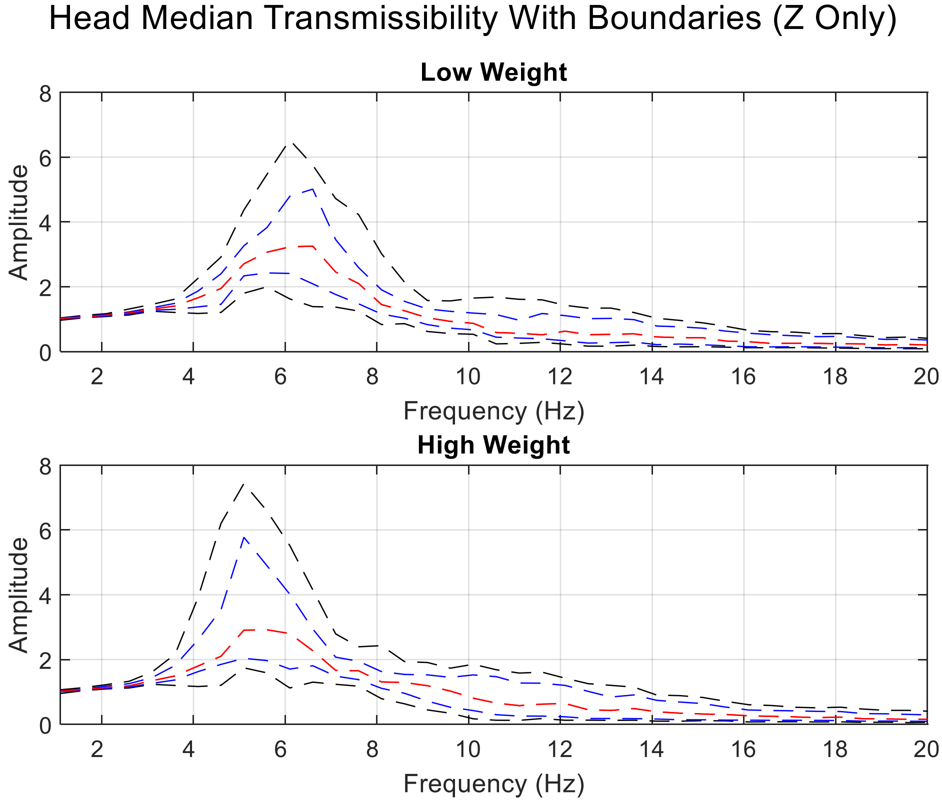

Figure 25: An overlaid transmissibility plot for the head comparing the LW and HW groups. The red line represents the subject median transmissibility, the blue line represents the 25th to 75th percentile, and the black line represents the 5th to 95th percentile

The median transmissibility for each weight group at the chest was analyzed in Figure 26. Only transmissibility along the Z axis was analyzed. The LW group had a transmissibility magnitude slightly higher than that of the HW subjects. In addition, the HW group resonated approximately 1 Hz earlier than the LW group. The HW group's 95th percentile was higher than the LW group's 95th percentile, and resonated nearly 2 Hz earlier than the LW group.

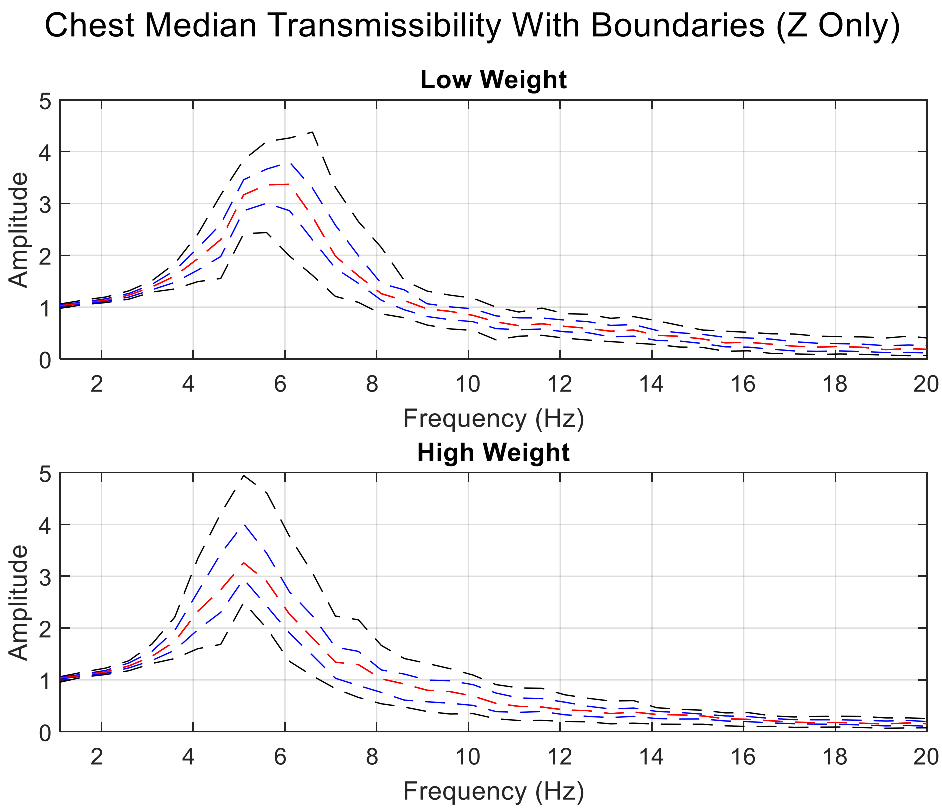

Figure 26: An overlaid transmissibility plot for the chest comparing the LW and HW groups. The red line represents the subject median transmissibility, the blue line represents the 25th to 75th percentile, and the black line represents the 5th to 95th percentile.

The median transmissibility along the Z axis for each weight group was analyzed in Figure 27. Only the hip was observed in this case. The median transmissibility magnitude was nearly the same between the two weight groups; in addition, both weight groups appeared to resonate at the same frequency. The 95th percentile was nearly identical in magnitude for both weight groups, but the HW group resonated approximately .5 Hz earlier than the LW subjects.

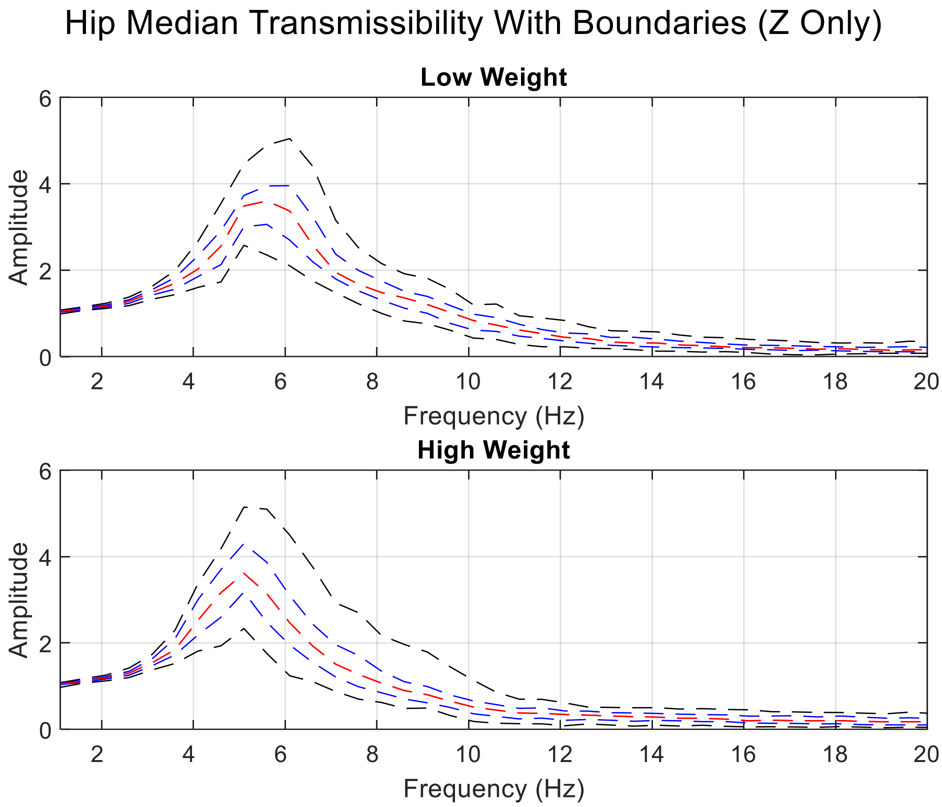

Figure 27: An overlaid transmissibility plot for the hip comparing the LW and HW groups. The red line represents the subject median transmissibility, the blue line represents the 25th to 75th percentile, and the black line represents the 5th to 95th percentile.

The median transmissibility along the Z axis for either immobilization condition was analyzed in Figure 28. Only the head was analyzed in this case. The median transmissibility magnitude was higher when no board was used, compared to when a spine board was used. The magnitude of the peak transmissibility was reduced by nearly 50 percent when a spine board was implemented. The spine board condition also saw its peak transmissibility shift back by approximately .5 Hz when compared to the no board condition; however, the spine board 95th percentile experienced its resonance around 1 Hz after the no board condition. After 10 Hz, the transmissibility magnitude continued towards 0 for the non-immobilized condition but remained at above 1 for much of the frequency content after 10 Hz for the immobilized condition.

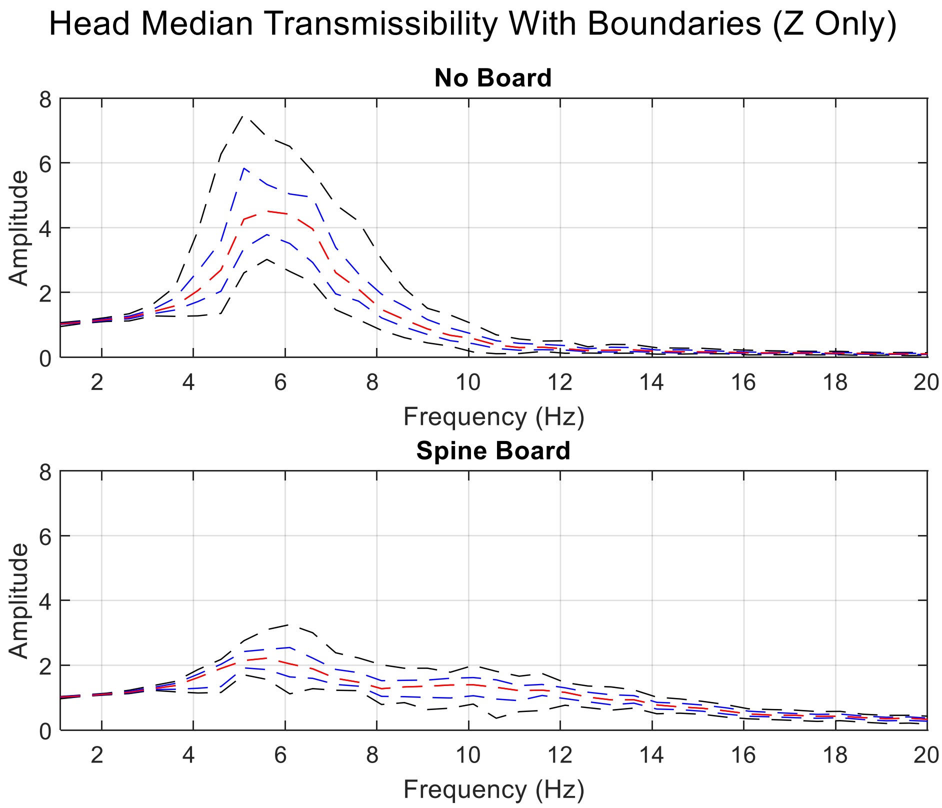

Figure 28: An overlaid transmissibility plot for the head comparing the immobilized and non-immobilized conditions. The red line represents the subject median transmissibility, the blue line represents the 25th to 75th percentile, and the black line represents the 5th to 95th percentile.

The median transmissibility for the chest with respect to each immobilization condition was analyzed in Figure 29. Only the Z axis was observed in this case. The spine board saw only a slight decrease in magnitude at its median, and the 95th percentile saw a drop when compared to the non-immobilized condition. Both immobilization conditions had a resonance that occurred at the same frequency at their medians; however, the immobilized 95th percentile had a resonance occur almost 2 Hz after the non-immobilized condition. Both immobilization conditions tended towards 0 magnitude after the resonance.

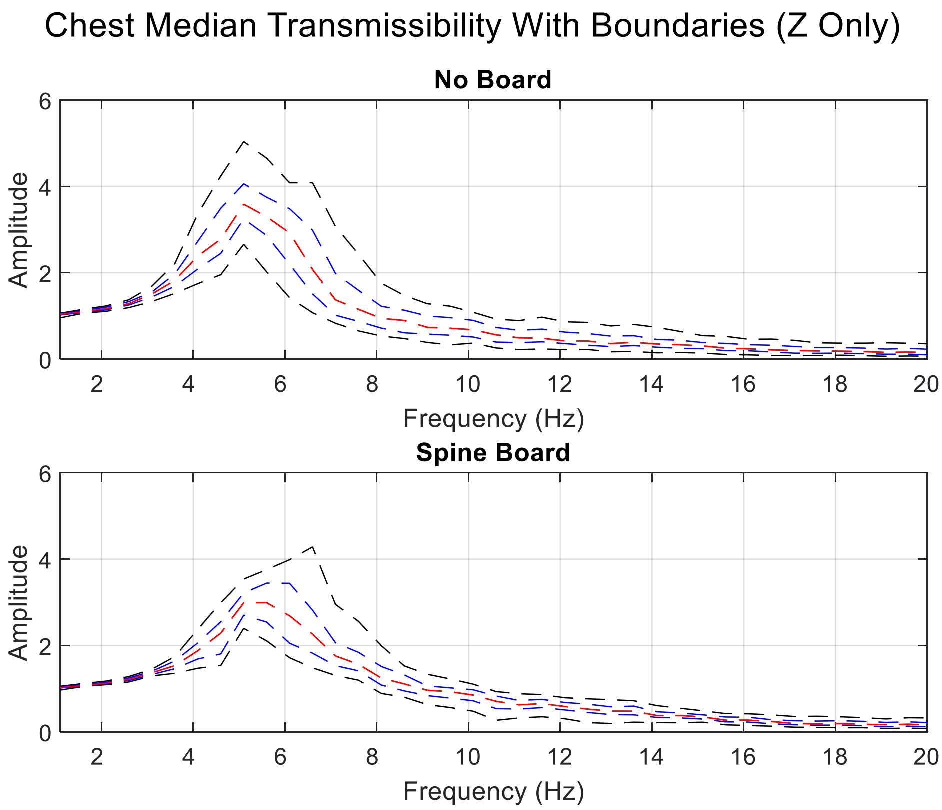

Figure 29: An overlaid transmissibility plot for the chest comparing the immobilized and non-immobilized conditions. The red line represents the subject median transmissibility, the blue line represents the 25th to 75th percentile, and the black line represents the 5th to 95th percentile.

The median transmissibility for the hip with respect to each immobilization condition was analyzed in Figure 30. Only the Z axis was observed in this case. The immobilized condition saw a slightly higher peak transmissibility magnitude at both its median and 95th percentile, when compared to the non-immobilized condition. The immobilized condition appeared to resonate less than .5 Hz after the non-immobilized condition at the 95th percentile. The non-immobilized condition tended towards 0 magnitude sooner than the immobilized condition.

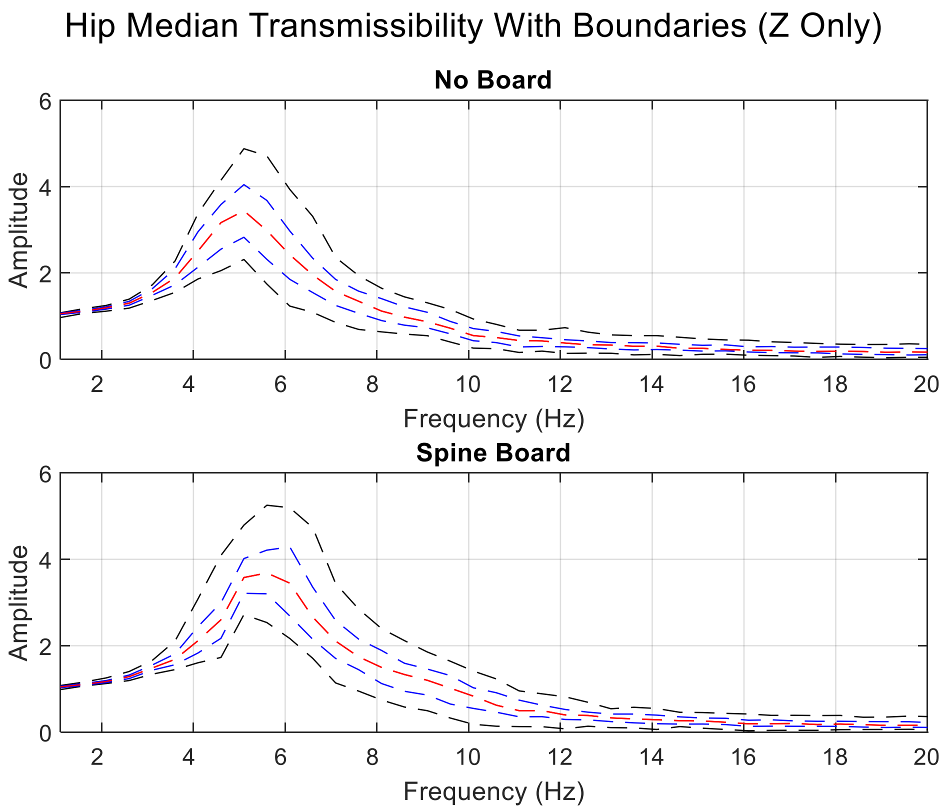

Figure 30: An overlaid transmissibility plot for the hip comparing the immobilized and non-immobilized conditions. The red line represents the subject median transmissibility, the blue line represents the 25th to 75th percentile, and the black line represents the 5th to 95th percentile.

Boxplots were used to describe the transmissibility data; an explanation of the boxplot can be found in Figure 3. Data was broken out into LW and HW groups and separated into non-immobilized and immobilized conditions (Figure 31-Figure 36).

An analysis of the peak transmissibilities for both weight groups at the head can be found in Figure 31. Along the Z axis, the peak median and mean transmissibility was higher for the HW group when compared to the LW group. The interquartile range and 5th to 95th percentile of the HW subjects was more widespread than the LW subjects.

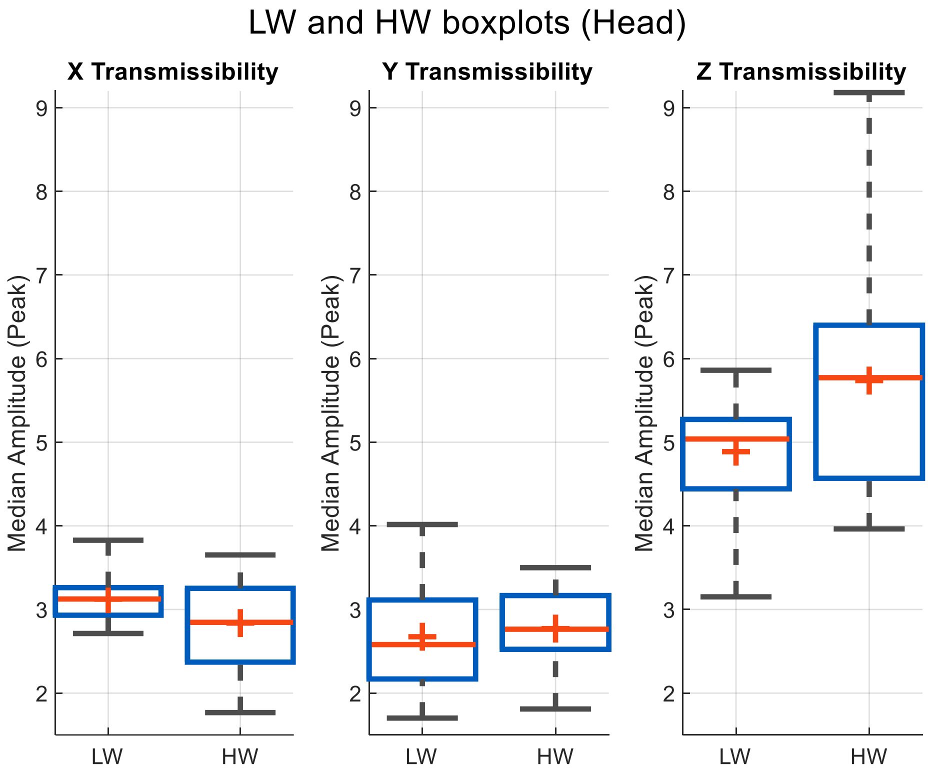

Figure 31: A plot comparing the peak median transmissibility of the LW subjects with the HW subjects. Transmissibilities are measured at the head.

The peak median transmissibilities for both weight groups measured at the chest can be found in Figure 32. Along the Z axis, the peak median transmissibility for the HW group is higher than the LW group. The interquartile range for the HW group is also larger than the LW group. The 5th to 95th percentile span is very similar between the two weight groups.

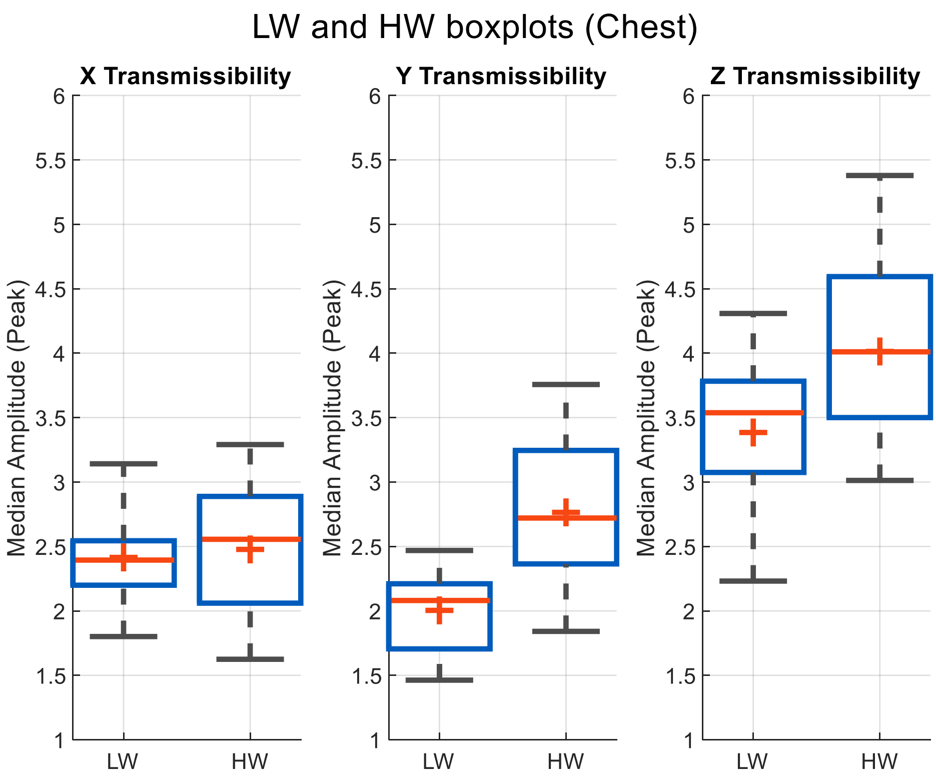

Figure 32: A plot comparing the peak median transmissibility of the LW subjects with the HW subjects. Transmissibilities are measured at the chest.

The peak median transmissibilities for both weight groups measured at the chest can be found in Figure 33. Along the Z axis, the peak median transmissibility is nearly the same between the two weight groups. The peak mean transmissibility is slightly higher in the HW group when compared to the LW group. The HW subjects' interquartile range and 5th to 95th percentile span is larger than the LW subjects.

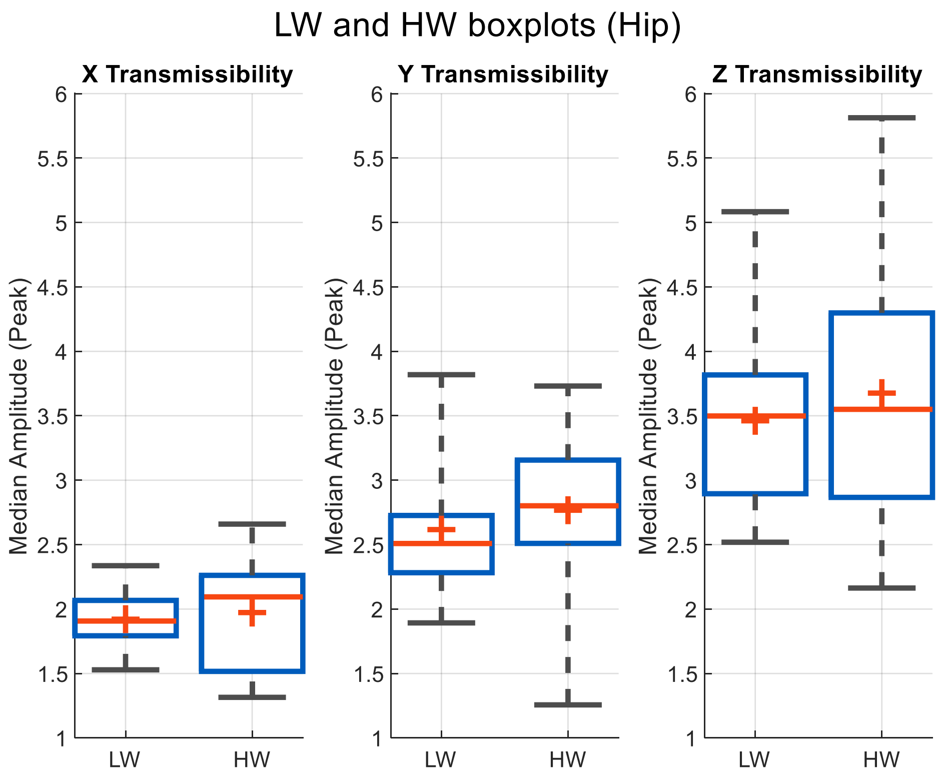

Figure 33: A plot comparing the peak median transmissibility of the LW subjects with the HW subjects. Transmissibilities are measured at the hip.

The peak transmissibilities for both weight groups at the head can be found in Figure 34. Along the Z axis, the immobilized condition had lower peak median and mean transmissibilities than the non-immobilized condition. The interquartile range and 5th to 95th percentile range is larger in the non-immobilized condition than the immobilized condition.

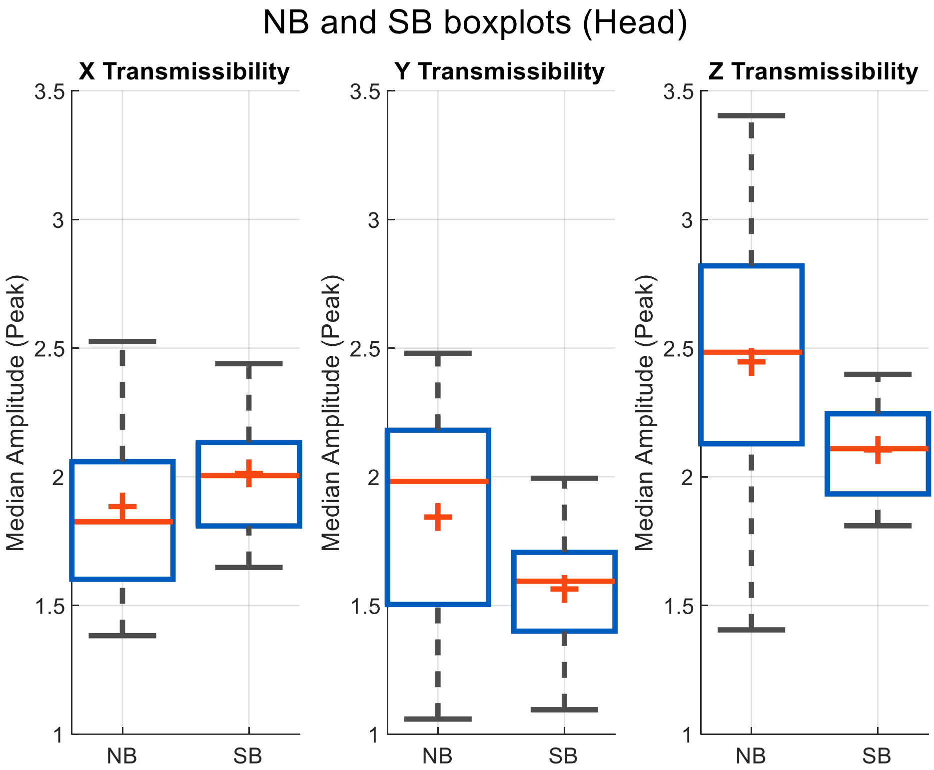

Figure 34: A plot comparing the peak median transmissibility of the non-immobilized and immobilized conditions. Transmissibilities are measured at the head.

The peak transmissibilities for both weight groups at the chest can be found in Figure 35. When analyzing the Z axis, the non-immobilized condition had higher peak median and mean transmissibilities than the immobilized condition. The non-immobilized 5th to 95th percentile range is larger than the immobilized condition, and as well as the interquartile range.

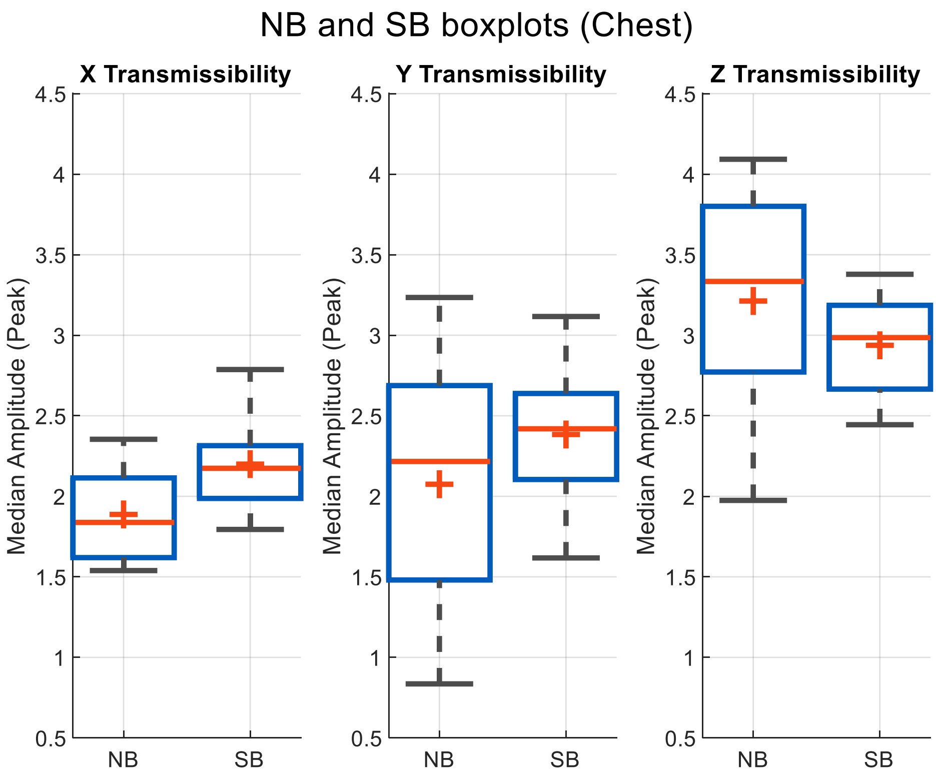

Figure 35: A plot comparing the peak median transmissibility of the non-immobilized and immobilized conditions. Transmissibilities are measured at the chest.

The peak median transmissibilities for both weight groups measured at the chest can be found in Figure 36. The peak mean and median transmissibilities of the immobilized condition were slightly lower than the non-immobilized condition. The interquartile range of the non-immobilized condition was larger than the immobilized condition. The 5th to 95th percentile range was nearly identical between the two immobilization conditions.

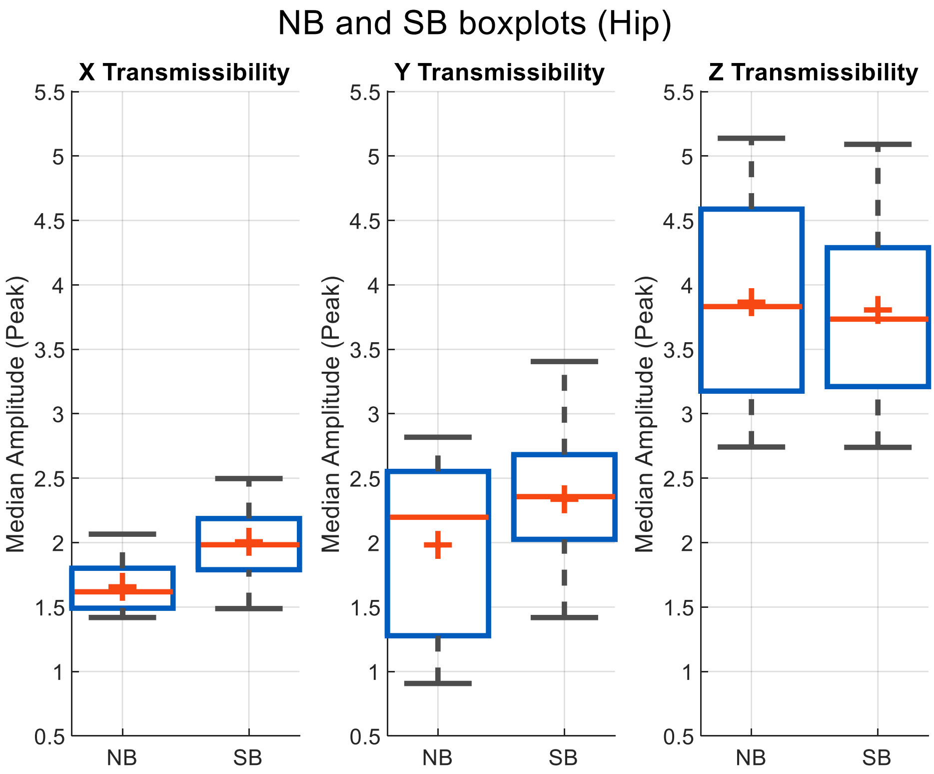

Figure 36: A plot comparing the peak median transmissibility of the non-immobilized and immobilized conditions. Transmissibilities are measured at the hip.

Area under the Transmissibility Curve

Transmissibility plots offer a plethora of information, describing the amplification of the input vibration as a function of frequency. The peak of a transmissibility graph is useful, as it shows the maximum amplification of the system as well as the frequency at which that occurs. However, examining the peak alone does little to quantify the frequency distribution of the amplification or quantify the overall energy transmission.

To extract more information from the transmissibility plots, the Area Under Transmissibility, was introduced. This metric is the integral of the transmissibility plot from 2 Hz to 10 Hz. These limits were chosen because they are equidistant from 6 Hz, the resonant frequency for most graphs. Furthermore, the transmissibility from 0 Hz to 2 Hz and 10 Hz to 20 Hz was very similar in most plots, and those ranges were assumed to have negligible impact on the integral results.

The area underneath the transmissibility curve can be found in Figure 37. The median and mean transmissibilities along the Z axis are similar and have a similar 5th to 95th percentile range. The no board subjects, however, have a larger 5th and 95th percentile value, and have a larger interquartile range.

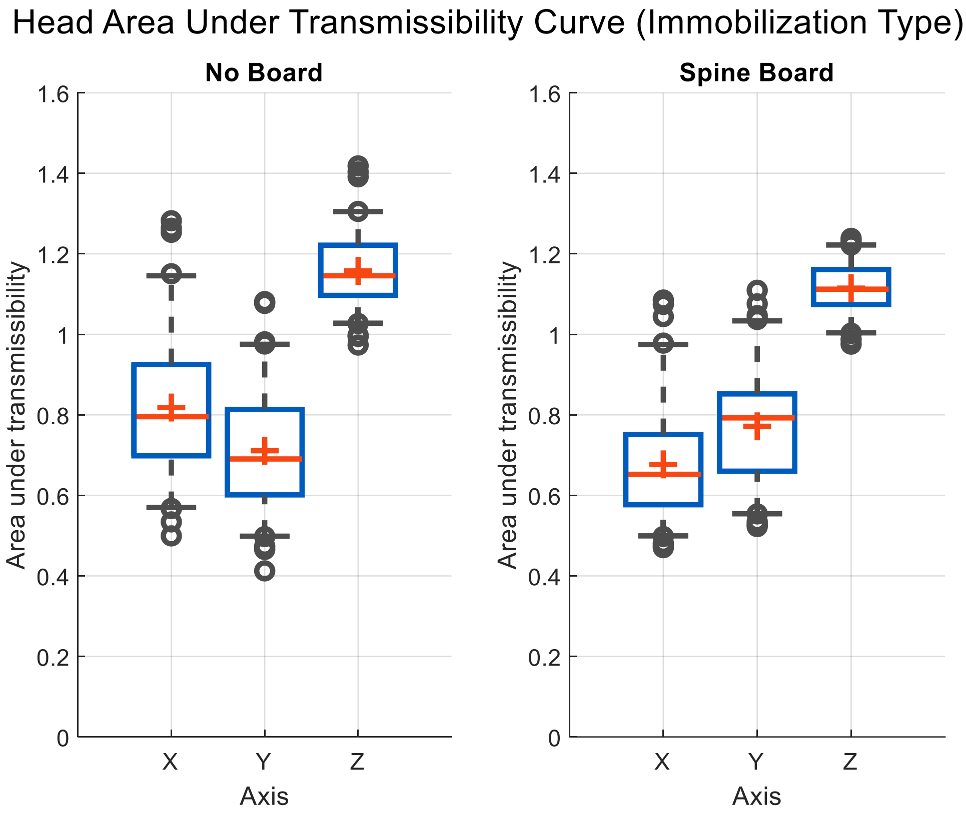

Figure 37: Boxplots representing the area underneath the transmissibility curve, measured at the head and dependent on immobilization.

Boxplots describing the area under the transmissibility curve at the chest can be found in Figure 38. When analyzing the Z axis, the median and mean area are within 5 percent of each other. The no board subjects have a larger interquartile range and 5th to 95th percentile range, as well as a larger 95th percentile value.

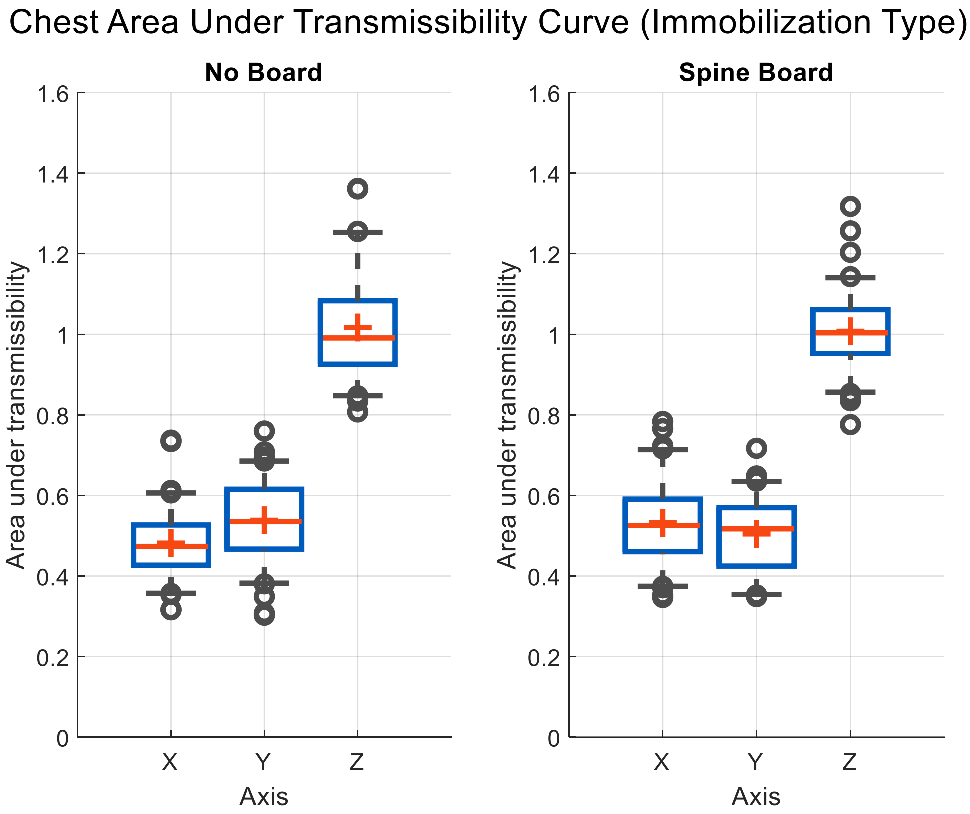

Figure 38: Boxplots representing the area underneath the transmissibility curve, measured at the chest and dependent on immobilization condition.

Figure 39 describes the area under the hip transmissibility curve using boxplots. In this case, only the Z axis was analyzed. For the spine board immobilization, the mean and median transmissibility were over 10 percent greater than the no board immobilization condition. In addition, the interquartile range and 5th to 95th percentile range was larger.

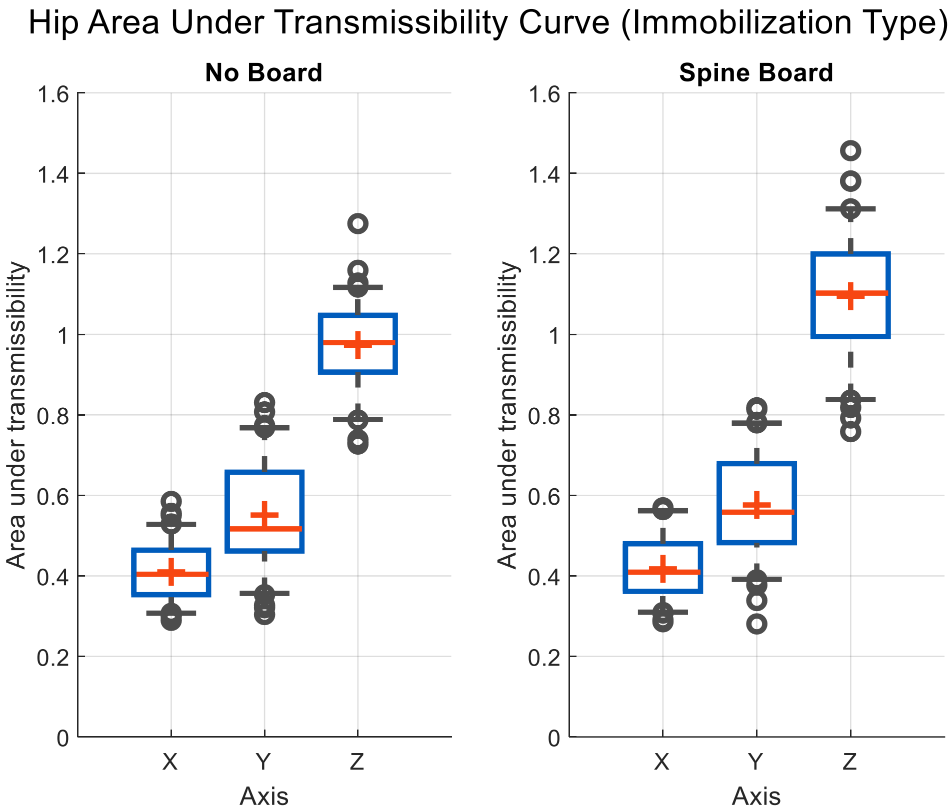

Figure 39: Boxplots representing the area underneath the transmissibility curve, measured at the hip and dependent on immobilization.

A depiction of the effect of subject weight on the area underneath the transmissibility curve can be found in Figure 40. In this instance, only the Z axis was analyzed. There was less than a 5 percent difference in mean and median area between the LW and HW groups. The LW group, however, had a larger interquartile range, and larger 5th and 95th percentile values. The 5th to 95th percentile range was similar between the LW and HW groups.

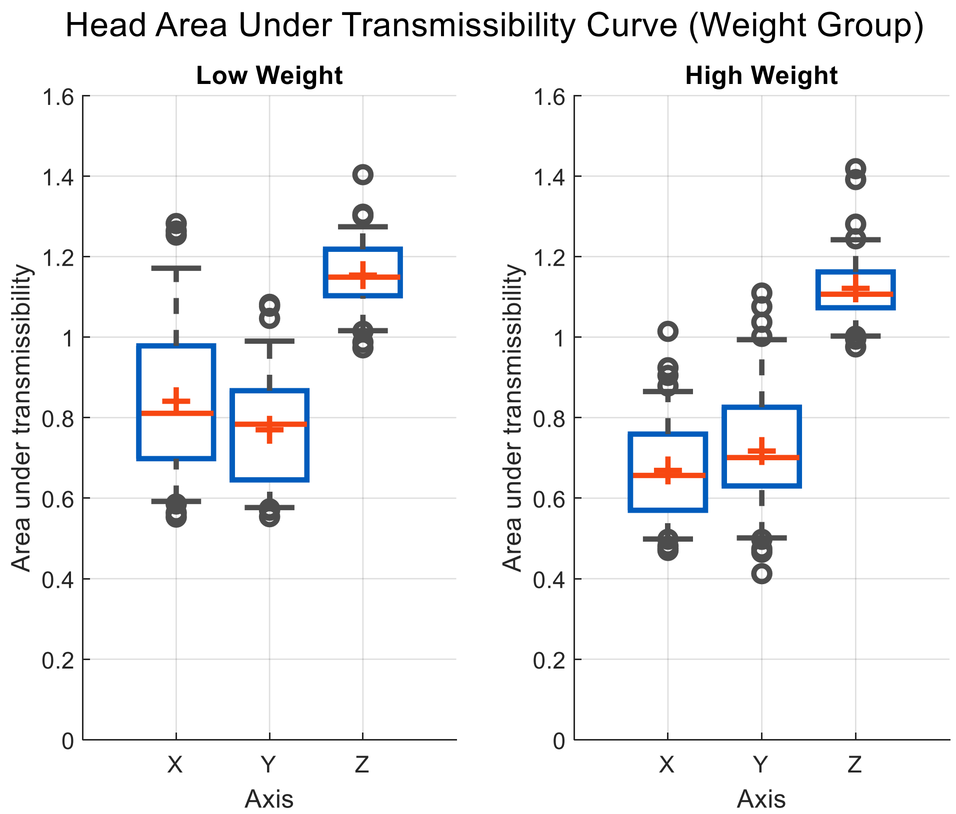

Figure 40: A representation of the effect of weight on area under the transmissibility curve, measured at the head.

Boxplots depicting the area under the transmissibility curve at the chest can be found in Figure 41. When analyzing the Z axis, the mean and median transmissibilities of the LW group were nearly 15 percent larger than that of the HW group. The LW group also had higher 5th and 95th percentile values, as well as a larger 5th to 95th percentile range. The interquartile range of both weight groups were similar, with the LW group having a slightly larger range.

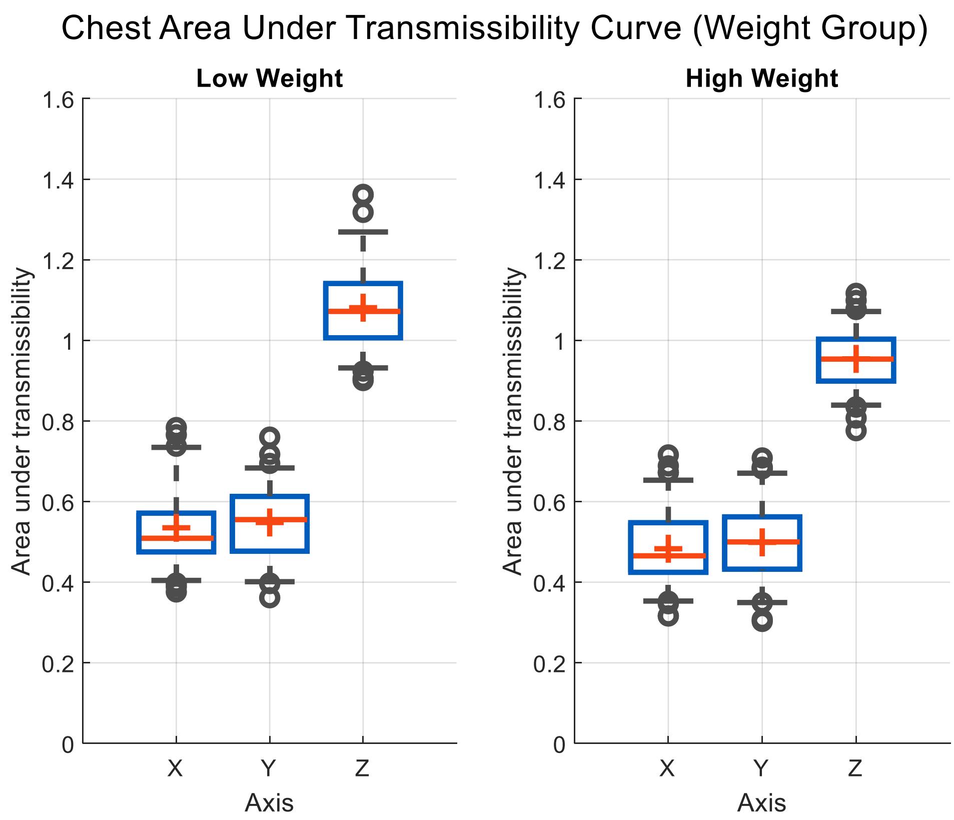

Figure 41: A representation of the effect of weight on the area under the transmissibility curve, measured at the chest.

The area under the transmissibility curve at the hip can be described by the boxplots shown in Figure 42. Only the Z axis was analyzed in this case. The HW group had a larger interquartile range, but smaller 5^{th} to 95^{th} percentile values. The 5^{th} to 95^{th} percentile range was similar between the two weight groups. The mean and median transmissibilities of the LW group were nearly 10 percent higher than those found in the HW group.

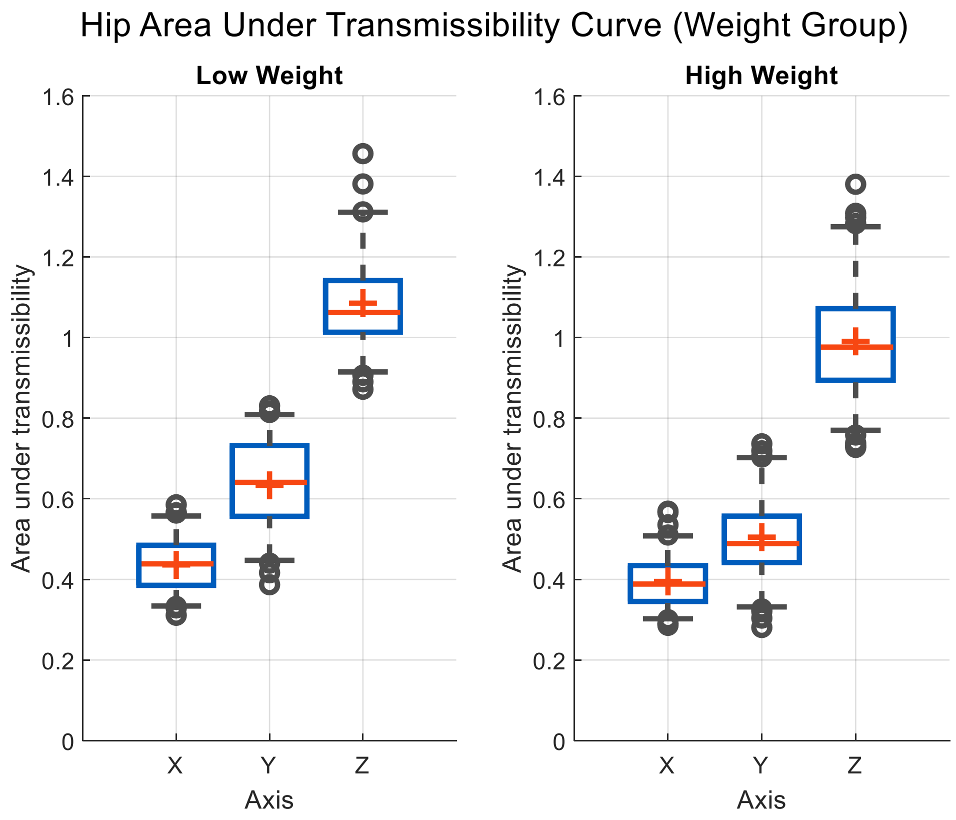

Figure 42: A representation of the effect of subject weight on the area under the transmissibility curve, measured at the hip.

Statistical Analysis

In order to provide a more comprehensive analysis of the gathered data, the results were subdivided based on three factors, as shown in Tables 1 and 2: weight (high or low), immobilization (spine board or no board), and ride profile (all profiles, ground vehicle, aircraft, and 3D vibration). For each subdivided set of results, a set of metrics were calculated, specifically the peak of the Z transmissibility, the area under the Z transmissibility curve (calculated via the integral from 2 Hz to 10 Hz), the resonant frequency (in the Z axis), the RMS Z acceleration, and the RMS of the gyroscope magnitude (the norm of the X, Y, and Z components). The gyroscope metric contains all three axes (rather than just the Z axis) because acceleration in the Z axis can cause rotational velocity about all three axes. The metrics were further analyzed for statistical significance using one-way ANOVA (Hogg, 1987). Results were deemed significant if $p < 0.05$.

Table 1: The effect of immobilization condition on various analysis quantities for low weight subjects. A '*' represents a statistically significant difference between the immobilization conditions, and a "^" represents a statistically significant difference ($p < .05$) between weight groups.

		Low Weight									
		Z Transmissibility (Peak)		Area under Z Transmissibility		Z Transmissibility Wn (Hz)		RMS Z Acc (g)		RMS Gyro (deg/s)	
Ride Profile	Segment	SB	NB	SB	NB	SB	NB	SB	NB	SB	NB
ALL	Head	2.74±0.45*^	5.49±1.06*^	1.12±0.06*	1.19±0.08*^	5.83±0.62*	6.39±0.41*^	0.16±0.04	0.20±0.08	10.04±5.77*	25.91±15.61*
	Chest	3.56±0.55^	3.72±0.54^	1.04±0.09*^	1.12±0.11*^	5.73±0.50^	5.81±0.54^	0.14±0.05	0.15±0.05	9.10±5.06*	12.39±5.86*
	Pelvis	4.24±0.77*	3.72±0.71*	1.15±0.11*^	1.02±0.09*^	5.75±0.45*^	5.22±0.45*^	0.15±0.06	0.14±0.05	14.25±8.03^	17.76±9.78
Ground	Head	2.80±0.44*^	5.75±1.15*	1.17±0.05	1.22±0.08	5.88±0.40*^	6.26±0.23*^	0.18±0.01*	0.22±0.01*	7.32±1.61*	17.73±2.41*
	Chest	3.46±0.53	3.75±0.38^	1.07±0.08	1.14±0.08^	5.84±0.37^	5.82±0.48^	0.17±0.01^	0.17±0.01^	7.24±2.80*	10.17±2.45*^
	Pelvis	3.95±0.68	3.45±0.63	1.13±0.11*	1.00±0.07*	5.82±0.37*^	5.15±0.45*^	0.18±0.01*	0.17±0.01*^	11.84±4.16^	13.64±4.38
Air	Head	2.82±0.51*^	5.52±1.19*	1.08±0.06*	1.17±0.10*	6.30±0.68	6.72±0.41^	0.11±0.01^	0.09±0.05	5.39±1.87*	13.35±3.64*
	Chest	3.81±0.63	4.05±0.61^	1.07±0.10*	1.17±0.12*^	6.09±0.46^	6.06±0.65^	0.08±0.02	0.09±0.02	5.48±1.99*	8.15±2.46*
	Pelvis	4.73±0.89	4.24±0.68	1.20±0.12*	1.07±0.10*^	6.09±0.34*^	5.42±0.51*^	0.07±0.01	0.08±0.01^	7.33±2.29*^	9.79±1.61*^
3D Vibration	Head	2.60±0.41*^	5.20±0.84*	1.11±0.04*	1.17±0.06*^	5.30±0.26*	6.18±0.36*^	0.20±0.01*	0.28±0.02*	17.41±2.97*^	46.65±6.36*
	Chest	3.41±0.45^	3.35±0.37	1.00±0.08^	1.05±0.09^	5.27±0.23^	5.54±0.36^	0.17±0.01^	0.18±0.01^	14.59±4.34*	18.85±5.17*
	Pelvis	4.03±0.49*	3.48±0.58*	1.11±0.10*	1.01±0.07*^	5.35±0.28^	5.09±0.35^	0.20±0.02	0.18±0.02	23.59±5.36*^	29.85±5.91*^

Table 2: The effect of immobilization condition on heavy weight subjects, reflected by various analysis quantities. A '*' represents a statistically significant difference between the immobilization conditions, and a "^" represents a statistically significant difference ($p < .05$) between weight groups.

		High Weight									
		Z Transmissibility (Peak)		Area under Z Transmissibility		Z Transmissibility Wn (Hz)		RMS Z Acc (g)		RMS Gyro (deg/s)	
Ride Profile	Segment	SB	NB	SB	NB	SB	NB	SB	NB	SB	NB
ALL	Head	2.31±0.27*^	6.25±1.60*^	1.11±0.07	1.13±0.09^	5.92±1.49*	5.41±0.43*^	0.16±0.04*	0.19±0.08*	9.11±4.41*	25.87±15.98*
	Chest	3.22±0.44*^	4.33±0.76*^	0.98±0.08*^	0.93±0.06*^	5.38±0.50*^	4.99±0.27*^	0.13±0.04	0.14±0.04	9.71±5.57	10.82±5.76
	Pelvis	4.28±0.77	4.00±0.92	1.05±0.16*^	0.93±0.10*^	5.36±0.43*^	4.82±0.24*^	0.15±0.05	0.14±0.04	20.76±11.66^	22.45±11.79
Ground	Head	2.42±0.29*^	6.43±1.42*	1.17±0.04	1.19±0.09	5.38±0.61^	5.35±0.40^	0.18±0.01*	0.21±0.01*	6.89±1.23*	17.85±2.74*
	Chest	3.23±0.42*	4.30±0.38*^	1.00±0.08	0.96±0.04^	5.45±0.40*^	4.97±0.33*^	0.16±0.01^	0.16±0.00^	7.39±1.96	8.11±1.82^
	Pelvis	4.13±0.71	3.73±0.62	1.04±0.16*	0.93±0.10*	5.38±0.33*^	4.82±0.22*^	0.17±0.01*	0.16±0.01*^	16.37±4.88^	16.62±3.29
Air	Head	2.26±0.28*^	6.50±2.22*	1.06±0.06	1.11±0.10	6.96±1.58*	5.63±0.54*^	0.10±0.01*^	0.09±0.01*	5.52±1.32*	12.54±1.55*
	Chest	3.40±0.49*	5.03±0.73*^	1.00±0.07	0.97±0.04^	5.65±0.56*^	5.12±0.24*^	0.08±0.01	0.08±0.01	5.82±1.84	6.41±1.83
	Pelvis	4.81±0.67	4.80±0.94	1.10±0.18*	0.97±0.10*^	5.65±0.42*^	5.01±0.18*^	0.08±0.02	0.09±0.01^	12.05±3.50^	13.88±3.74^
3D Vibration	Head	2.24±0.21*^	5.83±0.91*	1.10±0.04	1.10±0.06^	5.42±1.56	5.24±0.22^	0.20±0.01*	0.28±0.02*	14.91±1.66*^	47.22±6.52*
	Chest	3.04±0.36*^	3.65±0.35*	0.93±0.07*^	0.87±0.03*^	5.03±0.30^	4.88±0.20^	0.16±0.01^	0.16±0.01^	15.90±5.22	17.92±3.82
	Pelvis	3.89±0.66	3.48±0.57	1.01±0.16*	0.89±0.10*^	5.05±0.31*^	4.63±0.14*^	0.20±0.02*	0.17±0.01*	33.86±10.27^	36.83±8.64^

DISCUSSION

The study shows that on average among the subjects, RMS acceleration at the head is lower when immobilized than not immobilized; this is expected due to the head being secured inside a relatively soft brace. This effect can be observed in Figure 7. Chest acceleration is largely unaffected by immobilization condition, since the subjects are already strapped in around the chest regardless of whether the immobilization system is used or not. In all ride profiles, subjects experience approximately 5 percent more RMS acceleration at the hips when immobilized than when left not immobilized. This increase in acceleration may be caused by the spider straps inability to hold down the hips when moving vertically. Since most of the body is restrained when using spider straps, the energy imparted on the body during vibration escapes through the hips instead. The RMS acceleration of the chest and hips can be visualized in Figure 8 and Figure 9 respectively. These patterns can also be visualized in Figure 16, Figure 17, and Figure 18 when comparing raw RMS acceleration values between immobilization conditions for the head, chest, and hip respectively.

In general, higher weight subjects have a lower RMS vertical acceleration across the whole body in comparison to lighter subjects. Since the MARS can apply the same force to all subjects on all ride profiles, the heavy subjects must have a lower acceleration, due to their increased body mass. Figure 15 depicts this relation at the hips. Figure 13 and Figure 14 also depict this relation, but not as well as Figure 15 since the head acceleration is greatly affected by the subjects anthropometry, and the chest is restrained regardless of the immobilization condition.

At the head, higher weight subjects have a smaller interquartile range, as shown in Figure 7. This difference is thought to be caused by the weight variation between the subjects in the HW group and in the LW group. The heavy subjects' weights vary by a smaller percentage than the LW subjects, which may cause a decrease in the interquartile range. It is also thought that the anthropometry of each subject can play a role in transmissibility. The HW group was thought to have a more variable anthropometry when compared to the LW group. This variation in anthropometry may cause a wider RMS acceleration and rotational velocity range. The immobilization system reduces the effect of the heavy weight subjects' highly variable anthropometry, which in turn may have caused the reduction in the interquartile range. These responses are also true for the subjects' rotational data in the head and hips, but not the chest. HW subjects have a higher interquartile range in the chest when rotating, which may be caused by the increased inertia of their torsos.

In both weight groups, subjects' heads experienced a lower RMS rotational velocity around the Z axis when immobilized due to the head restraint restricting rotational motion. The chest and hips also experience a lower rotational velocity around the Z axis when immobilized because of the spider straps and spine board. These responses are also true when analyzing raw RMS rotation values, such as those found in Figure 22, Figure 23, and Figure 24.

At the head, the HW group will resonate at a lower frequency due to the increased mass in the head. This response can be predicted using Equation 2, and by referencing the data in Figure 25. The chest and hip data presented in Figure 26 and Figure 27 respectively also follow this trend. Also, heavy weight subjects appear to have a higher 95th percentile transmissibility, which may be caused by their highly variable anthropometry. This postulation also applies to the chest and hip data, and median peak transmissibility data found in Figure 31-33.

Two significant takeaways from the tabulated ANOVA analysis are as follows. First, use of the spine board had a significant impact on head motion (as compared to the no board condition) in both the high and low weight conditions. This significance was present in all ride profiles. The impact can most readily be seen as a large (often more than 50%) reduction in the peak Z transmissibility, though significant reduction in most of the other metrics is also apparent. This reduction with respect to the no board condition is logical given that in the spine board condition the head was constrained to the board via a foam block that greatly restricted any motion of the head with respect to the board.

Second, the resonant frequency was significantly impacted by weight. Specifically, the resonant frequency decreased by between 0.5 and 1.5 Hz from the low weight subjects to the high weight subjects. This decrease was statistically significant in every no board condition, as well as in most spine board conditions. Given the direct relationship between mass and resonant frequency (Equation 2), this reduction in frequency for higher weight subjects is not unexpected. Furthermore, though the magnitude of the reduction may seem small, its potential for vibration mitigation should not be underestimated. Even a small (0.5 Hz) shift in resonant frequency can reduce vibration magnitude if the subject’s resonant frequency would otherwise line up with the vehicle or aircraft he or she is traveling.

When analyzing Figure 29 and Figure 30, the 95th percentile transmissibility of the immobilized subjects had resonance frequencies that occurred before the non-immobilized subjects, occurring at approximately 2 Hz before and less than .5 Hz before respectively. This shift in resonant frequency was a result of the immobilization system. The spider straps held the subject tighter to the litter, therefore increasing their connection to the system and making the system more rigid. This relation can be described using Equation 2.

When looking at all transmissibility data points for each immobilization condition, such as those found in Figure 34-36, the immobilized subjects had lower median and mean peak transmissibilities. This was caused by the head restraint which significantly reduced the head motion. Across the whole body, immobilized subjects showed a lower interquartile range of transmissibility, as well as a lower 5th to 95th percentile. This may have been caused by increased system rigidity brought on using spider straps.

As evidence of the study, analysis was largely performed on transmissibility, accelerations, and rotations pertaining to the Z axis. These data were also affected on the X and Y axes when the spine board was implemented. Y transmissibility in the chest and hips was adversely affected by the implementation of a spine board, due to the contact surface between the board and the litter. Both the board and the litter had a stiff, smooth surface, therefore the friction between the two was low. This allowed the subject on the spine board to slide along the Y axis easier, increasing transmissibility. The X transmissibility also exhibits similar behavior.

REFERENCES

Hogg, R. V., and J. Ledolter. *Engineering Statistics*. New York: MacMillan, 1987.Ljung, L. *System Identification: Theory for the User*, Second Ed., Prentice Hall PTR, 1999.

Kinsler, R., Barazanji, K., Lee, J., Fulton, L., Hatzfeld, J. (2015). Analysis of Two Surveys Examining Enroute Care Technologies, Platforms, and Space Requirements. Poster Presentation at Military Health System Research Symposium. August 2015.

Kinsler, R., Khouri, R., Squire, C., Helgeson, S., Wurzbach, J. Immobilization and Vibration Mitigation Systems: Test and Evaluation of Current and Developmental Products, USAARL Technical Report No. 2018-13, 2018.

Ratanalert, S., Phuenpathom, N., Saeheng, S., Oearsakul, T., Sripairojkul, B., Hirunpat, S. (2004). ICP Threshold in CPP Management of Severe Head Injury Patients, Surg Neurol, 61(5):429-34.

Reno, J. (2010). Military aeromedical evacuation, with special emphasis on craniospinal trauma, Neurosurg Focus 28 (5):E12.

Moses, P. S. (2004). *Spectral Analysis of Signals.* New Jersey: Prentice Hall.

USAARL. (2019). Effect of Patient Weight as a Factor During Use of an Immobilization System Versus No Immobilization System. Research Protocol. April 15th, 2019.

LIST OF ABBREVIATIONS

3DOF: Three Degree of Freedom
6DOF: Six Degree of Freedom
HW: High Weight
Hz: Hertz
ICP: Intracranial Pressure
LW: Low Weight
MARS: Multi-Axis Ride Simulator
NB: No Board
PSD: Power Spectral Density
RMS: Root Mean Square
SB: Spine Board
USAARL: United States Army Aeromedical Research Laboratory

Department of the Army
U.S. Army Aeromedical Research Laboratory
Fort Rucker, Alabama 36362-0577
www.usaarl.army.mil

U.S. Army Medical Research and Materiel Command